Jül-4346

Peter Grünberg Institute/Institute of Complex Systems
Bioelectronics (PGI-8/ICS-8)

Tools for Non-Invasive Communication with Electrogenic Cells: Optogenetic Stimulation and Diamond Recording Devices

V. Maybeck

Mitglied der Helmholtz-Gemeinschaft

JÜLICH
FORSCHUNGSZENTRUM

Tools for Non-Invasive Communication with Electrogenic Cells: Optogenetic Stimulation and Diamond Recording Devices

V. Maybeck

Berichte des Forschungszentrums Jülich; 4346
ISSN 0944-2952
Peter Grünberg Institute/Institute of Complex Systems
Bioelectronics (PGI-8/ICS-8)
Jül-4346

D 82 (Diss., RWTH Aachen Universtity, 2011)

Vollständig frei verfügbar im Internet auf dem Jülicher Open Access Server (JUWEL)
unter http://www.fz-juelich.de/zb/juwel

Zu beziehen durch: Forschungszentrum Jülich GmbH · Zentralbibliothek, Verlag
D-52425 Jülich · Bundesrepublik Deutschland
☎ 02461 61-5220 · Telefax: 02461 61-6103 · e-mail: zb-publikation@fz-juelich.de

Contents

List of Tables

List of Figures

Chapter 1

Fundamentals

1.1 Decision Making and the Electrogenic Cell

Behavior is the outcome of a living system's ability to integrate millions of information processing events over the body of an organism. The smallest functional unit of this integration is the cell, which has evolved many ways to process information including chemical signals [33], mechanical cues [70, 82, 84, 60] and electrical signals [16, 99]. All of these inputs are spatially and temporially integrated in the cell to determine what output is progressed through the network. Though it is a single cell that decides whether or not to pass a signal to the next cell in the network, in order to understand cellular information processing perfect information about the single cell's connectivity and behavior in relation to the rest of the network is desirable, though as yet not achievable. This chapter will present a brief introduction to the cell and how electrogenic cells can process information within a network. Furthermore, existing techniques for gaining spatially and temporially precise information about the cell's situation in relation to the network are presented. Finally, an indepth discussion of two techniques used in this thesis (optogenetics and diamond electronics) will be expanded as a framework for the subsequent studies.

1.1.1 The Cell

The cell is the smallest unit of independently self perpetuating systems, i.e. life. Cells can first be categorized as prokaryote or eukaryote. The prokaryotes consisting of a single membrane bound volume without membrane defined internal structure. Their chromosomal DNA is in the form of a large ring within the cytoplasm bulk and accompanied by smaller rings of DNA (plasmids) which can be exchanged between individuals to increase the genetic diversity of a population (see Figure 1.1). The plasmids are typically between several and tens of thousands of bases long. These simple organisms, and in partiuclar *E. coli*, have become the workhorses of molec-

ular biology for their ability to produce large amount of long DNA chains with low error rates ($10^{-8} - 10^{-9}$, [131]) and produce simple proteins at a low error rate in an easily purified form ($10^{-3} - 10^{-4}$ misreads per codon [91]).

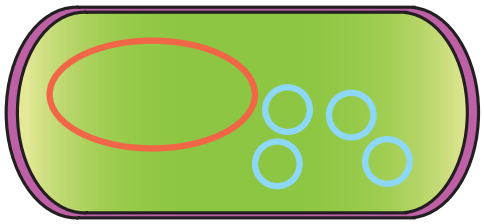

Figure 1.1: A prokaryotic cell (green) contains no membrane bound internal structures. The cell membrane (purple) defines the outer boundary of the cell. Inside the cell, a large circular chromosome (red) is often accompanied by small circular DNA plasmids (blue). The plasmids allow the exchange of genes between cells.

The eukaryotes, with internal membrane bound structures, have evolved a much more complex internal anatomy (see Figure 1.2). Like the prokaryotic cell, eukaryotes' boundaries are defined by the cell membrane. The organization of intracellular processes can then be divided among a number of sub-cellular organelles. A eukaryotic cell's linear chromosomes are contained within the membrane bound nucleus. RNA transcribed from the DNA exits the nucleus through the nuclear pores into the endoplasmic reticulum. The endoplasmic reticulum is the cell's transport system and consists of "rough"regions where ribosomes are embedded in the membrane and "smooth"regions that lack ribosomes. The ribosomes translate the RNA into proteins, and those RNAs not processed in the rough endoplasmic reticulum must be trafficked to the cytoplasm where they can be translated by free ribosomes. Proteins and carbohydrates destined to be secreted from the cell are passed from the endoplasmic reticulum to the golgi body where they can be processed for export. Additional organelles include the mitochondria, the main source of chemical energy in the form of adenosine tri-phosphate (ATP) in the cell; lysosomes, digestive vacuoles responsible for degrading cell invaders shuch as bacteria; and structural elements such as the cytoskeleton and centrosomes.

Eukaryotic cells may also be made transgenic by introducing plasmids with foreign DNA. This can confer new capabilities on the cell or allow monitoring of specific molecules or states. However, since the internal structure of the eukaryotic cell is more complex, the efficiency of transfection methods tends to be lower than that for prokaryotes. When planning the transfection of eukaryotic cells one must always consider the viability of the transfection process, the necessary amount of plasmid DNA for functional expression levels, and the potential toxicity of the plasmid DNA or the foreign protein it encodes.

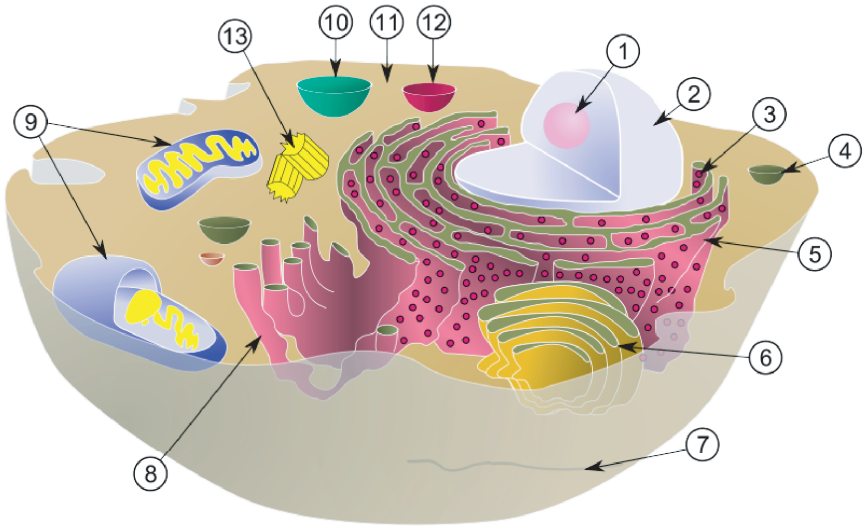

Figure 1.2: The eukaryotic cell contains many specialized membrane bound compartments. The nuclear membrane (2) contains the DNA, which is densest in the nucleolus (1). Ribosomes (3) transcribe RNA that is transported out of the nucleus, either in the cytoplasm (11) or bound on the Rough Endoplasmic Reticulum (5). The smooth endoplasmic reticulum (8) and Golgi Body (6) are responsible for non-protein metabolism and post-processing of proteins, respectively. Energy for cellular processes is supplied by the mitochondria (9) and support is provided by the cytoskeleton (7). Vacuoles (10) and lysosomes (12) allow the cell to sequester particular molecules, and the centriole (13) plays a supporting role in cell division [10].

1.1.2 Resting Membrane Potential

The homeostasis of all cells establishes a voltage across the cell membrane. The internal ionic concentration of the cell, versus that of the surrounding medium establishes an electrochemical gradient across the lipid bilayer, capable of driving ionic currents if the membrane becomes permeable to a charged particle. The lipid bilayer of the cell membrane acts as a barrier to charged particles, such that most polar entities must pass through transmembrane proteins. Active pumps and ion transporters, such as the sodium/potassium exchanger [144, 115] consume chemical energy to move ions across the membrane and maintain the concentration differences. The common concentrations of major charge carriers for one type of electrogenic cell, the neuron, at rest are given in Table 1.1. The generation of a resting membrane voltage and the mathematical description of that voltage holds true for all cells, but this discussion shall focus on their application to muscle and neuron cells, as these form the electrogenic cell networks of interest to the rest of this body of work. The Nernst equation describes the driving

Charge Carrier	Concentration In The Cell (mM)	Concentration Outside The Cell (mM)
K^+	400	20
Na^+	50	440
Cl^-	52	560
$Ca^{2+}*$	0.4	10
$Mg^{2+}*$	10	54
Organic anions	385	–

Table 1.1: Ionic concentrations inside a neuron versus extracellular fluid, from Kandel [50], $*$ adapted from Hodgkin [73].

force for a single ion species across the insulating membrane as

$$E = \frac{RT}{zF} ln \left(\frac{[I]_o}{[I]_i} \right) \tag{1.1}$$

where E is the Nernst potential across the membrane, $[I_o]$ and $[I_i]$ are the concentration of the ion outside and inside the cell respectively, R is the universal gas constant, T is the temperature, F is Faraday's constant, and z is the charge of the ion [16]. This Nernst potential is a combination of the electromotive and diffusive force on ion populations seperated by any insulating barrier, not necessarily across a cell membrane.

The insulating nature of the phospholipid bilayer would ideally act as a capacitor between these two concentrations of charge. However, the membrane's ion channels, pumps, and pores, allow parts of the cell surface to act as variable resistors. This is accounted for by introducing a relative permitivity term for each ion species and summing over all of the species (X) of interest

$$V_x = \frac{RT}{z_x F} ln \left(\frac{P_x[X]_o}{P_x[X]_i} \right). \tag{1.2}$$

Where V_x is the whole cell voltage across the membrane due to species X, R and F are the universal gas constant and Faraday's constant respectively, X is an ion species with a corresponding relative permeability through the membrane P_x and a concentration outside ($[X]_o$) and inside ($[X]_i$) the cell, and z has become z_x to denote that it is the charge of a specific ion. This can be calculated for each of the ion species inside and outside the cell. When the membrane has a permeability to multiple ion species, P of one ion is a relative permeability. Thus, when more than one ion can pass the membrane, the membrane voltage at any point in time is closest to the Nernst potential of the ion species with the highest permeability at that time. In neurons at rest, this is the potassium permeability (whose single ion potential would be -80 mV at 37°C using the values in Table 1.1) and the cell is usually at ($\sim$-50 to -70 mV) compared to the bath. The

Goldman equation (1.3) simplified the application of the above concept of permeabilities by condensing the various types of individual channels for a given ion into a single permeability and considering only the three ions with the highest currents across the membrane (K^+, Na^+, and Cl^-). This is expressed using the variables as above in

$$V_m = \frac{RT}{F} ln \left(\frac{P_K[K]_o + P_{Na}[Na]_o + P_{Cl}[Cl]_i}{P_K[K]_i + P_{Na}[Na]_i + P_{Cl}[Cl]_o} \right). \tag{1.3}$$

Note that in the Goldman formulation z_x has been evaluated within the terms for the individual ion species, as can be seen by the inversion of the concentrations of chloride due to its negative charge. It is not a direct substitution of the Nernst equation. For the full derivation of the Goldman equation see [59].

1.1.3 Action Potential

Many of the channels in the membrane have permeabilities which vary according to the state of the protein's environment. A channel may become more permeable due to binding of a ligand [16], a change in mechanical stress [38], temperature [34], light [121, 86, 72] (see also Sections 1.3.2 and 4.1), or a change in the voltage across the membrane [16]. As the relative permeabilities of different species shift due to these signals, the cell may become depolarized (more positive) or hyperpolarized (more negative) compared to the resting state. In electrogenic cells, when depolarization reaches a certain threshold, voltage gated channels in the membrane are activated triggering the action potential (AP). In neurons, the fastest responding of these channels is the voltage gated sodium channel with a threshold of approximately -45 mV [41]. When a cell is depolarized to threshold, these sodium channels open, greatly increasing the permeability of sodium ions and shifting the membrane voltage towards the Nernst potential for sodium ($\sim$+58 mV at 37°C using the ion concentrations in Table 1.1), accompanied by a sodium current into the cell. 2-3 ms after the depolarization, the slower rectifying potassium channels open. Their function is to repolarize the cell as the sodium channels inactivate. In the case of muscle cells, the depolarized phase is extended by release of Ca^{2+} from intracellular stores and an increase in membrane P_{Ca}. This is necessary to allow calcium to free the actin-myosin binding sites, and allow time for mechanical contraction. Though it is called the action potential, it should be noted that the voltage change is a passive process resulting from the changes in permeability of the membrane [59]. It is the resting membrane voltage which requires energy input from the cell to maintain the ionic concentration differences noted in Table 1.1. A typical action potential and the dominant currents at each time are shown in Figure 1.3 for a neuron and a cardiac myocyte.

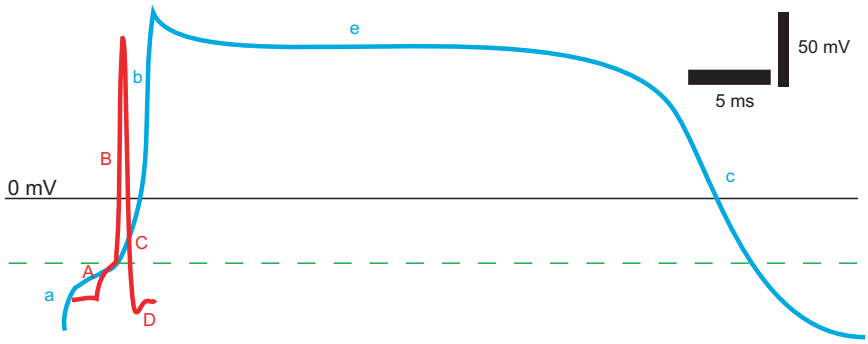

Figure 1.3: Sketches of a neuron action potential (red) and a cardiomyocyte action potential (blue). A and a, depolarization of the cell, which may be achieved by various means. B and b depolarization reaches threshold (green dashed line) causing voltage gated sodium channels to open and the cell to fire an AP. C and c repolarization due to the rectifying potassium channels. D the undershoot of the neuron repolarization due to potassium currents. e the plateau phase of the cardiac action potential due to calcium channels and calcium induced calcium release. Image adapted from [5, 112].

Neuronal networks rely on chemical signal transmission between cells and electrical conduction within a single cell. In cellular information processing, the neuron integrates the depolarizing and hyperpolarizing inputs it receives over its dendritic tree, and if this results in a depolarization above threshold the neuron fires an AP down its axon to subsequent cells in the network. In unmyelinated neurons, the AP initiated at the cell body travels at a speed of 1 m/s to 100 m/s down the axon depending largely on axon diameter [112]. The initial depolarization diffuses down the axon with some loss through the leaky membrane. As the increased concentration of sodium depolarizes the neighboring membrane, the voltage gated sodium channels in this region also open, propagating the Ap further along the axon. The system that has evolved to counteract the leakage and increase conduction speed is for Schwann cells to wrap around the axon and insulate it with layers of myelin. Since this region of the axon membrane has a very low conductance, and low capacitance the AP "jumps"to the points between Schwann cells (the nodes of Ranvier) where an increased concentration of ion channels allows the amplitude of the depolarization to be replenished [112].

In contrast, the AP can also propagate through a network with electrical syncintium. In the case of tissues with gap junctions, such as muscle, the AP in a cell depolarizes its neighbors by conduction of ions through the gap junctions. If the neighboring cell is not depolarized above the threshold voltage, the depolarization will decay as it radiates away from the source due to leak through the membrane at the sub-threshold permeabilities. However, if the cell is depolarized above threshold, a new AP is triggered in the second cell and the process of propagation is repeated in the neigh-

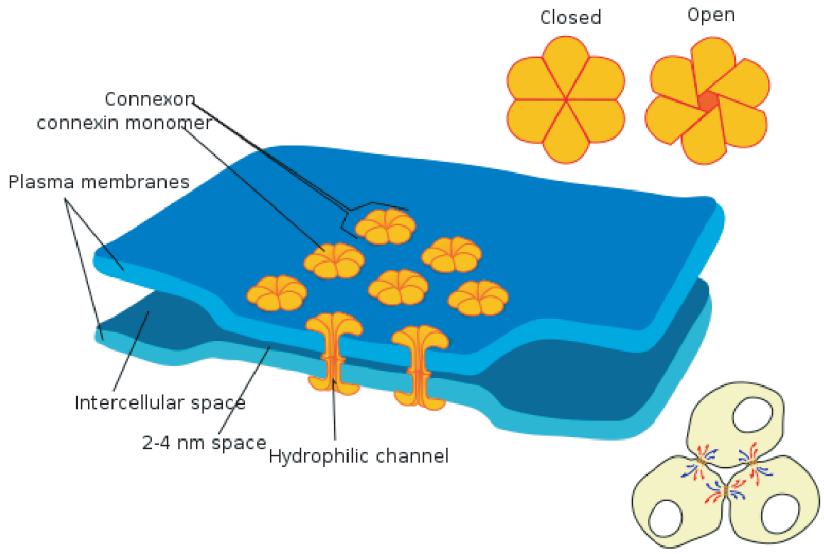

Figure 1.4: Gap junctions (yellow) form a direct passive connection between two cells, capable of conducting ions and small molecules across both membranes (blue) without entering the extracellular space. From [112].

boring cell (see Figure 1.4). Despite the direct connection between cells, the flow of information within a cell network containg gap junctions can be regulated. This is accomplished by the thresholds and dynamics of the conductive channels in the membrane. The clearest example of this is in the heart, where a unidirectional wave of AP propagation is necessary to ensure a coordinated pumping action. In these cells, as in other muscle cells, voltage gated calcium channels and calcium induced calcium release extend the depolarization phase into a plateau. During the plateau phase voltage gated sodium channels inactivate, and cannot be reactivated until the cell repolarizes. Therefore, the AP cannot propagate in the reverse direction, because the calcium driven depolarization has prevented the relaxation of the sodium channels to an excitable state. The calcium channels eventually close based on their own slow channel kinetics and the cell returns to the resting membrane voltage (see Figure 1.3), by which time the AP wave is far enough away to not induce backflowing APs.

1.2 Traditional Manipulation of Electrogenic Cells

The gold standard to investigate the electrical response of cells has been the patch clamp technique. It can be used to both record a cell's response to external conditions and to depolarize or hyperpolarize the cell from within.

In this technique, a glass capillary is drawn to a fine taper (1-3 μm in diameter). In the drawn glass, the difference between the inner and outer diameter is negligable. The pipette is then filled with electrolyte of similar composition to either the intracellular or extracellular fluid. An electrode is inserted in the back of this pipette and used to measure voltages or currents at the tip with reference to a Ag/AgCl bath electrode. The tip of the pipette is brought in close contact with the cell membrane until the lipid bilayer seals onto the glass tip with greater than 1 GΩ resistance [11]. It is then inferred that any current detected at the tip during a constant holding voltage, with reference to the extracellular fluid, is due to opening of ion channels within the patch of membrane attached to the end of the pipette. Using fine tipped pipettes on membranes with low protein concentrations, stochastic current events were observed, leading to the theory that ion channels switch between conductive and nonconductive states only, without graded conductance of a single channel [89]. The graded response of the cell comes as the integration of the conductance of all the channels in the membrane. To investigate this with the patch clamp technique, underpressure is applied to the pipette once it is sealed to the membrane. This ruptures the membrane within the inner diameter of the pipette tip and forms a continuous electrolyte between the cytosol and the patch pipette fluid. The edges of the ruptured membrane remain sealed to the glass with GΩ resistance such that the pipette can be considered an extension of the cell interior connected by the tip resistance (determined by the diameter) and the capacitance of the glass. In this way, the summed action of all the cell's channels can be measured. See Figure 1.5 for a pictorial representation of these two types of patch clamp technique.

Patch clamp has allowed investigation of the affects a single channel type can have on a cell. If a single protein channel is cloned into a normally non-electrogenic cell (i.e. *Xenopus* oocytes or HEK cells), the contribution this channel makes to the cell membrane voltage can be investigated [30, 150] (see also Section 2.4.1). This system can then be used to determine which ions the channel can conduct by varying the pipette solution's composition to omit ions one at a time. Drugs or toxins can also be added to the pipette to determine which factors can block the channel being investigated.

The investigation of individual neuron's behavior is the most widely used application of patch clamp. Excised neurons have been investigated while the holding voltage is varied or current pulses are applied with the pipette [16]. This elucidates the change in response of a single neuron to different environmental conditions or over short periods of time ($\sim$1 hour). To investigate neural processing, small portions of neural networks have been mapped using rabies based reporters loaded into a single neuron via the patch pipette [123]. This allows the investigator to see which neurons provided input to the cell being patched. It is far more complicated to predict exact cell-cell connections for double patch experiments. These double patch investigations allow correlation between the electrical behavior of the two

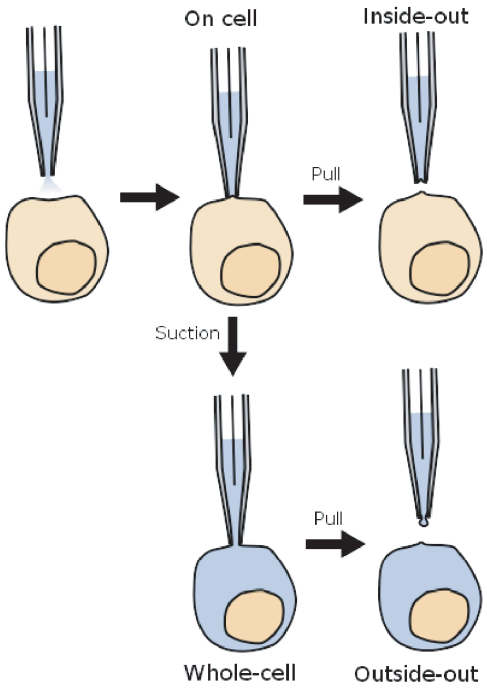

Figure 1.5: Four modes of the patch clamp technique. For each, a glass pipette filled with electrolyte and an electrode approaches a cell. The On-cell mode seals the outside of the membrane inside the pipette and inside of the membrane inside the cell. It has the possibility of measuring single channels if the tip is small enough and the channel density low. If underpressure is applied to the On-cell mode, the membrane ruptures so that the inside of the entire cell is continuous with the pipette electrolyte. Whole-cell measures the sum of all channel activity in the membrane, but also exchanges the pipette electrolyte with the cytosol. Withdrawing the pipette from On-cell mode removes a patch of membrane with the side formerly inside the cell now exposed to the bath, and the former outside of the cell inside the pipette. Withdrawing the pipette from Whole-cell mode results in a patch of membrane being removed, with the former inside of the cell inside the pipette and former outside of the cell exposed to the bath. Figure from [11].

neruons, but rely on established maps of physiologic connectivity, or carefully planned small *in vitro* networks where much of the connectivity can be evaluated visually. The patch clamp data has formed the basis of our understanding of neuronal processing at the single cell level, in comparison to studies of large areas of brain activity such as Functional Magnetic Resonance Imaging (fMRI) [7].

However, there remain several drawbacks to the patch clamp technique. First is the difficulty in assessing multiple cells in the network. Double or triple patch clamp setups are routinely used, but adding more points of investigation quickly consumes the available space for equipment, as each pipette must be accompanied by a micromanipulator, pre-amplifier, and associated electronic control system. This means that patch clamp is poorly suited for investigating the coordinated electrical activity of neural networks larger than several cells. Second, the setup is very sensitive to vibrations or drift, which detach the pipette from the target cell. Third, is the viability of the patched cell assuming a stable setup. Since the whole cell patch configuration leads to a hole in the cell membrane, the contents of the pipette are slowly transferred into the cell and vice versa. Intracellular patch solutions are good ionic approximations of the cytosol, but lack the full complexity

of cytosol and therefore lead to a dilution of normal intracellular components. This limits a typical patch clamp experiment to at most several hours. If one would like to investigate processes in neural networks over a longer timescale, such as long term potentiation or synapse formation and pruning, experiments on the time scale of days are desireable. To this end, less detrimental recording and stimulation methods have been developed.

1.3 Techniques Beyond Classical Electrophysiology

The time limitation of patch clamp experiments has prompted the development of new non-invasive means of monitoring and manipulating electrogenic cells. These approaches are broadly categorized as optical and electrical. Optical cell signal detection has relied on calcium sensitive dyes or membrane integrated voltage sensitive dyes [45] or proteins (see Sections 1.3.1 and 1.3.2 respectively). Extracellular electric devices for recording and excitation have also been developed and are reviewed in Section 1.3.3. For the reasons presented in their respective sections, one sees that optical stimulations and extracellular electronic recording are complimentary techniques. The drawbacks of optical AP detection (slow kinetics of calcium sensors and low dynamic range of voltage sensors) are the points where high sensitivity, high bandwidth electronics excell. Conversely, stimulation with electronic devices has limited spacial resolution and the point in the array delivering the stimulation pulse is unable to record from the cell for several milliseconds as the charge applied disappates. In this case, optical methods benefit from the versatality of light guides, genetic targeting of optical actuators, and since the stimulation and recording are in decoupled systems, the point of manipulation can still be recorded, i.e. all sensors on an electrical measuring array could detect changes in the culture while light is applied to points coincident with the sensors.

1.3.1 Dye Based Electrophysiology

Optical measurements of electrophysiology (voltage-sensitive dye imaging or VSDI) were first made by Tasaki et al. in 1968 [62]. However, even in the early 1980s the technique was still taking root and more dyes and better photodiode detection systems were being sought. Dyes such as RH-414 were found to show fluorescence changes ($\Delta F/F$) on the order of 10^{-3} in response to voltage changes in the cell membrane [61]. These early studies aimed to capture the same number of action potential events as electrical recordings were capable of at the time. One major hurdle, the fluctuation of fluorescence *in vivo* due to hemoglobin absorbtion, was overcome at the turn of the century with the advent of blue voltage sensitive dyes. However,

these dyes still achieved only a 21% change in fluorescence over a 100 mV range and had millisecond time resolution [142].

Alternatively, calcium imaging uses the cation chelating properties of a modified BAPTA (1,2-bis-(2-aminophenoxy)ethane-N,N,N′,N′-tetraacetic acid) molecule to monitor changes in calcium from nanomolar to millimolar concentrations. Among the benefits of calcium imaging is the ratiometric nature of the measurement. By using excitation shift or emission ratioing, fluctuations in the concentration of dye without bound calcium, as well as bleaching, are controlled for. Later dyes based on fluorescin or rhodamine allow ratiometric measurements based on intensity alone, instead of comparing wavelengths [13]. The case of the long term quantification of calcium concentration from fluorescence remains a challenge, because the calcium indicators photobleach over long recording periods (>60 s) [97]. FRET pairs allow a constant ratiometric re-adjustment, but require monitoring seperate wavelengths, which requires expensive equipment to correlate images with high time resolution [97]. Despite this tradeoff in quantitative and temporal sensitivity, calcium imaging fills an important role in not only tracking cell membrane voltage changes, but also the distribution off this important cell signaling molecule. Further advances in optical calcium sensing have used genetic methods to incorporate protein fluorophores, see Section 1.3.2. Among the advantages of genetically encoded methods are cell targeting and repleneshment of the fluorophore to combat bleaching.

1.3.2 Optogenetics

Introducing foreign genes into a cell allows the reseacher to add functionality that has evolved for a different purpose into a desired cell for investigation. In a strict definition, optogenetics should include the use of any light responsive, genetically encoded element to investigate or manipulate the cell. In this sense, optogenetics started with the use of green fluorescent protein (GFP) to label proteins of interest and track them within cells [130]. Fluorescent protein tags have been designed to cover most of the visual [140] and approach the near infrared spectrum (655/40 nm) [105]. Fluorescent tags have also been developed that are only activated after exposure to light with a shorter wavelength than the excitation light so that the movement of localized populations of proteins can be tracked within the cell [128]. Förster Resonance Energy Transfer (FRET), Fluorescence Recovery After Photobleaching (FRAP), and Fluorescence Lifetime Imaging (FLIM) all added to the detailed information that one can deduce about the movement or environment of a tagged protein using optical methods.

However, it was the advent of optically triggered actuators (light responsive control of the cell's internal condition) that led Miller to coin the term Optogenetics [110], and in the literature the term is almost exclusively reserved for proteins using light to manipulate the cell, rather than just observe

it. This manipulation has been predominantly in the field of electrophysiology, with recent expansion into gene expression (see Transcription Factors, later in this section). One slight deviation from this in the literature is the inclusion of genetically encoded sensors for electrophysiologically important conditions such as calcium, voltage, pH, chloride, glutamate, or acetylcholine in "optogenetics". This is related to the predominantly electrophysiological applications of the early optically controlled genetic actuators.

Given this range of genetically encoded elements, we can group the constructs broadly as (1) Sensors, which report a change in state of the cell or protein, (2) Hyperpolarizers which make the interior of the cell more negative with reference to the bath, (3) Transcription Factors, which change the expression of another gene within the cell, and (4) Depolarizers, which make the the cell more positive with reference to the bath. A brief introduction to each of the types is provided here. Optogenetic depolarizers are addressed in depth in Section 1.4, as they are the most relevant to the subsequent work described here.

Sensors

Genetically encoded fluorescent sensors have taken both a structural and a methodical approach to quantifying conditions within the cell or across the cell membrane. The structural approach uses proteins whose fluorescence is only possible when the analyte (or voltage) to be sensed is present. In the case of voltage sensors, the depolarization of the membrane leads to a conformational change of the membrane bound part of the protein, resulting in a change in position of the fluorophore. Proteins have been designed as voltage sensors by bringing together FRET pairs, or by quenching a single fluorophore against the membrane upon depolarization [104]. FRET based systems were also employed with the calcium binding domain of calmodulin to generate optogenetic Ca^{2+} sensors [117]. The fluorescent calcium indicators have also been paired with G-protein coupled calcium increases to detect small molecules that provide inputs to the signaling cascade [134]. Though these systems provide long duration, high viability measurements, work continues to improve the dynamic range of optogenetic voltage sensors, which currently show a fluorescence change of 1-2% over the range of -90 - 110 mV [103]. Used in parallel experiments these tools may provide insight into the role that secondary calcium signaling plays in neuronal changes in conjunction with and independent of voltage changes, and vice versa.

Hyperpolarizers

Of course, it is not only of interest to monitor what is happening inside the cell, but also to control some cellular actions, i.e. specifically timed suppression of spontaneous activity. Among the first genetically encoded

silencing systems used in neurons was the modified Shaker channel SPARK. SPARK uses an externally applied azo moiety to bind the modified Shaker channel and prevent potassium currents in the absence of light. Light with a wavelength of 390 nm then causes a conformational change in the azo group to remove Shaker channel blockade and induce hyperpolarizing potassium currents. This was shown to silence hippocampal neurons expressing the SPARK channel and exposed to the azo blocking agent [26]. Subsequently, interest was renewed in the protein Halorhodopsin. *N. pharaonis* posseses a Halorhodopsin (NpHR) capable of pumping chloride ions into the cell upon exposure to yellow light [138, 95]. NpHR allowed researchers to suppress spontaneous activity in neural networks and depolarize specific cells using optogenetic depolarizers [68]. The proton pump Archaerhodopsin-3 (Arch) from *H. sodomense* was also used to hyperpolarize large regions of brain to manipulate behavior in virally transfected rodents [37]. The advantage of NpHR and Arch are that they can form active chromophores using the retinal naturally produced by mammalian neurons instead of needing to be transfected and then have an additional co-factor added, as in SPARK.

Transcription Factors

A further optogenetic actuator has been developed to control gene expression. Plant phytochromes were found to dimerize with phytochrome interacting factors (PIFs) upon illumination with specific wavelengths, and remain bound until illuminated with a different wavelenght [133]. These plant transcription factors directly translocate into the nucleus to modify gene expression once dimerized. However, they introduce the possibility to use their dimerization to bring together signaling molecules [90] or to re-join proteins that have been engineered in a split form [149]. It has been shown by Tabor et al. that color specific induction of gene transcription could be achieved in *E. coli*, see Figure 1.6 with at least 3 states (two different illumination colors and one dark state) [149]. This opens the possibility of using light to bypass early events in signaling cascades, potentially increasing the response speed within a pathway. It also suggests the possibility of splitting any biologically interesting protein to control its spatial and temporal activity in the cell, bringing optogenetics well beyond the realm of just electrophysiology.

Depolarizers

As Green Fluorescent Protein formed the basis of fluorescent labeling protein technology, Channelrhodopsin has formed the basis of optogenetic depolarizers. The advantage of this algal protein is that because it direclty conducts ions, it has a faster response time than G-protein coupled photoreceptors ($0.008 - 0.090$ s [100] vs $0.03 - 50$ s [113]) and can be transferred to differ-

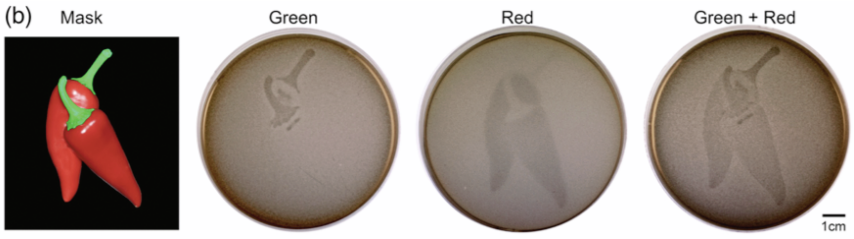

Figure 1.6: Two-color bacterial photography. A two-color mask of color-enhanced chili peppers was projected onto bacteria that produce β-galactosidase when a PIF re-assembles the transcription factor. Green sensor-only strain is JT2 carrying the pJT118 and pPLPCB(S) plasmids and the red sensor-only strain is JT2 carrying pCph8, pPLPCB(S), and pJT106b plasmids. The green + red strain is JT2 carrying plasmids pJT122, pJT106b3, and pPLPCB(S). Reproduced from [149].

ent cell systems as an independently functional unit. Channelrhodopsins 1 and 2 were first discovered by Nagel et al. in *C. reinhardtii* as directly light gated cation channels [120]. Much of the structure of Channelrhodopsin 2 is based on its homology to the well studied proton pump Bacteriorhodopsin. In these transmembrane proteins, a molecule of trans-retinal is bound inside of the channel via a Schiff base to a lysine on trans-membrane domain seven (on K216 in Bacteriorhodopsin [56] and K257 in Channelrhodopsin 2). Isomerization of the 13C upon absorbance of a photon rotates the retinal into a cis conformation (see Figure 1.7). In Bacteriorhodopsin, this rotation leads to a series of proton transfers from coordinated water in the channel to move charge across the membrane [56]. Though they share significant structural homology, the Channelrhodopsins differ in over 50% of amino acids, partly owing to their larger nature. Channelrhodopsins are more likely pore-like channels, as evidenced by their lack of selectivity. A more thorough description of Channelrhodopsin and its relation to the current work can be found in Section 1.4.3.

Optical depolarization has also been achieved by the modification of channels to accept a light sensitive co-factor, similar to the modified SPARK channel used for hyperpolarization. In this case an ionotropic glutamate receptor was engineered to thether the receptor agonist on the end of a maleimide anchor via an azobenzene linker. Exposure to 380 nm light brings the agonist to the channel, activating it and causing depolarization of the cell [152].

1.3.3 Extracellular AP Detection

Introduction

Several extracellular electronic devices are routinely used to detect cell signals. However, these are continuously being improved in terms of signal

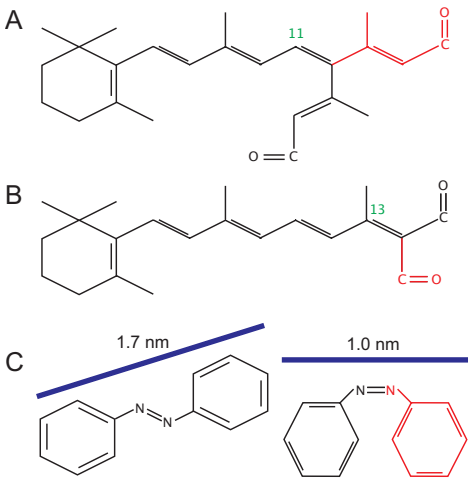

Figure 1.7: Different chromophore control mechanisms for ion currents can be seen. Rotation of retinal about C-11 from cis to trans activates G-protein coupled responses in the mamallian eye. B) Direct channel gating by rotation of retinal about C-13 from trans to cis. C) PTLs control potassium channels by dual wavelength controlled switching of an azobenzene molecule between trans and cis states. A and B induce changes in cell membrane voltage by interaction with the Schiff base inside the chromophore. C can be used to move molecules into or out of a conductive form by spatial arrangement alone i.e. physical blockage of a channel.

detection limit, resolution, speed, and an effort to combine sensing and stimulation capabilities. These efforts have benefitted from novel processes which allow fabrication of ever smaller features, currently into the nanometer scale, and new materials with beneficial combinations of physical and electrical properties.

Biocompatibility is the foremost requirement of a device. Materials that induce an immune response, such as nickel, should be avoided. Similarly, mercury has desirable electrical properties such as a large potential window on the cathodic side [87], but is toxic to cells. The reverse is also true, as the device must withstand the salty, aqueous environment of the cell for weeks or more during operation as well as resist fouling. Loss of function in such an environment can occur due to the breakdown of the sensor material itself, as in corrosion, or by the accumulation of biologic material (protein, sugars, decomposed cell signaling molecules, etc.) on the surface of the sensor, as in fouling. In the first case the sensor is no longer capable of detecting (the properties of element (1) in the point contact model have been changed for the worse, see Figure 1.8), while in the second case a functional sensor is separated from the cell by a physical barrier (in Figure 1.8 the connection between V_J and (1) is severed).

Among the more tunable qualities desirable in a device are high temporal specificity, low noise, affordable production, and high detection efficiency. In this case detection efficiency is meant as the amount of signal detected per one analyte unit. For example, in fluorescence recording this would be the intensity change per calcium ion bound, in field effect transistors the transconductance, and in metal electrodes the change in voltage per ion movement through the membrane or in the cell. Often, the tradeoff between different qualities (i.e. production cost vs. detection efficiency) must be considered for the partiuclar application of the device.

Field Effect Transistors

Field effect transistors (FETs) can be used to detect cell signals if their gate is influenced by the junction voltage, V_J between the gate and the cell. Fluctuations in V_J change the conductance between the FET's source and drain by altering the size of the inversion layer. FETs are desirable cell sensors because the classical electronics industry has well developed industrial scale production of high density and high quality FET arrays as well as the implementation of on chip amplification [53]. Improvement in FETs for bioapplications include the use of new materials such as single crystal diamond [42] and size reduction to achieve subcellular resolution, see also Section AP Detection at the Nano-Scale, later in this Section.

MicroElectrode Array

Microelectrode arrays (MEAs) also have a long history of use in biological recordings [27, 147]. However, these devices still suffer from several limitations. Some of the optimal metals for microelectrodes are not biocompatabile, i.e. mercury. Therefore, gold and platimum have been the standard materials used for MEA fabrication. Due to their ability to stimulate as well as record, MEAs are key systems for implantable technology. One approach to improve implanted MEAs is to construct three dimensional electrodes. When these devices are implanted, the sensors project away from the implantation site and can extend through the glial scar which forms, into the active neural tissue. When coupled with appropriate insertion methods to overcome the viscoelasticity of tissue these devices provide access to cells deep within a tissue.

MEAs have furthermore been structured to interface with specific anatomical formations, such as the cochlea, or to incorporate additional functionalities. These multifunctional MEAs include incorporation of optical fibers [153] and construction on flexible substrates. Flexible MEAs achieve tight conformational contact with whole tissue preparations such as brain or retina [116, 81]. An additional function is to use the electrodes of the array to stimulate electrogenic cells instead of just recording from them. This can be achieved by current injection or by capacitive depolarization of the attached area of the membrane. Different electrode materials have been investigated to prevent electrochemical reactions during stimulation [40] and to improve charge transfer capabilities [49]. The drawback of using the electrode of the MEA for stimulation is that the charging and de-charging of the electrode creates a "blind time"during which the electrode cannot be recorded from. This necessitates the use of a complimentary recording method, such as calcium imaging or patch clamp recording, to monitor the efficacy of MEA based stimulation.

AP Detection at the Nano-scale

To increase resolution, sensitivity, and improve cell-device coupling, both FETs and MEAs have been modified at the nano scale. Nanowire FETs were shown to detect intracelluar AP propagation in a single neuron [127]. High density arrays have also been developed with resolution of less than 10 μm using CMOS technology [94]. Nanowire FETs with free standing wires are further proposed to not only provide a structure that the cell can wrap around [52] but also structures that allow surface properties of materials rather than bulk properties to be utilized [88].

MEAs have also taken advantage of nanoscale modifications. Nano or small micro structuring of the electrode surface can lower the impedance of the electrode without decreasing array resolution [31]. Electrodes with gold nanopillars [31], gold microspines [70], and carbon nanotube spheres [143] have all shown improvement in cell signal detection compared to planar metal MEAs. Silicon nanospikes have also been shown to penetrate the cell membrane and contact the cytoplasm without injuring the cell [139] suggesting that nanostructured electrodes could provide a route for non-damaging intracellular electronic recordings.

Modeling

The current extracellular electronic AP detection devices rely on close contact between the cell and a substrate integrated electronic sensor. Several models have been proposed for the coupling of the cell to the underlying sensor including the point contact [54], sheet conductor [154], and finite element methods [114]. The point contact model depicts the features of interest for cell-device coupling in the barest form. In this model, the substrate embedded electrode is seen as a capacitor and resistor in parallel connected on one side to ground and on the other to the cleft between the cell and the sensor. One possible current leaves the cleft via the leak conductance G_J, which is defined by the distance between the cell and the substrate and the conductance of the gap between the cell and substrate. The other possible current into and out of the cleft is across the cell membrane, which also acts as a capacitor and resistor in parallel (see Figure 1.8). The ohmic component of the membrane is defined by the transmembrane ion channels and pumps, and as discussed in Sections 1.1.2 and 1.1.3 these have variable permeability (variable conductance for their specific ion species) depending on the local conditions, including chemical agonists [9], voltage across the membrane, pH [79], or illumination [120]. The capacitive component of the cell membrane is determined by the phospholipid structure of the membrane and typical specific membrane capacitance is normally 1 μF/cm^2 [111].

Additional models have tried to more accurately describe the signal shape detected at extracellular sensors. The sheet conductor model is one

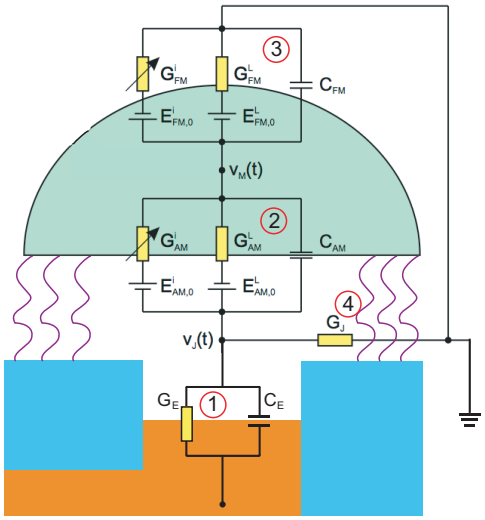

Figure 1.8: The point contact model simplifies the cell-electrode interface to three current paths converging in the cleft between the cell and the device. The parallel capacitance and conductance of the electrode (1) are defined by the material properties of the device and remain static during recording, whereas the conductance in parallel with the membrane capacitance (2) is variable and depends on the permeability of ion channels and pumps in the membrane. The free membrane has a corresponding electrical equivalent, however currents flow out of the cell and into the bath instead of into the cleft (3). The seal conductance, G_J, provides a path for ions to flow out of the cleft instead of being detected by the electrode (4). The higher G_J is, the less sensitive the device is to cell signals, and the more charge needs to be transfered to stimulate the cell. Adapted from [74].

such elaboration. The sheet conductor model defines the membrane attached to the substrate as a different two dimensional feature than the free membrane. In this case, the conductance of the membrane interacting with the surface at each area of contact is separated from the neighboring patch of membrane by a conductance in the cleft media in addition to the leak conductance between the area under the cell and the bath [154]. The point contact and sheet conductor models focus on the electrical equivalents of the different regions of the cell and their connectivity to the sensor. In an extension of this, finite element analysis has been used to model each conductance in the cell membrane as a point current distributed in space near an electrode and simulate the voltage record. This model utilizes a bulk area with conductive properties and therefore has a high dependence on the relative position of the electrode, simulated neuron, and electrode shank [114]. All of these models allow the investigator to predict the influence of the experimental design. However, we may focus on the point contact model to understand the features that are desirable in extracellular recording devices and devise methods to improve these factors.

1.4 Topics Specific to This Body of Work

This work aims to utilize the complimentarity of MEA recordings and optogenetic stimulation to study the behavior of electrogenic cell networks. Both

techniques allow long term interfacing with electrogenic cells. The goals are to achieve single cell resolution interfacing for both signal input and signal recording. Optical stimulation is expected to provide more flexibility of stimulation points and lower interference with simultaneous recording than using extracellular electrodes to stimulate cells. As a new MEA material, the use of boron doped nanocrystalline diamond (BNCD) is investigated for its ability to detect cell signals with single cell resolution and to compare the quality of signal detection (signal to noise ratio, bandwidth, etc.) to that of the current state of the art. To stimulate cells optogenetically, the Channelrhodopsin 2 protein was selected as a depolarization tool. The following section will give a more in-depth introduction to these themes.

1.4.1 Device Improvement Strategies

Surface Modification

To improve the impedance of MEA recordings, traditional microelectrodes have been modified with high surface area materials. These materials include nano- or micro-structured gold [31, 66], platinum black [44, 155, 71], iridium oxide [49], or carbon nanotube spheres [143]. These modifications address region (1) of the point contact model's equivalent circuit (see Figure 1.8). By increasing the surface area of the electrode, these materials increase sensitivity without increasing electrode diameter beyond a size capable of single cell resolution. Nanogap electrodes have also been used to provide large surface area electrodes coupled to high resolution measurement points within the passivation surface [77]. These surfaces improve the electrical coupling at G_E and C_E (see Figure 1.8 (1)), but can suffer from poor mechanical stability, particularly in the case of platinum black, surface structuring, and carbon nanotube spheres [69]. Finding new materials that are stable and have low impedance in a small perimeter electrode is the first improvement strategy.

Decrease G_J

A decrease in G_J (see Figure 1.8 (3)) prevents electrical changes over the sensor from escaping before they can be detected by the device. This usually involves adhering the cell as close as possible to the sensor surface (see also the discussion Reduce Scarring/Fouling later in this Section), since it has been estimated that on a planar substrate less than 20% of the membrane is tightly sealed to the surface [159]. The protein coating of many extracellular sensors for *in vitro* experiments utilizes extracellular matrix proteins, either in their naturally occurring mixture or in more singular purifications. These proteins are on the order of 100 nm long and form a matrix that allows many ions to leak out between the cell and the device. The use of peptide fragments derived from extracellular matrix proteins has reduced the gap

between the cell and the surface to 3.5 nm at adhesion points. However, peptide fragments require covalent linkage to the surface to prevent them from washing away during cell culture [74]. Furthermore, the use of carbon nanotubes or fine woven filter paper has allowed cells to wrap fully around structures, but this idea of using materials that cells wrap completely around is currently being adapted to stable recording devices [69]. Wrapping of cells around protrusions has already been applied to increase the fraction of the membrane in close contact with the surface [66].

Reduce Scarring/Fouling

For sensing devices that are intended to be implanted into the body, a major concern is scar formation at the insertion site. Inactive scar cells can form an isolating barrier between the sensor and the cell of interest. In this case, G_J may be high, but the connection between $V_J(t)$ and the cell of interest (see Figure 1.8) is severed or extrememly weakened. Here, biologically inert materials have been shown to reduce scar formation and cell accumulation on implants. In one approach, coatings of bioactive substances can be applied to devices to prevent scarring [146]. Alternatively, the device itself could be made of a material that induces less scar formation. For example, nanocrystaline diamond (NCD) has been shown to induce less scar formation in retinal implants than traditional implant materials [129].

Summary

The overarching themes of each of these improvement strategies is to have a stable electrode with low impedance and close contact with cells. The field is constantly investigating new materials to address these issues. Particularly as we move to a greater use of sophisticated electronic implants to both investigate and repair biologicial systems, MEA devices will require optimization in each of these areas.

1.4.2 Diamond Electronics

Diamond has many interesting material properties due to its sp^3 bonded crystal structure. Its hardness, has long made diamond a useful abraisive or an anti-abraision coating. However, more recent developments have permitted the growth of artificial diamonds. With this, comes the ability to tune properties such as the roughness and conductivity of the diamond. This allows the inherent hardness and inertness of diamond to be exploited for the field of bioelectronics.

Diamond Types

It must first be noted that many of diamond's electrical properties are most strongly influenced by defects in the sp^3 lattice. They may be grain or edge boundaries, impurities, or sp^2 phases. Diamond films can therefore be classified by the crystal size range in the film as well as by doping. The largest is single crystal diamond, which denotes any diamond with the lowest number of grain boundaries possible during production. This material is commercially available up to 7.5 x 7.5 x 1.2 mm in size [6]. Polycrystaline diamond (PCD) has a grain size of 1-100 μm [12], while microcrystalline diamond (μCD) denotes grain sizes from 0.1-5 μm ([36] and [20] respectively), nanocrystalline diamond (NCD) refers to 10-500 nm grains ([20] and [151] respectively), and ultrananocrystalline diamond (UNCD) refers to grains of 2-10 nm ([20] and [36] respectively) forming the film. All of the above forms are used as a bulk material or are grown as a film over a supporting substrate. Nanodiamond (ND) powder, formed by explosions can also be resuspended such that dispersed particles with diameters of about 5 nm [160] and consisting of one or very few grains can be used. It can be seen that the size delimiters of each type of diamond film vary slightly within the literature. For this body of work, NCD is used to denote material with grain sizes from several hundred nanometers to half a micron.

The second order of classification is the doping of the diamond. "Pure" carbon films of all types mentioned above grown by plasma enhanced chemical vapor deposition (PECVD) contain a small amount of hydrogen termination from the carrier gas at their grain boundaries [135, 122]. However, these undoped films retain an insulating character, with conductivity below $10x10^{-10}$ $\Omega^{-1}m^{-1}$ [55]. The addition of dopants, most often boron, can increase the conductivity and the electrochemical stability of the film. Boron doped nanocrystalline diamond (BNCD) contains $3x10^{20} - 2x10^{21}$ [151] boron atoms per cubic centimeter between the quasi-metallic transition (when the conductance mechanism ceases to be hopping between carriers and returns to carrier mobility) and the phase separation limit (when the film contains distinct regions of diamond and regions of boron). The corresponding conductivities achieved are 0.81 up to 63.6 $\Omega^{-1}m^{-1}$ at room temperature. Boron doping has also been used in SCD and polycrystalline diamond [55] to achieve quasimetallic or semiconductor films. Nitrogen may also be incorporated into diamond films, and in nitrogen doped UNCD conductivity of 260 $\Omega^{-1}cm^{-1}$ was observed [20].

Diamond Biocompatibility

NCD has been shown to be a usefull material for cell culture. Argonne National Labs uses UNCD as a passive coating to make silicon chip implants more biocompatible [108]. Cells could furthermore grow on NCD substrates

Diamond Type	Crystal Size
Single Crystal Diamond	100 μm
Polycrystalline Diamond	1-100 μm
Microcrystalline	0.1-5 μm
Nanocrystalline	10-500 nm
Ultra Nanocrystalline Diamond	2-10 nm

Table 1.2: Diamond types are classified by their grain size. There is some overlap in the rage of sizes for each term. Data compiled from [6, 12, 36, 20, 151].

without coating the substrate with adhesive proteins [102]. The cells' ability to adhere to the uncoated surface is attributed to the surface roughness and surface energy of the diamond [21]. Furthermore, implanted diamond devices were shown to induce less gliosis at the implant site than traditional gold/kapton devices [102]. This not only signals that diamond induces less of a response to implantation, but also shows that implanted diamond devices are expected to be in better contact with their target cells than traditional materials.

Prior Art in Diamond Bioelectronics

Much development of diamond electrodes for biosensing applications has focused on electrochemical measurements. The large electrochemical window of diamond (-1.5 V [126] to 3.2 V [151]) is promising for the development of an electrochemical device which can discriminate a larger number of biologically relevant analytes than conventional metal electrodes. However, diamond electrodes may also be used to directly measure the electrical activity of cells such as neurons and muscle. Polycrystalline diamond electrodes with a diameter of 20 μm have been used for *in vivo* measurement of neuronal signals, achieving a peak to peak signal of 0.07-0.08 mV [35, 18]. Large electrodes (1 mm) of hydrogen terminated diamond recorded signals up to 0.08 mV from multiple GT1-7 cells cultured on the surface. If a device with electrical recording and electrical stimulation capabilities is desired, then the large electrochemical window of diamond allows the device to deliver a larger voltage step without inducing irreversible reactions at the electrode surface.

1.4.3 Optogenetic Depolarizers

As mentioned in Section 1.3.2 Channelrhodopsin 2 has been the main protein used for depolarization of electrogenic cells and will be further addressed in this body of work. Channelrhodopsin's adoption by the scientific community has largely driven the rise of optogenetics and can be seen by the rapid development of Channelrhodopsin uses and variants.

Channelrhodopsin 2 was first utilized as a transgenic construct in 2003. Nagel cloned the Channelrhodopsin 2 gene and expressed it in *Xenopus* oocytes and HEK cells with the aim of determining the Channelrhodopsin 2 light-driven response from that of Channelrhodopsin 1. It was then shown that Channelrhodopsin 2 is a passive cation channel with less selectivtiy than the Channelrhodopsin 1 proton channel and whose C-terminal tail is not necessary for channel function [121]. One advantage of using Channelrhodopsin 2 in animal cells is that native production of retinal is sufficient for generating functional chromophores [29], and though supplements may be provided in cell culture systems they are not strictly required. This is in contrast to genetically engineered channels which require the addition of a non-native photo tethered ligand (PTL) (see Section 1.3.2). Engineered channels using PTLs have been used to activate cation channels [152], in addition to the blockade of potassium channels [26] noted in Section 1.3.2. The independence of Channelrhodopsin 2 means that it is a more easily tailored tool for a number of cell systems.

After it was shown that the Channelrhodopsin 2 protein was capable of depolarizing mammalian cells, the next logical step was to transfect electrogenic cells. Channelrhodopsin 2 was first used in neurons in 2005, in culture [29, 83] and to elicit changes in behavior in *C. elegans* [119]. Furthermore, in Drosophila, Channelrhodopsin 2 specifically targeted to nocireceptors using the a *painless*-GAL4-UAS expression system triggered "pain"responses upon blue light illumination [163]. This showed not only Channelrhodopsin 2's applicability to various model systems in experimental biology, but also the specificity with which the protein could be expressed in neural subpopulations.

In addition to the expansion of use into numerous experimental systems, Channelrhodopsin 2 has been specifically modified for targeted applications. Key moieties in the channel have been identified (H134) and mutated to alter channel currents [119]. Other mutations have been introduced to improve channel kinetics such that fast and frequent current pulses can be applied without a plateau due to unclosed channels (E123) [65], or to provide step function opening and closing of the channel using two different wavelengths of light (C128) [28]. A chimera of Channelrhodopsin 1 and Channelrhodopsin 2 has also been introduced, which shows superior resistance to deactivation [101]. For an overview of the top performing published Channelrhodopsins in several parameters of interest see Table 1.3.

Despite intensive recent work in the development of different Channelrhodopsin variants there remains several areas for investigation. It remains to be seen if a toolbox of individually specialized constructs or one variant with good performance across several factors (even if not the top performer in each single characteristic) is useful for general use. The expression vectors used could furthermore influence the availability of channels or the viability of expressing cells.

Parameter	Best Construct	Performance
Least Deactivation	ChIEF	20%
Fastest Kinetics	ChETA	0.86 ms
Highest Conductance	ChIEF	1.46 pS/channel ‡
Greatest Light Sensitivity	ChEF	0.72 mW/mm^{-2}

Table 1.3: The top performance in a number of key parameters is shown with the associated specialized Channelrhodopsin construct. Data from [100] except for ‡from [101].

1.4.4 Complimentarity of MEAs and Optogenetics

Since, directly light gated channels maintain the speed of stimulation possible with electrical methods, but have greater flexibility of position and do not cause "blind time"on the electrode coupled to the cell they are the stimulation method of choice for non-invasive bi-directional communication. The combination of genetic targeting and illumination projections available, offers the opportunity to stimulate single cells, and even manipulate subcellular regions. This is complimentary to the sub-millisecond speed and single cell accuracy of extracellular MEA recordings for long term cell measurements. New materials for MEA construction, such as diamond, provide further opportunities to improve MEA recordings. The superior biocompatibility and durability of diamond suggest it can be a superior MEA material. Additionally, its optical clarity suggests such MEAs are better suited for optogenetic studies. This work aimed to develop the two fields of optogenetic stimulation and diamond MEAs for their convergent use at the level of single cell studies.

Doing so requires the selection of an optogenetic depolarizer that can be used for single cell stimulation of *in vitro* networks with 10^2-10^4 cells. This must be expressed in neuronal cultures for several weeks to ensure mature networks with functional synapses have formed. This protein should have fast response times and suitable currents for triggering action potentials.

The cells should be cultured on a MEA with single cell resolution of the electrodes and sufficient signal to noise ratio to detect neuronal signals. Advanced MEA materials are sought for this requirement because planar gold electrodes with areas less than the circumference of one cell have difficulty detecting neuronal signals. It remains to be shown that diamond microelectrodes can be used to detect cell signals with single cell resolution. The biocompatability of diamond also suggests that a tighter seal with the cell could be achieved, and therefore a better signal to noise ratio than conventional microelectrodes.

The following body of work details the selection of such an optogenetic tool and the development of a diamond based MEA recording device to-

wards the implimentation of combined optogenetic stimulation and extracellular MEA recording at the single cell level. Such a system is aimed at understanding single cell contributions to network information processing over the timescale of days or more.

Chapter 2

Material & Methods Overview

The present work aims to integrate optogenetics and extracellular cell recordings. Doing so requires a wide range of techniques including optical control, genetic manipulation, cell culture, and MEA utilization. This chapter provides a brief overview of the techniques used. It's aim is to introduce the reader to the method so that the results presented can be understood in context, rather than to provide protocols for reproducing the results. For complete protocols please see Appendix B, and for manufacturer's details and reagent specifications see Appendix A.

2.1 Measuring Setup

2.1.1 Optics

The measuring setup allows for several forms of stimulation and recording. At the heart of the system is a Zeiss Axio Scope upright microscope with three illumination sources. A switchable, wide-field white or UV illumination (HXP, Zeiss) is provided along with a coupled 473 nm laser (Rapp OptoElectronics) as a blue point source. An additional filter option at the wide-field illumination sources makes it possible to illuminate with long wavelength light over large areas, while applying point illumination with the laser. This is useful for using red-shifted calcium imaging dyes during laser stimulation and for allowing global light based manipultion that is different from point manipultion, i.e. for global suppression using Halorhodopsin and yellow light with point stimulation of Channelrhodopsin using blue light (see Chapter 1 for a discussion of Halorhodopsin vs. Channelrhodopsin). A schematic of the beam paths possbile can be seen in Figure 2.1.

In the standard case of an upright microscope (Figure 2.1(A)), a broad spectrum of light from either the white light or HXP source is bandpass

or long pass filtered for the excitation wavelengths immediately before the dichroic beamsplitter. Excitation light is reflected to the sample by the beamsplitter where it interacts with the sample and is reflected or reemitted at a longer wavelength. The beamsplitter passes the longer wavelengths produced by fluorescence or interaction with the sample to the emission filter which passes only the color of interest for observation. In the original laser excitation setup (Figure 2.1(B)), the laser was coupled into the beam path between the wide-field light sources and the excitation filter. This allowed high power laser excitation, but forced observation with blue wide-field light, in some cases leading to an apparent background activation of Channelrhodopsin. This wide-field illumination was necessary because the excitation filter was between the laser coupling and the dichroic mirror. The final option (Figure 2.1(C)) implements the excitaiton filter at the wide-field source, before the laser is coupled into the beam path. This allows, for example, observation of the red fluorophore mKATE with green excitation light, while exciting Channelrhodopsin expressed by the cell with blue laser light.

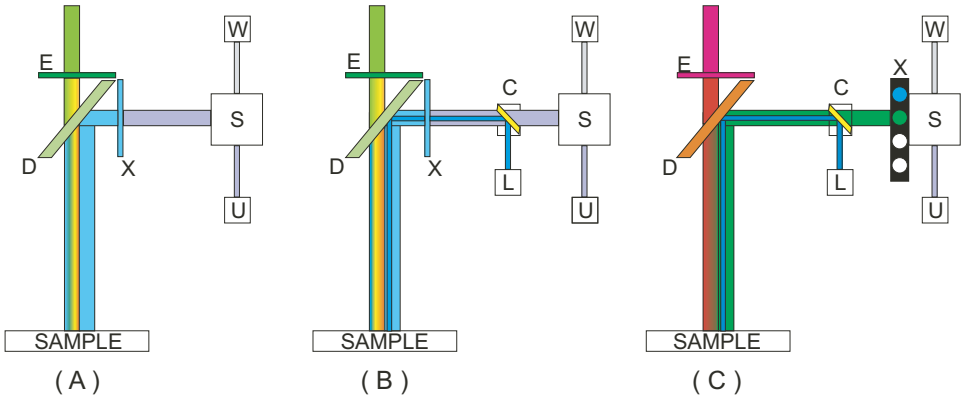

Figure 2.1: Schematic depiction of the measuring setup's illumination options in comparison to standard wide field fluorescence microscopy. A standard fluorescence microscopy setup can be seen in (A), the original laser coupled setup is shown in (B), and the current setup for long wavelength wide-field illumination with point 473 nm illumination is seen in (C). Filters and sources are labeled as follows; W - white light source (halogen bulb), U - ultraviolet light source (HXP from Zeiss), S - widefield illumination switch, L - 473 nm, 100 mW laser, C- coupling dichroic mirror to reflect the laser into the microscope optics, E - emission filter, X - excitation filter, D - dichroic beamsplitter.

The laser is controlled by UGA targeting software (Rapp Optoelectronics). The software interface allows the micromanipulator for laser spot position to be calibrated to any image detected by the camera, and therefore the field of view from any objective and tube lens combination. The position of the laser spot is also marked on the image for later reference. Laser

flashes can be manually triggered, electronically triggered, or continuously on. Electronically triggered trains of flashes can be programmed into the targeting software with a single pulse time and delay time for each spatial point targeted. Alternatively, an external TTL pulse can be supplied for the electronic trigger. By coupling the stimulation output of the HEKA EPC9 patch amplifier (see Section 2.1.2) into the laser TTL, specific pulse trains with varying time courses could be applied to a single point using the TIDA (HEKA) software to program stimulation files. To provide a record of the illumination time directly on the recording trace, the TTL pulse can be split at the input port and passed via a voltage divider to the recording amplifier. When a portion of the TTL trigger is taken for recording synchronization, the signal input from the laser control system cannot be further split without becoming too week to trigger the devices. This means that input signals from the UGA control box cannot be simultaneously combined with TIDA programmed flash programs in the current hardware setup. Coupling for signal synchronization could be achieved for both patch clamp and MEA recordings, though for MEA recordings, one of the 64 channels must be sacrificed from the recording array to receive the laser input.

The microscope is further equipped for standard fluorescence, DIC, and brightfield imaging with a Zeiss Axiocam MRm running AxioVision image acquision software. AxioVision is designed for high quality image acquisition and processing. The UGA laser interface software provides image acquisition, but its main goal is to precisely control the laser spot position and duration of illumination, therefore it is not as good for image measurements as the AxioVision software. However, AxioVision and UGA cannot be run simultaneously, so during laser stimulation the UGA interface must suffice for image acquision (see further comments in Section 4.2.3).

2.1.2 Electronics

Two electrical recording devices were used for the majority of this work. The first is an EPC9 patch clamp amplifier by HEKA electronics. This is a double patch system operated by the software TIDA (HEKA). The EPC9 has automatic compensation functions for the pipette offset, C_{fast} and C_{slow}. The bandwidth of this amplifier is 100-15,000 Hz [57].

The second is a custom built 64 channel MEA amplifier system "BioMol" [158]. A signal can be fed out of any single channel of the MEA and into one of the EPC9 inputs, or conversely a signal from the EPC9 (or any other device, such as the laser TTL discussed above) can be coupled into channel 1 of the MEA amplifier. The MEA amplifer provides a theoretical 1033x amplification of the chip signal using two inverting and one non-inverting amplifiers. The amplifyer system has built in drift correction with τ of $\sim$1 ms for 56 channels in columns one through six and eight, and τ of 11 s for the eight channels in column seven. This arrangement allows comparison

of column seven to the other channels to determine if slow components of the signal are being removed by the drift compensation. MEA data was collected and analysed with MED64 Controler software (Panasonic). Furthermore, MEA data was also post processed in MatLab including the programs M64 [145] and BioMas Analyzer [85], Origin 8, and Excel. Since MED64 Controller is commercially available for use with a triple inverting amplifier system, the 'raw'data from MED64 was inverted to obtain the trace from the double inverting amplifier system. All electrical measurements were made against a silver/silver chloride bath electrode.

2.2 Chip Production

Chip production comprises several steps from deposition and patterning of the electronic device, to packaging it in a state that can survive the wet and salty environment of cell culture. The sensor array itself is produced in batches on commercial wafers of oxidized silicon or borofloat glass. Then conductive elements are applied, patterned, and passivated with an insulating layer. The passivation layer covers all of the surface of the chip except for the electrodes and the bond pads. The bond pads are connected to the inner gold contacts of a printed circuit board (PCB) carrier, which expands the radius of the contacting lines and provides the base on which to build the culture space. A water-tight culture area is then built up on the carrier leaving only the center of the chip where the sensor array is exposed to the culture (see Figure 2.2).

2.2.1 Metal MEAs

Metal electrode MEAs were produced in house by our cleanroom team, or in collaboration with the University of Bonn. Gold feedlines and electrodes were deposited on oxidized silicon wafer or borofloat glass substrates using standard photolithography techniques and passivated with $SiO_2/Si_2N_3/SiO_2$ (ONO) or alternating layers of Si_3N_2/SiO_2 (NONONO). Metal electrodes were used as fabricated or with surface modifications including electrochemically deposited platinum black and gold nanopillars. Electrodes were arranged in an 8 x 8 square array and had a diameter of 8, 10, or 20 μm. The pitch, or center to center distance between electrodes, was 200 μm. Feedlines connected the electrodes to the bond pads in a star formation. For some comparisons, gold electrodes of the same size and pitch, but with a cross layout for the feedlines and produced in the University of Mainz, were also tested. For images of the chip design see Figure 2.2.

Metal MEAs could be further improved by electrodeposition of a porous platinum layer on the electrodes. Encapsulated chips were filled with hydrogen hexachloroplatinate(IV) solution (Fluka) and mounted in a socket with selectable channels and a platinum counter electrode in the bath. The

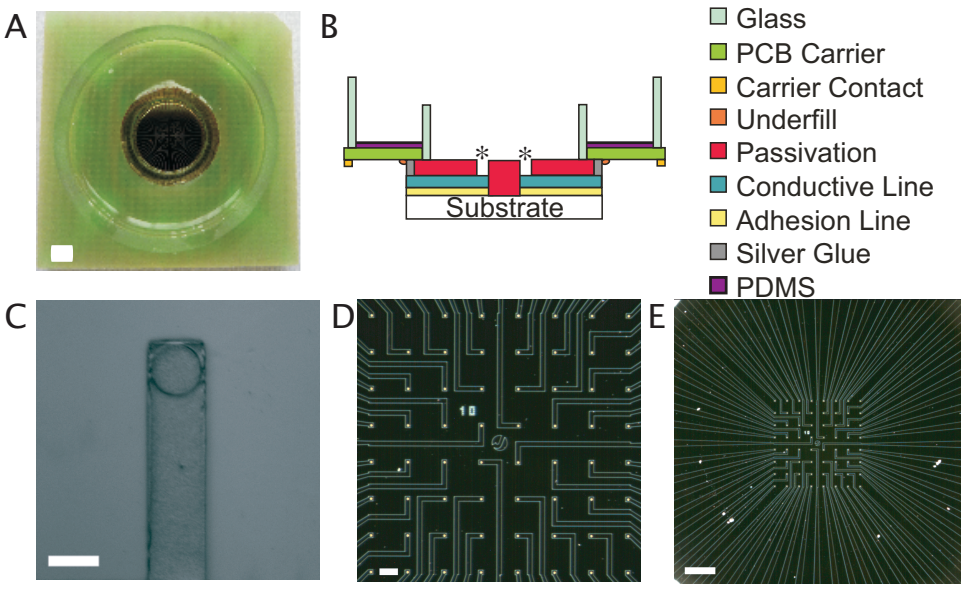

Figure 2.2: The standard layout of a MEA chip with 20 μm electrodes and 200 μm pitch. A) top view of a fully encapsulated chip, scalebar equals 2 mm. B) schematic of a cross section of the encapsulated MEA showing conductive lines patterned on a support substrate, not to scale. The passivation is open only at the electrodes (*) and bond pads, where silver glue provides a contact between the chip and carrier. Underfill isolates the individual silver contacts and seals the chip to the carrier. Glass rings and a PDMS coating produce the culture dish on chip. C) Micrograph of a single electrode, scalebar equals 20 μm. D) The array of 64 electrodes in a micrograph, scalebar equals 100 μm. E) Micrograph of the exposed area of the chip. The edge of the inner glass ring is visible in the corners, and the star arrangement of the feedlines is clear. Scalebar equals 500 μm.

socket switches were used to deactivate voltage cycling for channels 62 to 64 in all platinizations as an internal control (performance of the unplatinized electrodes serves as an indicator of any general defects in chip production, such as poor adhesion of feed lines etc.). The voltage was then cycled from 0.7 to -0.8 V in 0.1 s steps for up to 2500 cycles. Platinization was monitored electrically (I/V curves) and optically (formation of bubbles during deposition and deposition of domes or mushroom structures instead of filled electrode cavities).

2.2.2 Encapsulation

Encapsulation is required both for the sake of protecting the electronics and protecting the cells. In the first case, the encapsulation seals off conducting elements from the wet culture environment except for the electrodes. In the second case, the encapsulation prevents chemicals from the plastic in the PCB carrier from leaching into the media and poisoning the cells. Since

the photolithography steps leave the electrodes and the bond pads both on the top side of the chip, silver glue or wire bonding must be used to attach the chip to a carrier which expands the space for a culture volume to be built upon. Polydimethylsiloxane (PDMS) is the most versitile encapsulation material, but is succeptable to swelling during long culture periods. Therefore, more durable chips can generally be produced using the silver glue / flip-chip method than wire bonded chips where the wires become embedded in PDMS. The flip-chip method was therefore applied for all of the MEAs discussed in this work.

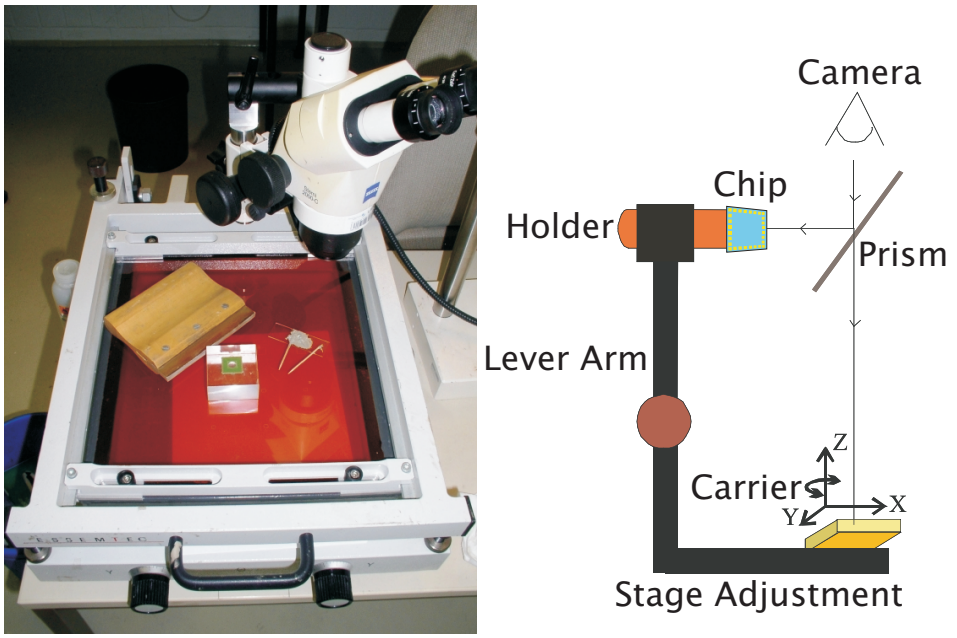

Figure 2.3: Images of the flip-chipping equipment including screen printer, silver glue, carrier, chip, and fine placer (left), and schematic of the fine placer used for flip-chipping (right). Adapted from [74].

The bond pads of individual MEA chips are aligned to a PCB carrier with gold inner and outer contacts using a fineplacer, see Figures 2.2 and 2.3. A conductive attachment between each pad and the carrier is achieved with conductive silver glue. After baking the chip and carrier to cure the silver glue, a thin layer of epoxy is applied as underfill to insulate between the individual silver glue contacts. The chips are baked again to cure the epoxy and then fitted with glass rings to form the culture area on chip and the culture volume. After another baking step to cure the PDMS or epoxy that affixes the glass rings, the PCB carrier is coated with PDMS or epoxy in all remaining places that will be exposed to the culture media.

Several factors must be taken into consideration for the exact encapsulation procedure. For example, the material for encapsulating the PCB carrier

is determined by the cell type to be used and the base material of the chip. It was previously known that PDMS but not epoxy encapsulation was suitable for growth of HL-1 cells (see Table 3.2 and Section 2.4.1), though neurons were successfully cultured with both encapsulations on metal MEAs built on silicon wafer or borofloat glass substrates. Additional considerations are discussed in Section 3.1.2, and the specific combinations of materials for encapsulation and their processing are summarized in Tables 3.1.2 and 3.2.

2.3 Chip Usage

Methods related to chip usage are the processes necessary to apply cells for a viable culture and remove them again to allow re-use of the chip. This involves cleaning and coating before the culture and removal of both the coating and cell material after the culture.

2.3.1 On Chip Culture

The encapsulated MEA requires several more steps of preparation before each use with cells. These steps prepare a cell adhesive surface for the culture to grow on and sterilize the system so there are no contaminating microbes in the culture. Encapsulation must only be perfromed once in the building of a chip, but the preparation steps outlined in this section are performed before each culture.

Metal MEAs were activated with oxygen plasma, sterilized with UV light, and coated with cell adhesive proteins, such as poly-D-lysine plus extracellular matrix gel (pECM) mixtures, pECM with gelatin (GpECM), or a fibronectin/gelatin mixture. After one hour of adsorbtion, excess protein was rinsed away by washing the chips once with the solvent the protein is suspended in, see further details in Appendix B.4. Sterilized and coated chips could be stored for up to one week at 4°C.

Freshly dissociated cells were plated directly in the inner ring of encapsulated and coated MEA chips. If cells were plated in a low volume to ensure high density on the array, media was topped up after four hours of adhesion to fill the outer ring of the chip. Similar to cells in traditional culture wells, cells on chip were cultured on at 37°C, 5% CO_2 in a humidified incubator. The media of chips with HL-1 cultures was changed completely each day, while the media of neuronal cultures was exchanged by half every other day. If transfection was carried out on chip, an additional complete media change was carried out on the day after transfection to remove remaining transfection reagent, see Section 2.4.3.

2.3.2 Cleaning

Chips could be cleaned and reused for several cultures. However, reuse requires removal of cells and debris from the previous culture. Depending on the material of the chip and the cleaning procedure used, chips lasted between three and ten cultures before degradation of the chip prevented sensible measurements. The standard cleaning protocol kills the cells immediately after the culture is measured and mechanically removes cell material. The chips are then cleaned in an ultrasound bath with 2% Helmanex in Bidest, followed by a rinse step in ultrasound with pure Bidest. This cleaning protocol works well for metal MEAs with ONO passivation stacks.

2.4 Cell Preparation

Cells cultured on chips may be either primary cells directly prepared from a tissue, or cells from a cell line that is maintained in culture in the lab. This work utilizes primary cortical neurons, the HL-1 cardiomyocyte-like cell line [39], and Human Embryonic Kidney (HEK) cell lines. For optogenetic studies, foreign DNA containing the light sensitive gene must be inserted into the cells. In this work, electrofection was used to introduce DNA to cells in suspension, and as an alternative route, a chemical transfection reagent was ussed to transfect adhered cells.

2.4.1 Cell Lines

HL-1 Cells

HL-1 cells are a cell line derived from a mouse atrial heart tumor, capable of dividing indefinitely but also maturing when a confluent layer is formed. The mature layer forms gap junctions and begins to spontaneously send action potentials across the sheet of cells. With further maturation, the cell sheet becomes contractilely active and each wave of action potentials can be seen as a movement of the cells. Thus, this system is ideal for the first validation of new electronic devices. The presence of electrical signals can be confirmed optically by the contraction of the cells in mature cultures and since signals propagate through the sheet, the detection on each sensor of an array must have a time shift correlated to the propagation speed of the action potential.

HL-1 cells are maintained in Claycomb's Media supplemented with glutamine, Norepinepherine (NorA), penicillin/streptomyocin, and 10% Fetal Bovine Serum (FBS) [39]. Cells were removed from a confluent T-25 culture flask by digestion with Trypsin EDTA and one eightyth plated onto 7 mm ⌀ devices coated with fibronectin/gelatin. The culture media was changed every day and the activity of the confluent layer was measured on day *in vitro* (DIV) 3 or DIV4. Cultures longer than DIV4 were rare but possible

if the cells had not formed multilayers that reduce nutrient diffusion to the lower layers of cells. If no contraction of the cells could be seen in a confluent layer, cells were stimulated with an additional 1x dose of Norepinepherine.

HL-1 Test System

The signal reliability and shape analysis make the HL-1 cell system a good candidate for validating new cell sensing devices. The confluent layer formed assures that most, if not all, sensors on an array are in close contact with at least one cell. In addition, optically confirmed spontaneous activity prevents false negatives in the evaluation of the device. Finally, signal propagation prevents false positives in the evaluation of the device, by having more characteristic features, and therefore the ability to align and average spikes over time, than spurrious noise. The ability to average peaks also exists in randomly occurring cell signals (i.e. from neuronal networks) but these are more difficult to identify if the ability of the device to operate as a cell sensor is still in question. The HL-1 system was therefore used in proof-of-principle experiments with new devices and to evaluate device performance due to the ability to accurately eliminate both false positive and false negative signals.

Since the beating of the HL-1 cells generates a wave of action potentials that propagates across the cell sheet, one key factor to suggest that the signals recorded are indeed cell signals is to look at the propagation speed and direction across the sensor array. Typical HL-1 action potential propagation speeds are $7 - 30$ mm/s [49, 106]. Additional evidence that recorded signals are due to cell activity and not to external interference or noise is an increase in beat rate upon the addition of NorA and pacemaker switching in recently matured cultures. Pacemaker switching is most easily seen as a change in propagation direction when there is a long delay (i.e. >10 s) between each beat. The final piece of evidence that the signals are truly from the HL-1 cells is that if the spikes from one channel are aligned according to their sodium peak, each channel should produce a characteristic spike shape. The differing cell configuration over each channel leads to the variation in shape from channel to channel. Noise should flatten the average of the spikes on a single channel, while systematic interference would produce the same signal shape on all channels. It is also possible that the spikes from particular propagation directions have their own characteristic shape for a channel. This may arise when more than one cell contributes to the recording from a single electrode. For a schmatic illustration of this concept see Figure 2.4.

It must be further noted that the shape of the extracellularly recorded HL-1 action potential is quite different from that expected from a neuron, see Figure 2.5. Because the HL-1 cells form a sheet connected by gap junctions, the AP wave first depolarizes the cell without the opening of any channels on the cell surface. This depolarization is capacitively coupled to the electrode

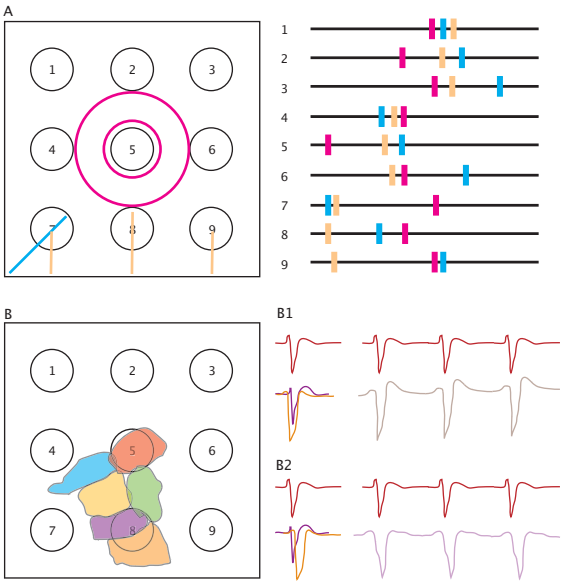

Figure 2.4: Schematics of evidence that signals are from cells and not noise or interference. A) The timing for a beat wave moving over a small array in different directions; concentric circles from a pacemaker on electrode five (pink), bottom to top from an off-array pacemaker (orange), and from bottom left towards top right from an off-array pacemaker (blue). There array occupies 1.4 x 1.4 mm of a 7 mm ⌀ culture, so a distant off-array pacemaker's point source appears as a plane wave. On the right, a color matched relative time recording from each channel. B) Signal shape evidence for cell signals. B1) Signal shapes from channel five (red) and channel eight (lavender) during bottom to top propagation. B2) Signal shapes from channel five (red) and channel eight (brown) during top to bottom propagation. The red cell dominates electrode five's response, so the signal is the same in both propagation directions and beat to beat. Channel eight outputs the combined activity of the orange and the purple cell, each with its own shape. The sum of their output depends on which cell fires first. However, when beats propagate in a single direction, the measured signal shape (the sum of the orange and purple cell) is the same from beat to beat.

and makes the electrode surface more positive. As cellular depolarization continues, the cell reaches threshold and voltage gated sodium channels in the membrane open. This leads to a flow of positive ions from the cleft between the cell and electrode into the cell, leading to a negative deflection in the potential detected. The cell then repolarizes and the electrode surface is made more positive. At the end of the action potential, a broad (>10 ms) positive peak is seen from the extracellular electrode. There is a contribution to this peak that is biological and a contribution that is purely the effect of the measuring setup. The biological source of this deflection is the plateau phase of the myocyte action potential. This continued depolarization of the cell may couple to the electrode capacitively (as the initial

depolarization did) to make the electrode surface more positive. The purely systemic contribution to this peak originates from the baseline correction of the measuring electronics. To account for drift in the system, the measuring setup brings the baseline to 0 mV with a time constant on the order of 1 s for 56 channels [46] and 11 s for one column of 8 channels. This means for example that after a 5 ms, 0.5 mV negative measurement due to the sodium current, the zero point has been shifted 2 μV negative to the real zero point in the case of the 11 s time constant. Thus, when the electrode has returnted to the initial state (the real zero point), the electronics has reset this state to a positive value. The contribution of the baseline compensation in this case is small because the sodium based signal has a duration of only a few milliseconds and an amplitude rarely exceeding 1 mV. The effect is much more prominent when sustained potentials are generated, as in the case of continuous currents (see Section 5.3).

HEK Cells

Human Embryonic Kidney (HEK) cells are a well established expression system in mammalian cell culture. The cells are robust in culture and divide approximately once per day. The wild type cell line is HEK 293, and several variants have been permanently transfected to express ion channels relevant for electrophysiological studies. Among these are Ether-a-gogo, voltage gated sodium channels, and Channelrhodopsin 2. HEK cells are useful for electrophysiological studies because of their low intrinsic channel expression and morphology which allows them to be easily measured by patch clamp.

HEK Cell Test Systems

HEK cells were chosen as a model system for validating the new protein construct due to their high expression rate, low intrinsic channel activity, and the availability of an existing line carrying a Channelrhodopsin 2 variant. The wild type HEK 293 cells were maintained in Dulbecco's Minimal Essential Media (DMEM) + Glutamax supplemented with 10% FBS,and penicillin/streptomycin. Cells were removed from culture flasks by Trypsin EDTA digestion and plated onto poly-L-lysine (PLL) coated glass coverslips. HEK 293 cells were transiently transfected with the TO_Ch2opt_mKATE plasmid and maintained in culture media supplemented with all trans retinal. These cells were investigated by patch clamp experiments between DIV3 day post transfection (DPT) 2 and DIV6 DPT5.

The ChR2 HEK cell line [118] carries a Channelrhodopsin 2 construct with inducable expression by the addition of tetracycline to the media. ChR2 HEK cells were maintained in Ion Gate media, with zeocin and blastocidin selection for the expression system plasmids, see Figure 2.7 for an explanation of tetracycline controlled transgene expression. The cells were removed

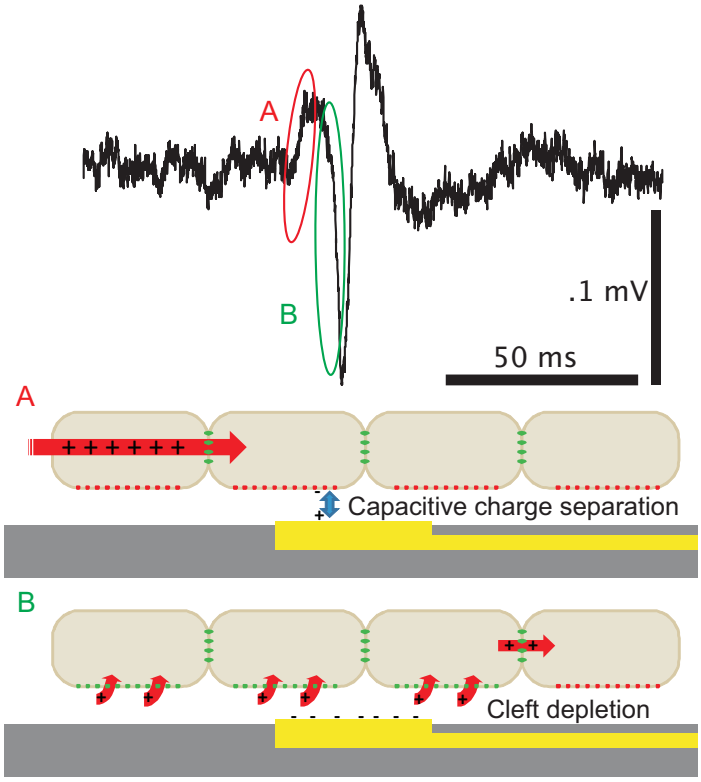

Figure 2.5: The difference in shape of an AP recorded extracellularly from HL-1 cells is shown. The HL-1 AP contains a first peak due to the capacitive coupling between the gap junction depolarization of the cell and the electrode. Once the voltage gated sodium channels in the membrane open, the positive current into the cell depletes the cleft and causes a negative potential at the electrode. The slow final peak is a combination of the slow calcium current and the baseline correction of the amplifier. Adapted from [78].

from culture flasks and plated onto coated glass substrates as described above for wild type HEK cells. On DIV1 the Ion Gate media was supplemented with tetracycline and all trans retinal. The cells began expressing Channelrhodopsin 2 within hours and were measured by patch clamp techniques on Day Post Activation (DPA) 1. For a further discussion on the viability of the ChR2 HEK cell line see Section 4.3.

2.4.2 Primary Cortical Neurons

Wild Type Neurons

Wild type primary cortical neurons were prepared as described in Appendix B.1. Briefly, corticies were removed from E18 Wistar rats in ice cold Hanks Balanced Salt Solution without calcium or magnesium (HBSS−). Cells were

dissociated in cold HBSS− with a fire polished, silanized, glass pipette. Two volumes of cold HBSS+ (with calcium and magnesium) were added and the suspension allowed to settle for 3 minutes on ice to allow aggregating glia to sink to the bottom. The top half, to two thirds, of the suspension was pelleted at 200 G and used for further experiments. Pellets of wild type neurons were resuspended in 1% neurobasal media (NB) and plated onto substrates. After 10 minutes at room temperature, the cells were moved to a humidified 37°C, 5% CO_2 incubator. This preparation results in low glia containing cultures that remain viable in culture up to at least DIV51.

If cells were plated at low density ($<$ 1300 cells per mm^2 over less than 50 mm^2), i.e. for chip cultures that also allow patching, a co-culture was included on a glass substrate placed higher in the culture volume than the experimental substrate as described by Hofmann [74]. Even though cells are only grown on the small active area of the chip ($\varnothing$7 mm or less) the cell culture volume cannot be scaled down with the culture area due to an increase in fluid surface area to volume ratio, which results in the culture evaporating and undergoing a large change in osmolarity at each media change. The co-culture maintains the total cell density at a healthy level ($\sim$ 200,000 cells per ml) without overgrowth of patterns or for small culture area per volume systems such as FETs and MEAs. Co-cultures could also be produced with higher glia populations by taking the lower fraction of dissociated cells after settling, see Figure 2.6. Co-cultures also provide a reference substrate when new materials are tested for neuron viability, i.e. new passivation stacks or encapsulation proceedures, see Table 3.2.

Genetically Modified Neurons

Primary neurons could be transfected prior to cell plating. For the details of alternative transfection methods see Section 2.4.3. Primary cortical neurons transfected by electrofection underwent the following additional steps before plating. The cell pellet was resuspended in 200 μL of Lonza's Nucleofection Kit transfection solution with 10 μg of plasmid DNA. Cells were electrofected using the Amaxa system (Amaxa). After transfection cells were resuspended in a plating volume of Roswell Park Memorial Institute (RPMI) recovery media supplemented with FBS and glutamine. The use of RPMI induces glial division due to the presence of FBS, but FBS containing media is necessary at this step for the cells to re-seal after electrofection. The RPMI suspension was then plated and treated as above. Irrespective of the initial plating media, cultures were changed to fresh 1% NB media after 4 hours of adhesion to remove dead cells from the preparation and/or transfection procedures. Since primary cells are always electrofected during the preparation, electrofected cells must have equal DIV and DPT numbers.

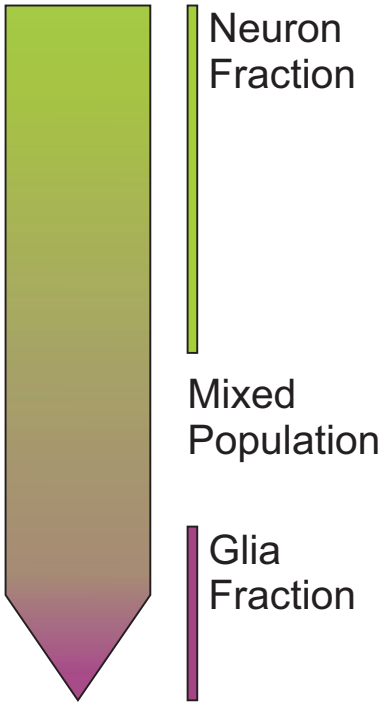

Figure 2.6: The differential settling of neurons and glia is depicted schematically. The top fraction can be used for a nearly glia-free culture, which is best suited for a neural network to be measured. In the middle region, a mixture of neurons and glia can be collected, which is well suited for co-cultures which can then condition the media with secretions from all naturally occuring cell types.

2.4.3 Transfection

Electrofection has been described in Section 2.4.2 as a method to introduce foreign DNA into cell suspensions. Though it was presented for primary cortical neurons, cell lines could also use this method to introduce plasmid DNA. In this case, the cells from adherant lines were digested off of the culture flask with Trypsin EDTA and pelleted by centrifugation. The pellet was re-suspended with approximately one million cells and 5 μg DNA per 100 μl transfection solution. The suspension was electrofected in the Amaxa system with a cell type appropriate transfection program as supplied by the manufacturer, i.e. HL-1 cardiomyocyte-like cells were transfected with the manufacturer loaded program "Cardiomyocytes".

An alternative to electrofection is chemical transfection. Cells adhered to a substrate may be chemically transfected at any time after plating. Invitrogen's Lipofectamine™, Roche's FuGENE® 6, and Roche's FuGENE® HD were tested on primary neurons. Invitrogen's protocol was longer and had poorer viability with equal transfection efficiency to both Roche products and therefore use was discontinued. Discussions here all utilitze a FuGENE® HD transfection, since this product was able to be standardized for both serum containing cell line cultures and B-27 supplemented primary culture media. Cells were plated and transfected between DIV1 and DIV3. In this case even toxic constructs not under the control of an inducable promoter may be expressed for a short time in adhered cells, because a mature

culture can be developed before the construct is added.

Cell lines were amenable to both transient and permanent transfection with the methods above. Electrofection was used to create working cultures of transfected cells, which were maintained by antibiotic selection. It was tested for the case of HL-1 cells if wild type and permanently transformed cells could be plated together on chip to observe any interactions, but in this case the difference in growth rates and selection requirements between the cells prevented consistent confluent mixed layers. Instead, if wild type and transfected cells are desired in a mixed population, chemical transfection is suggested.

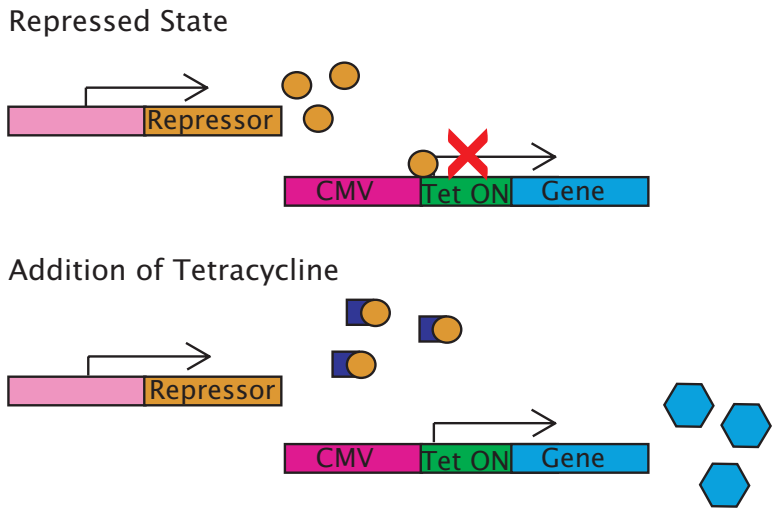

Figure 2.7: The gene of interest is cloned into a plasmid downstream of the tetracycline on (TetON) promoter. If this plasmid is transfected alone into cells the gene will be constitutively expressed. If a Tet Repressor plasmid is co-transfected into the cells, the Tet Repressor blocks transcription downstream of TetON until the addition of tetracycline prevents Repressor binding.

2.5 Cloning

Standard cloning methods were used to manipulate DNA constructs in the modification of Channelrhodopsin 2 for use in primary cortical neurons. This section describes the production of plasmid material and its manipulation as was undertaken in-house. All constructs were produced in TOP10 *E. coli* (Invitrogen) that had been transformed according to the manufacturer's protocol. Constructs were not seen to cause any reduction in viability of the *E. coli*. Transformed colonies were detected by Quick CloneCheck [22]. Briefly, individual colonies were picked and resuspended in 6 μl culture media. 3 μl of the suspension was lysed, direcly digested in the media-lysis

buffer mixture, and examined by gel electrophoresis for characteristic bands.

Plasmids were purified from bacteria using a scalable Midi to Maxi Prep protocol as can be found in [137]. Bacterial cultures were grown over night in Luria Broth containing a selective antibiotic. Bacteria were pelleted by centrifugation and resuspended in lysis buffers I-III (see Appendix B.11 for buffer composition). The nucleic acid containing suspension was filtered to remove lipids and proteins. Sequential precipitations were then carried out to remove the bacterial chromosome and bacterial RNA. Any remaining bacterial RNA was destroyed by digestion with RNAse A for one hour at 37°C. The sample was cleaned by phenol-chloroform-isoamyl alcohol extraction and purified plasmid was precipitated with LiCl. All plasmids were resuspended in MilliQ water and stored in aliquots of 0.7 to 1 μg/μl at -20°C.

The CUCY plasmid (see Section 4.1.3 was created by insertion of the human Ubiquitin C promoter (hUbiC) from the plasmid pUB (Addgene) into Ch2_K315_YFP (a gift from the Bamberg group). hUbiC was cut out of pUB using the restriction endonuclease SalI and purified by agarose gel electrophoresis in Tris Acetate EDTA buffer (TAE) followed by gel extraction by centrifuging through silanized glass wool. The acceptor plasmid was prepared by digestion of Ch2_K315_YFP with PspXI for one hour, followed by heat inactivation of the enzyme at 65°C for 30 minutes. hUbiC insertion fragments were combined with the linearized Ch2_K315_YFP plasmid in a 4:1 ratio and ligated with T4 DNA ligase.

2.6 Summary

This chapter has presented the standard methods which provided the starting point for the work discussed later. Specific modifications made to these techniques and their justification are discussed in the results sections that prompted the changes. Appendix B gives the final protocol after experiment sepcific optimization in an end user ready format.

Chapter 3

Diamond Based MEAs

3.1 Introduction

Diamond as an electronic material is making inroads into the field of biosensing due to its durability in biologic environments, high biocompatibility, and range of tunable electronic properties. Within the current body of work, the use of boron doped nanocrystaline diamond (BNCD) as an electrode material in MEA devices was evaluated. It was hypothesized that diamond's biocompatibility and low scar induction would make it a better material for extracellular sensing implants than existing metal or silicon technologies. The EU Project Diamond to REtina Artificial Micro-interface Structures (DREAMS) aimed to produce improved extracellular cell recording devices by using diamond as a new sensor material. The consortium consisted of research groups in Paris, France, London, United Kingdom, Munich and Jülich, Germany, and Prague, Czech Republic. In parallel parts of the DREAMS project it was shown that field effect transistors (FETs) made with surface conductive single crystal diamond were able to detect cell signals [42]. However, the use of diamond MEAs with single cell resolution had not been validated, and MEA devices would allow additional functionality for stimulation of cells by the device.

3.1.1 Diamond Introduction

Diamond can take several forms in electronic devices, three of which will be discussed in this chapter. BNCD is a conductive material suitable for making electrodes. In this work, BNCD with a boron concentration of 10^{21} B/cm^{-3} was used [102], and therefore had an expected conductivity of 30 Ω^{-1} m^{-1} [55]. In contrast, undoped nanocrystaline diamond (NCD) can be used as an insulator, with not-intentionally-doped diamond showing a conductivity of 1.5 x 10^{-8} Ω^{-1} m^{-1} [55]. Both of these materials are produced by CVD to form a sheet of material over large areas. Typical grain sizes in BNCD or NCD are on the order of 100 nm [107]. The third type of diamond relevant to

the current investigation is dispersed nanodiamond (ND). NDs are produced by exploding TNT and RDX within a confined space and re-dispersing the particulate matter that forms. NDs tend to form aggregates, and it was only recently shown that they can successfully be re-dispersed in solution [92]. Typical crystal sizes of dispersed NDs used here are on the order of 10 nm [47]. For a full discussion of current diamond electronic technology, the reader is referred to Section 1.4.2.

3.1.2 Diamond MEA Preparation

Diamond MEAs were developed in an iterative process utilizing close collaboration between the production and cell culture teams. All DREAMS chips use the 20 μm electrode size, 200 μm pitch, and star formation of feedlines, as shown in Figure 2.2. They vary in the passivation material used and material of the bond pads. Diamond lift-off processes were shown to be possible onto clear, flexible substrates. However, to test the functionality of new diamond electrodes, a rigid substrate was selected to eliminate effects of mechanical manipulation. Initial titanium silicide coatings on oxidized silicon wafers were supplied by M. Jansen, Jülich, Germany. Conductive diamond was applied by R. Kiran, Paris, France, and patterned by R. Edgington, London, United Kingdom. Chips were then passivated in Jülich, Germany, or London, United Kingdom, or Paris, France for SU8, ONO, and NCD, respectively. This work will begin with the chips' encapsulation in Jülich, Germany and include electrical characterization and use for cell culture experiments. As such, details of the exact growth and etch conditions are not provided here, and the interested reader is referred to the the relevant collaboration partners [48, 136, 156].

	Metal MEA	**DREAMS MEA**
Silver glue curing	1 hour 150°C	2 hours 80°C
Underfill curing	1 hour 150°C	2 hours 80°C
Ring attachment curing	1 hour 150°C	2 hours 80°C
Encapsulation material	PDMS or Epoxy	PDMS
Encapsulation curing	1 hour 150°C	2 hours 80°C

Table 3.1: Material, curing time and curing temperature comparison for metal MEAs, i.e. gold, versus DREAMS MEAs.

Several modifications were made to the encapsulation protocol to accomodate the use of diamond chips. Due to oxidation of diamond surfaces at high temperatures in atmospheric conditions, all diamond containing substrates were baked at 80°C for two hours instead of the standard 150°C for one hour during the encapsulation process. Additionally, they were sterilized by 70% ethanol instead of UV exposure. Furthermore, when single crystal

Base Material	Surface	Encapsulation	Neuronal Growth	HL-1 Growth
Glass	Glass	Epoxy	+	NA
Glass / Gold	ONO	Epoxy	+	- *
Glass / Gold	ONO	PDMS	+	+
Silicon / Gold	SU8	PDMS	+	+
Silicon	SU8	Epoxy	+	NA
SCD	SU8	Epoxy	-	NA
SCD	SU8	PDMS	+	+ *
BNCD	SU8	PDMS	+	+
BNCD	ONO	PDMS	+	+
BNCD	NCD	PDMS	+	+
Glass / Gold	ND	PDMS	NA	+

Table 3.2: The viability of neurons and HL-1 cells is shown for various combinations of chip material, passivation material, and encapsulation material. Particular care must be taken if ONO passivated chips are encapsulated with epoxy, as this limits the types of cells that can be used. Due to poor viability of SU8 passivated diamond encapsulated with epoxy, PDMS was made the standard encapsulation material for all DREAMS chips. Combinations marked with an $*$ were known in the lab prior to this work and not re-examined [75].

diamond was used as a chip substrate, epoxy encapsulated chips did not support neuronal growth, though PDMS encapsulated diamond substrates still supported growth. For this reason, all diamond chips were encapsulated with PDMS. For a summary of the encapsulation material combinations and their viability see Table 3.2.

Diamond MEAs were not activated before culture. After they were sterilized in 70% ethanol and aspirated dry, protein coatings for the diamond chips used a mixture which always contained gelatin to compensate for the lack of activation of the surface. The exact method of gelatin's action as a coating carrier remains unknown, but concentrations as low as 2×10^{-6}g/ml were effective in allowing coating of unactivated surfaces.

Due to the limited number of diamond MEAs produced in the DREAMs consortium, and the lower (SU8) or unknown (NCD) stability of the passivation layer a more gentle cleaning procedure was sought for these chips. A contactless cleaning protocol was adapted from that of J. Eschermann [51]. Immediately after the culture, cells were removed from the device by digestion with trypsin EDTA solution for >15 min at 37°C. The loosened cells were removed with a stream of water before the chip was sterilized with 70% ethanol. Chips were then cleaned for one hour in 2% Helmanex in a rocking bath, followed by four hours of rinsing in flowing deionized water. Under these cleaning conditions, the SU8 passivation lasted for four

to five cultures before peeling and pin holes prevented further use. Initial cultures with ONO and NCD passivated DREAMs MEAs also used the contactless cleaning protocol. Later, these two types of DREAMs chips were also cleaned using the standard procedure. In the case of ONO passivation, degradation from one culture to the next was not noticably more than with the contactless cleaning. However, for the NCD passivated chips, the surface roughness makes the mechanical cell removal in the standard cleaning procedure problematic. In some cases, the Q-tip becomes tangled on the surface and in more extreme cases the edges of the passivation are scratched or cracked by the scraping. It is therefore reccommended to continue with the contactless cleaning for all DREAMs chips to maintain consistency between samples.

3.1.3 Bandwidth Measurements

Band pass measurements of an artificially generated sine signal were also used to characterize the DREAMS measuring setup. A lock-in amplifier (Stanford Research, SR830) provided a variable frequency sine wave from 1-10,000 Hz with 4 mV amplitude. This was applied to all 64 channels of the chip simultaneously over the bath electrode. A single channel was then read out from the main amplifier of the BioMol MEA system and passed via a voltage divider back to the lock-in amplifier. The voltage divider is necessary because if the minimum applied pulse (4 mV) is amplified to the theoretical maximum of the BioMol device (1033x), the signal returned would overload the lock-in amplifier. The lock-in measurement then returned the phase shift of the BioMol signal and its amplitude relative to the input signal (software correction was used account for the voltage divider). A schematic of the bandwidth measurement setup can be seen in Figure 3.1. The length of cables, particularly on the signal input side were minimized as much as the space constraints of the Faraday cage allowed.

3.1.4 Analysis

Cell signals with varying signal-to-noise ratios (SNRs) are observed on the different working channels of any MEA measurement. The major contributing factor to the variability between channels is the cell-electrode coupling. This means the exact position of a cell over the electrode, in particular with consideration for the position of other neighboring cells, will make a strong contribution to the signal amplitude and, to a lesser extent, signal shape. Due to this dominance of the cell-device coupling in signal amplitude, evaluation of the SNR can be performed using the best performing channel of the array when comparing across devices. It is assumed that this channel represents the optimal cell-device coupling achieved for the culture, and therefore the SNR of the device itself.

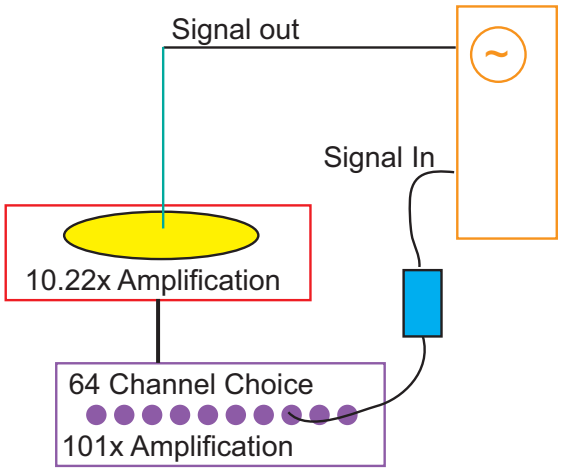

Figure 3.1: Schematic of the bandwidth measurement setup. The lock-in amplifier (orange) applies a variable frequency 4 mV signal to the encapsulated chip (yellow) via the silver/silver chloride bath electrode (green). The signal is amplified by the pre-amplifier stage (red) and then the main amplifier (purple), where a single channel is selected to be fed back to the lock-in amplifier. A voltage divider (blue) protects the lock-in amplifier from overload.

SNRs were evaluated using signal peak-to-peak height versus noise peak-to-peak height. This was chosen because the root mean squared (RMS) value of a cell signal does not embody any information applicable to biological measurements. Comparing the peak to peak value of the signal to the RMS value of the noise would artificially inflate the SNR. Of interest for biological investigations is the ability to decipher cell signals from the noise and evaluate their shape. Therefore, peak-to-peak signal versus peak-to-peak noise SNRs acurately reflect a device's ability to detect signals. The device's influence on signal shape can be characterized by bandwidth measurements.

Bandwidths of the devices were calculated in conjunction with the measurement setup as a whole. The bandwidth passed by the device was defined as:

$$A\left(_{\nu=\nu_{cutoff}}\right) = \left(\frac{1}{\sqrt{2}}\right) A_{max} \tag{3.1}$$

Where ν_{cutoff} is the cutoff frequency for the bandwidth passed and A_{max} is the maximum amplification achieved. That A_{max} is rarely at the theoretical maximum amplification is due to factors such as parasitic currents from any defects in the passivation and the connections feeding the signal back to the lock-in amplifier. A continuous phase shift is expected when the frequency is swept, therefore measurements with irratic changes in phase were disregarded for further analysis of the bandwidth. Furthermore, due

to the number of channels that could reasonably be sampled for bandwidth measurements, SNRs were calculated using the as-recorded signals, without back transformation to account for differential amplificaion at different frequencies. All of the figures in this work are presented using the data as recorded, without the back transformation according to the bandwidth dependent amplification.

3.2 DREAMS1

The consortium's first production run resulted in a single 64 channel diamond MEA suitable for encapsulation and cell experiments. A schematic of the material layout for the DREAMS1 design can be seen in Figure 3.2. The chip was encapsulated on a PCB carrier using 10:1 PDMS and silver glue to contact the BNCD bond pads of the chip to the carrier. HL-1 cells were cultured on the fibronectin/gelatin coated chip for three days, followed by recording with the BioMol MEA recording setup (see Section 2.1.2).

These proof-of-principle experiments showed that BNCD MEAs with electrodes sized for single cell resolution (20 μm $\varnothing$) are able to detect electrical activity from cells *in vitro*. Over two seperate cultures on the single chip, a total of 38 channels were able to detect cell signals. This number reflects a 59% success rate in the production of the chip. Potential sources of defective channels include; processing a single chip wafer fragment encountered difficulties in achieving a homogeneous SU8 coating, silver glue contacts to the bond pads may not make an ohmic connection or may make short cuts, or damage/degradation of the electrode during culture. Because only two HL-1 cultures were grown on a single chip, one cannot perform significant statistical analysis on the degradation of the chip from one culture to the next (see Section 3.3 and 3.4 regarding passivation stability), however, the best channel's peak-to-peak signal to peak-to-peak noise ratio (SNR) only changed from 5.3 to 4.9 between cultures. This suggests that the culture conditions themselves do not drastically degrade the performance of the electrodes, i.e. by fouling, over time.

3.2.1 Electrical Measurements of DREAMS1

The DREAMS1 chip yielded a band pass of approximately 55-2200 Hz ($\frac{1}{\sqrt{2}}$ of maximum signal passed). The lower bound of this band pass could be useful as it would reduce 50 Hz noise from nearby electronic devices. Furthermore, since the fast sodium current of cellular action potentials has a rise time of 1-2 ms, the setup should be suitable for measuring the biologically relevant range of signal frequencies. From the theoretical amplification for the BioMol MEA system of 1033x, we expect a perfect amplification to result in a signal of 4.132 V (with software correction to account for the

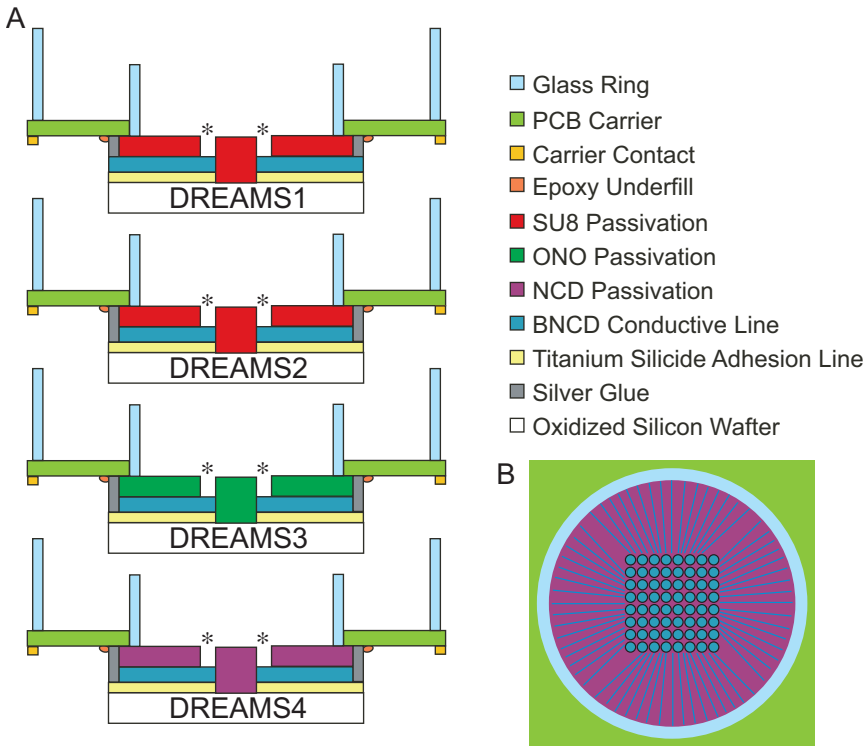

Figure 3.2: Schematic representations of the layered structure of the different DREAMs MEAs. A) The diagrams represent a lateral view of a device sliced through from top to bottom. The contact between the chip bond pad and the carrier is visible, as are the various passivation types used for each version. The open area marked by the $*$ represents the electrodes. B) The top view of a chip showing the materials exposed to the cells are the electrodes, the passivation,and the glass ring. The feedlines are made of BNCD but depicted in lighter blue because they are burried under the passivation. Drawings are not to scale.

voltage divider). The DREAMS1 device had a maximal signal amplification of 2.768 V (67% of the theoretical). Therefore, the frequencies with the maximum gain were only read out with a real amplification of 692x.

3.2.2 HL-1 Recordings with DREAMS1

Figure 3.3 shows one beat as it propagates across the upper right corner of the chip. Three of the nine channels plotted do not detect signals, but from the remaining six a wave propagation from the lower left to the upper right of the chip can be seen. The initial culture on the DREAMS1 device was measured as soon as it was electrically active. This led to a slow beat rate of 14 beats per minute (BPM) which allowed pacemaker switching to occurr. Eight switching events were observed in a two minute recording between a pacemaker to the left of the array to a pacemaker below the lower

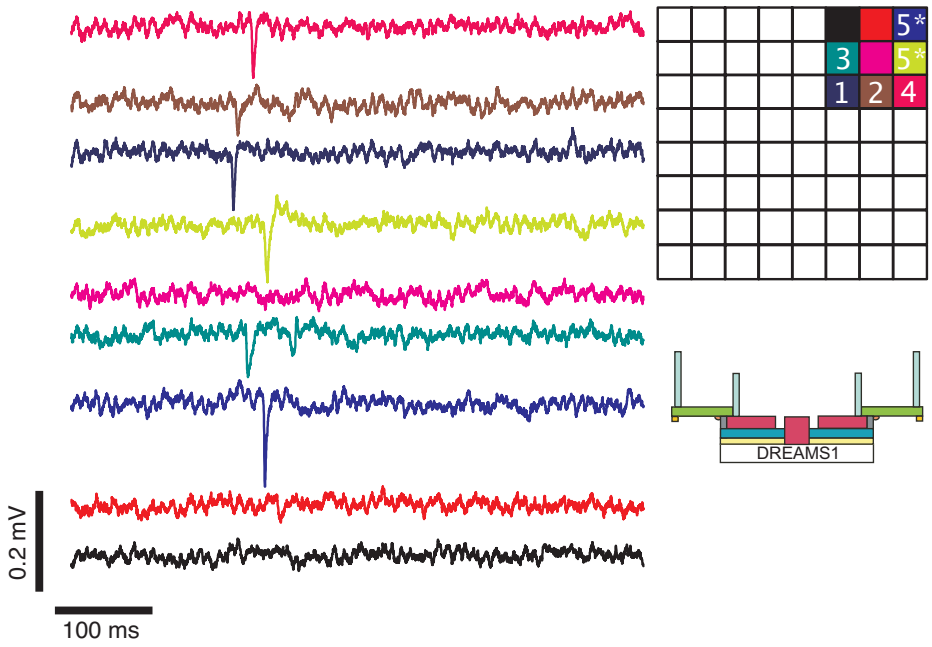

Figure 3.3: On the left, an excerpt from the DREAMS1 recording is expanded. For demonstration purposes, only nine of the 64 channels are plotted. Each channel's recording is plotted with a potential offset from one another to allow clearer visualization of the temporal separation between peaks. On the top right is a schematic of the chip array, showing the location of the recorded signals in space. White numbers indicate the order of arrival of the signal on different channels relative to each other. * indicates a tie between the channels for the fifth signal to arrive. A schematic shows the features of the DREAMS1 chip in the lower right (see also Figure 3.2).

right corner of the array. Furthermore, when subsequent beats from the same pacemaker were analyzed, slightly different beat rates were observed for the left propagating and right propagating waves (14.7 and 14.1 BPM, respectively). This provides further evidence that the DREAMS1 device was detecting true cell signals.

The DREAMS1 SNR was at the edge of statistical significance ($p = 0.05$) in differing from the SNR of planar gold electrodes of the same size (See Figure 3.14, 5.1 vs 10.9 $p = 0.05$, two-sample t-Test assuming unequal variances). The chip also had higher noise than expected. The noise ranged from 0.03 to 0.15 mV peak-to-peak. A large increase in the noise was observed when the chip was exposed to white light during the recording. This can be seen in Figure 3.4. For a full discussion of the effect of illumination on various types of chips, see Section 5.3.

Since only one DREAMS1 chip was successfully produced, the chip serves as proof-of-principle that electrical cell signals can be detected with BNCD

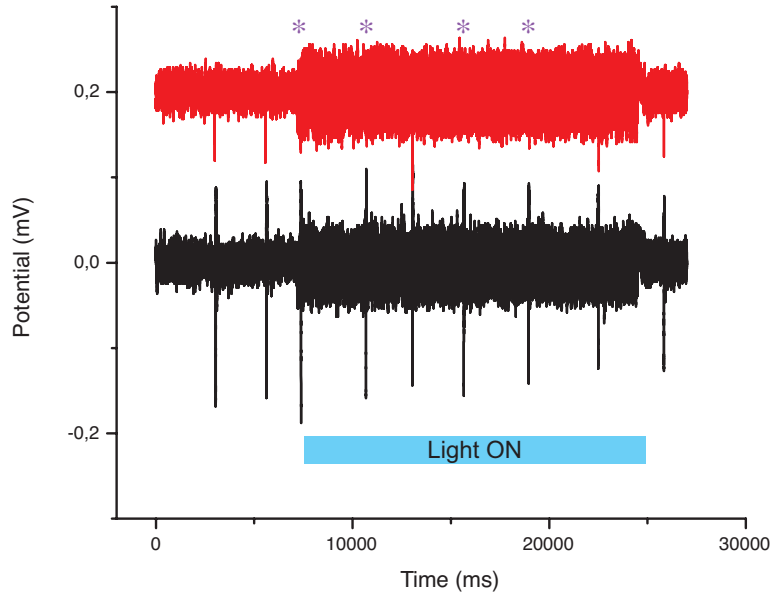

Figure 3.4: An increase in the noise is observed on all channels when widefield white light from a halogen lamp is applied to the surface of the DREAMS1 chip. Two exemplary channels are shown. In some cases, the decrease in SNR does not interfere with signal detection (black trace), while in other channels the increase in noise makes it impossible to detect some or all of the beats during the illuminated period (red trace, $*$ marks undetectable beats).

electrodes at a size that allows single cell resolution. Improvements in the design for the second processing batch of BNCD MEAs (DREAMS2) were intended to reduce the overall noise of the device and improve signal to noise ratio. With the improved processing we also expected a larger number of working electrodes on the DREAMS2 devices.

3.3 DREAMS2

The first issue to address in the second iteration of the DREAMS MEA was to improve the SNR to be clearly as good as state of the art metal MEAS. One possible cause for the poor performance of the DREAMS1 chip was the contact between the bond pads and the carrier. From standard MEA production in our group, it is known that the gold carrier - silver glue junction does not pose a problem for electrical readout. However, the BNCD - silver glue contact may degrade performance of the device. The solution to this problem was to etch the bond pads down to the titanium silicide adhesion layer so that the bond contact was gold - silver glue - titanium silicide, and then using the large area of titanium silicide under the whole feedline and electrode to contact the BNCD, see Figure 3.2.

The production run for DREAMS2 generated eight finished devices, five of which were able to detect cell signals from HL-1 cells. A contracting culture could be confirmed on one of the chips which detected no signal. The remaining two chips were cultured with cells at the same density, passage number, and culture conditions, suggesting that even in the absence of mechanical contraction the cells were expected to be electrically active. These samples therefore represent devices with no working channels. Furthermore, in the best cases approximately half of the channels on each chip were able to detect cell signals (mean = 19, maximum = 33, minimum = 3 channels). This continued production problem may be related to the stability of SU8 as a passivation layer. After two to three cultures and subsequent cleaning procedures, SU8 passivation can be seen peeling off of chips or cracking. This is true even for the gentle, "contactless cleaning"procedure (see Section 2.3.2).

3.3.1 Electrical Measurements of DREAMS2

Three of the DREAMS2 devices were tested in the bandwidth measurement setup. The maximal amplification achieved by these devices was 85 ± 12% of the theoretical amplification (mean ± standard deviation). One device showed particularly poor performance in signal amplification. In later experiments, this device continued to underperform the rest of the batch (see Section 3.3.2).

The DREAMS2 MEAs exhibited a band pass of 50 ± 40 to 800 ± 200 Hz (mean ± standard deviation, n = 8 channels over three chips). This bandwidth shift to lower frequencies compared to DREAMS1 could increase the amount of 50 Hz electrical noise detected by the chips.

The channels tested in the bandwidth measurements are a random sample of the 192 channels available on the three chips considered. Since typical cell signal shapes were observed during the HL-1 recordings, the bandwidth sampling was to rule out extreme distortions of the signal amplitude due to frequency characteristics and evaluate the percent of the theoretical maximum amplification achieved. In order to have a small enough standard deviation to back transform the recorded signal into a real voltage trace, one would need many more measurements per chip and to characterize each electrode of each device. This may be useful if neuronal signal shape is to be investigated using the DREAMS device, but was beyond the scope of these validation experiments.

3.3.2 HL-1 Recordings with DREAMS2

Though the yield of functional channels per chip was lower than DREAMS1, their performance was slightly better than the DREAMS1 chip. The SNR for DREAMS2 was 7.6 ± 3.6 (mean ± standard deviation, n = 5) as opposed

to DREAMS1's 5.1 (no statistics were carried out because only one chip and two cultures were available see Section 3.2.2). The high standard deviation of the DREAMS2 SNR stems largely from one device with a SNR of 2.0. This device was also only able to detect cell signals on three channels. This further suggests that production or stability issues remain the limiting factor for BNCD MEA performance.

A major improvement of the DREAMS2 device was that the sensitivity to white light was no longer detectable. The peak to peak noise did not change when white light was applied broadly to the chip surface via the microscope optics. Figure 3.5 shows the response of the DREAMS2 chip in the same experiment as Figure 3.4 for comparison.

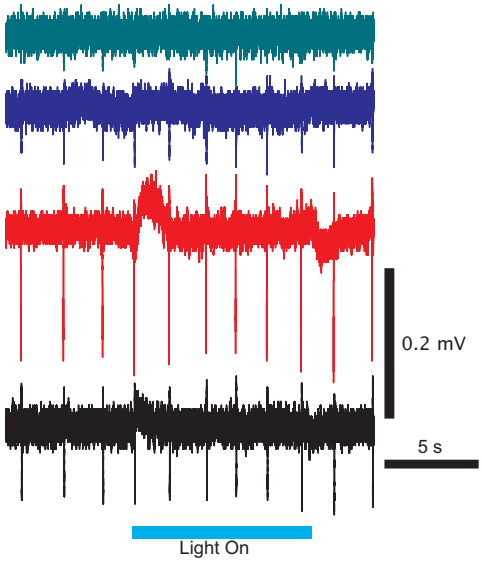

Figure 3.5: An increase in the noise is not observed when widefield white light from a halogen lamp is applied to the surface of the DREAMS2 chip. There is an offset of ∼100 μV seen, which the baseline correction of the amplifier compensates for. For comparison see Figure 3.4.

3.3.3 Neuron Recordings with DREAMS2

After testing with HL-1 was completed, DREAMS2 chips were cultured with dissociated cortical neuron cultures. E18 rat cortical neurons were grown on GpECM coated DREAMS2 MEAs (see Section 2.4.2 for culture condition details) to see if neuronal action potentials could be detected by the devices. Neuron cultures on DREAMS2 chips were viable (see Figure 3.6) at DIV7. This was the fourth culture for these devices.

On one device randomly timed spikes were detected that had a shape suitable to be an action potential. The spikes were all a similar shape to each other and could be averaged to a smooth spike in the channel recording (see Figure 3.6). Upon optical investigation, no neuron could be identified on the electrode from the channel in question. However, several neurons were spaced along the feedline of the channel. The signal was not present on any other channel and its reproducibility indicates it was not likely outside

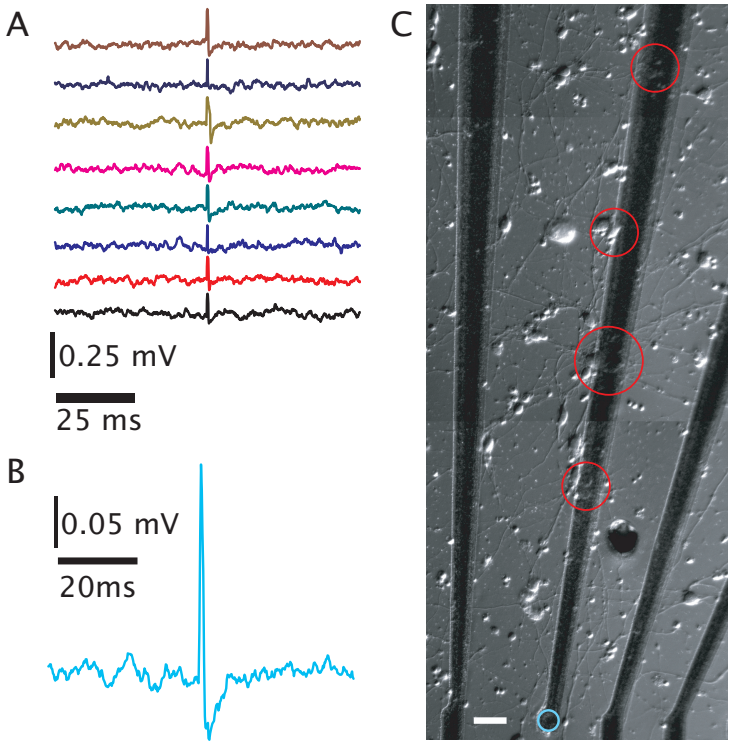

Figure 3.6: Possible spontaneous neuronal recordings on a diamond MEA are shown. The signals can be aligned (A) by the peak of the spike and (B) average to a reasonable shape for a cell signal that first capacitively couples to an electrode and then induces a current in the cleft. This would be expected of an AP traveling down an axon. (C) Optical investigation shows that no cell is on the electrode (blue cirlce) of the channel detecting the signal, suggesting the recording is made through a pinhole in the passivation. Cells are situated at several positions over the feedline (red circles). Scalebar of the photo is 50 μm.

interference from other equipment in the area or noise, respectively. This suggests that one or more of the neurons on the feedline was situated over a crack or hole in the passivation and the cell signal was detected through this defect. Because the exact cell being recorded could not be determined, correlative patch clamp data from the neuron could not be obtained to confirm without doubt that the signal was truly neuronal action potentials. The recording does suggest that neuronal recording with BNCD electrodes is possible with single cell resolution. However, these results emphasize the need for a stable passivation layer that can be used for multiple cultures.

3.3.4 DREAMS2 Summary

The DREAMS2 devices continued to be statisitically as good as planar gold electrodes of the same size ($p = 0.25$, two tailed, two-sample t-Test assum-

ing unequal variances). They also exhibited more consistent performance across various lighting conditions in widefield illumination. Amplification was also closer to the theoretical maximum output of the amplifier system. These factors all indicate the continued suitability of BNCD electrodes for biological recordings and the improvement conferred by contacting the chip via titanium silicide bond pads instead of BNCD bond pads. The dominant problem which remained was the ability to produce a stable chip with 64 working sensors.

3.4 DREAMS3

To address the stability of chips passivated with SU8, the third iteration of DREAMs MEAs were produced with a $SiO_2/Si_2N_3/SiO_2$ (ONO) multilayer structure (stack) with 500 nm thickness of each layer. ONO passivation stacks are routinely used by our group and others, and are known to be biocompitible as an *in vitro* culture substrate [96, 109, 74]. This passivation is far more durable than SU8, with metal electrode chips still able to measure after more than five standard cleaning procedures (see Section 2.3.2). ONO stacks were also the passivation used for the metal electrodes in control experiments in this work.

ONO passivation was produced at University College London (UCL), UK, immediately after the etching process to pattern the BNCD feedlines and electrodes. DREAMS3 chips were again etched through the BNCD to expose the titanium silicide bond pads to contact the carrier, see Figure 3.2. The passivated chips were received in Jülich and encapsulated as described in Section 2.2.2, as for the previous versions. This production process again resulted in eight finished devices, all of which were able to detect cell signals from HL-1 cultures. The 64 electrode arrays had a mean number of 42 channels that detected cell signals ($\pm$ 14, standard deviation), showing that the production process and/or stability of the chips was improving.

3.4.1 Electrical Measurements of DREAMS3

All eight DREAMS3 devices were measured in the lock-in setup to determine their bandwidth and amplification capabilities. The frequency range passed was 40 $\pm$ 40 to 2000 $\pm$ 300 Hz, with a maximum real amplificaiton of 74 $\pm$ 5% of the theoretical maximum. Therefore, ONO passivation did not significantly affect the bandwidth of the DREAMS3 device, and the electrodes remain capable of detecting the relevant frequencies for cell signals.

3.4.2 HL-1 Cell Recordings with DREAMS3

Though the ONO passivation was more durable and allowed multiple recordings from each chip with very little degradation or loss of channels, the

recordings from these chips showed that the passivation layer was not completely sealed. Pinholes in the passivation led to double spikes as the AP wave propagated not only over the electrode, but also over defects located over the feed lines (see Figure 3.7). Since a large number of channels were working on most chips, it was possible to determine which spike in these multiple peaks was recorded from the "real"electrode. One may first reason that if a channel detects signal, then the connection to the carrier and packaging is intact. If only one spike is detected, it is most likely to come from the "real"electrode. From these single spikes the position of the propagation wave at a particular time could be determined. For neighboring electrodes with two spikes, it is most likely that the spike closest in time to that recorded as a single spike on the neighboring channel is the AP passing over the "real"electrode. If there is still ambiguity, the propagation direction can be determined using spikes that are distinctly over the electrode using the first two methods. Based on the propagation direction and the star shaped layout of the feedlines (see Figures 2.2 and 3.2) the relative order of pinhole and electrode detected spike can be determined and from this the correct spike selected. For example, if the propagation direction is from left to right, electrodes with left projecting feedlines will have the pinhole spike preceeding the "real"electrode's spike and electrodes with right projecting feedlines will have the "real"electrode recording preceeding the pinhole spike. For all subsequent analyses with HL-1 cultures, only the spikes determined to be recorded from the "real"electrode were considered.

It must be noted that the amplitude of the signal is not a suitable factor to evaluate if a spike is from an electrode or a pinhole. It has been shown that at a given point in time, less than 20% of the cell membrane is in close contact with a the planar culture substrate [159]. For electrodes with a size on the order of the cell diameter, this means that the majority of the membrane is loosely attached and and does not have the minimal G_J (see Section 1.3.3 and Figure 1.8 for the point contact model). Because the pinhole diameter is presumed to be small, it can be completely sealed by closely attached membrane. This would lead to a very low G_J and high amplitude signals from the pinhole. The pinholes introduce additional complications when cells that do not form a confluent sheet are recorded. This is because confirmation of cell signals would then require coordinating secondary recording methods with the MEA signals, see Section 3.3.3.

When the performance of the electrode detected spikes are analysed for SNR, DREAMS3 chips had a SNR of 8.4 ± 2.1 (average $\pm$ standard deviation, $n = 8$), which is not significantly different from planar gold electrodes of the same size ($p = 0.31$, two tailed, two-sample t-Test assuming unequal variances). The noise level also remained unchanged whether the chips were in the dark or exposed to widefield white light. Thus the passivation layer was not a defining factor in the performance of the chips. The higher percentage of functional sensors and greater durability of the ONO stack would

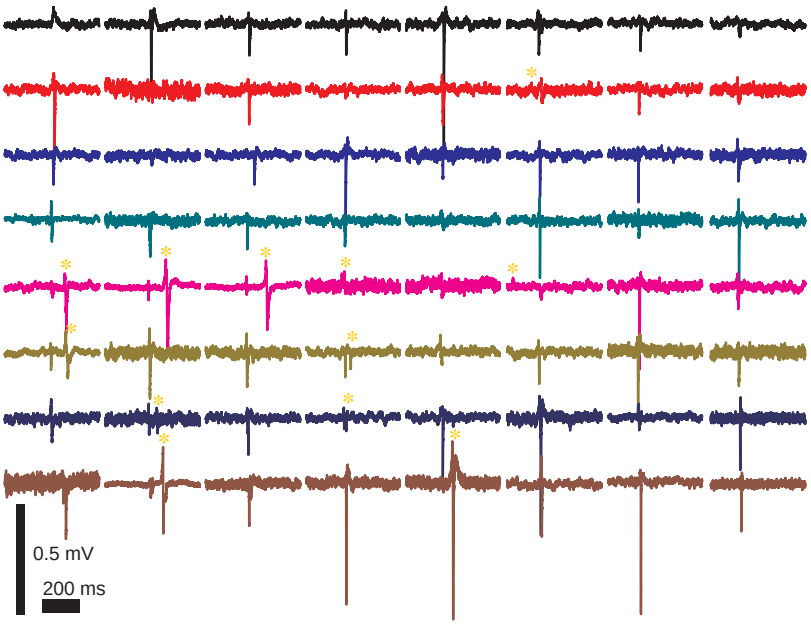

Figure 3.7: 500 ms of recording from a DREAMS3 chip with beating HL-1 culture is shown in the layout of the electrodes in the array. It can be seen that on some channels double spikes are detected. Using the propagation direction and the timing of spikes on channels with only one spike the false spike from the pinhole in the passivation can be identified (yellow $*$). In some cases the recording through the pinhole has a much larger amplitude than the signal from the electrode. Vertical scalebar is 0.5 mV, horizontal scale bar is 200 ms.

mean this layout would be superior to the SU8 passivation of DREAMS1 and DREAMS2 chips if deposition of the passivation layer could be achieved without pinholes.

Due to the inability to identify the cell being recorded from in neuronal cultures on ONO passivated chips containing pinholes, further investigation using neurons with these devices was not successful. The problem thus remained to find a suitably durable and well-sealed passivation layer for the BNCD MEAs' use with neurons.

3.5 DREAMS4

When the question of passivation materials is raised, one may also consider the original goals of developing a diamond MEA. One of the desired characteristics is the biocompatibility of diamond. In the DREAMS1-3 devices, the only diamond the cells were exposed to was from the surface of the electrodes. This amounts to .05% of the total culture area. Therefore, the ideal situation would be to introduce a diamond passivation layer in combination with the BNCD electrodes. Thus, for the DREAMS4 iteration of chips,

undoped NCD was used for passivation.

BNCD deposited by CEA on the titanium silicide prepared substrates was patterned at UCL, and then returned to CEA for fixation of seed NDs and growth of NCD over the entire surface. Passivated wafers were then returned to UCL for opening of the passivation layer at the electrodes and opening of the bond pads down to the titanium silicide. Chips were then received in Jülich and encapsulated as previous (see Section 2.2.2).

3.5.1 Electrical Measurements of DREAMS4

Bandwidth measurements of the as-received DREAMS4 chips showed unusual characteristics. None of the channels tested (n = 7, over 2 chips) showed a smooth phase shift transition over the frequency range. This alone would disqualify all measurements for bandwidth analysis given the current study's criteria. However, examination of the amplification at each frequency showed further inconsistencies, with individual frequencies showing higher amplification than the preceeding or following measurements without a smooth transition during the frequency sweep (see Figure 3.8). A larger number of amplitude spikes are observed in the low frequency domain than the high frequency regime, therefore even without the calculation of clear cutoff frequencies for the bandwidth, it can be inferred that the bandwidth for DREAMS4 has shifted to lower frequencies compared to DREAMS1-3. This is further supported by the cell signal shape recorded from DREAMS4 (see Section 3.5.2).

3.5.2 HL-1 Measurements with DREAMS4

Five of the 16 chip production run of DREAMS4 were tested with HL-1 cultures in the first instance. The performance of these chips was initially far worse than any of the previous designs. The SNR was 3.7 ± 2.1, which is significantly worse than the performance of planar gold electrodes ($p = 0.01$, one tailed, two-sample t-Test assuming unequal variances). The chips also had only 28 ± 7 working channels per chip (average $\pm$ standard deviation). Furthermore, an extreme light sensitivity was again seen in the DREAMS4 (see Figure 3.9).

The signals detected were also of an abnormal shape. The APs detected had a sodium current rise time of approximately 10 ms, or an order of magnitude slower than expected from the physiological process underlying it.

3.5.3 Post Processing of DREAMS4

This was a surprising loss of functionality until UCL reported that the opening process used may not have completely removed the seed NDs from the chips. Seed NDs were heat fixed to the patterned BNCD MEA to provide

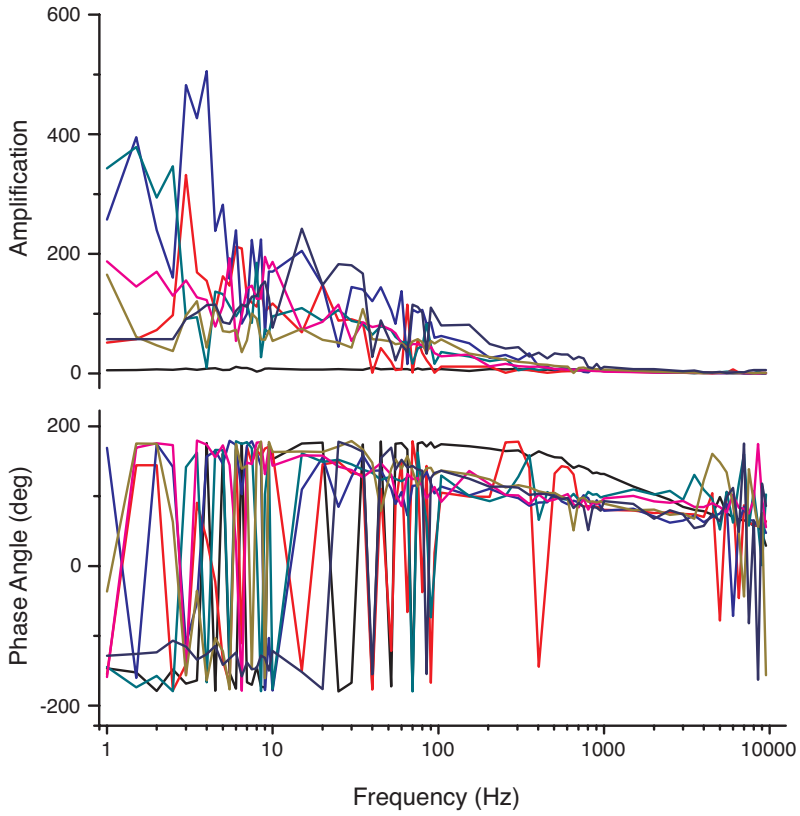

Figure 3.8: The phase shift and amplification during a frequency sweep of seven channels from DREAMS4 chips are shown. The amplification and phase both lack a smooth transition from point to point.

crystalization centers for the CVD growth of the NCD passivation. Etching parameters had been designed to remove these but the remaining ND presence was reported after chips were fully encapsulated, preventing a reprocessing. It was shown that a thin ND layer ($\sim$ 10 nm) does not prevent cell signal detection (see Section 3.6). However, AFM measurements at UCL suggested up to 70 nm of NDs may still be present on the surface of the electrodes. Three alternative processes for removing the NDs from the encapsulated chips were suggested; mechanical abrasion, an acetone wash, or an oxygen plasma treatment.

Acetone alone was used as a cleaning procedure for two chips that had not yet been subjected to cell culture. These continued to have poor performance, with SNRs of 1.5 and 5. As an alternative, mechanical abrasion with a cotton bud soaked in acetone was used. Mechanical cleaning may have contributed to cleaner electrodes, but upon visual inspection scratches or chipping of the passivation surface could be seen in mechanically cleaned chips. It is therefore expected that areas mechanically cleaned are also most

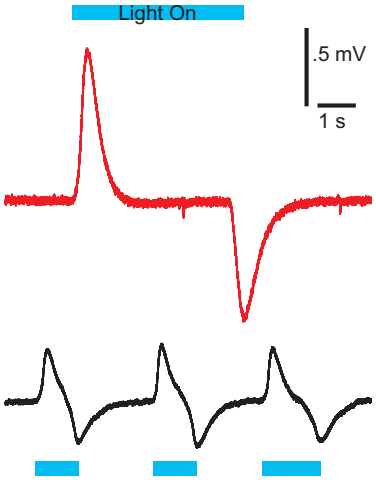

Figure 3.9: The effect of white light on DREAMS4 chips. In red, a DREAMS4 chip as received. In black, DREAMS4 chip after cleaning (see Section 3.5.3). The long illumination was from a 100 W halogen bulb with a beam path 90° to the chip, the short illuminations were from a 60 W incandescent bulb with an incidence angle of approximately 40°.

likely areas where no signal can be detected due to large scale damage.

Five chips were cleaned with either oxygen plasma alone or oxygen plasma plus the acetone wash. These five included two chips which had been used for HL-1 culture prior to any cleaning process. In one of the repeated use chips the SNR decreased from 7.0 to 4.7 while the other chip improved its SNR from 2.8 to 40. Overall, the average performance of the cleaned DREAMS4 chips was an improvement over previous chips (22.6 ± 16.1, $n = 5$, mean $\pm$ standard deviation). This average is more than double the performance of planar gold electrodes. However, the variability of the cleaned chips was too large to make any significant comparisons ($p = 0.08$, one sided, two-sample t-Test assuming unequal variances for planar gold versus cleaned DREAMS4 SNR performance). The distribution of SNR from cleaned and uncleaned DREAMS4 chips can be seen in Figure 3.10. If the DREAMS4 chips are divided into "Cleaned" and "Uncleaned" groups, the standard deviation of the Cleaned group is still more than half the average (22.6 ± 16.1, $n = 5$).

If the seed NDs that remained on the surface of the MEAs were unevenly distributed, then processes designed to remove diamond layers could eat into the underlying chip structure in places where the seed NDs were thin or leave residual non-conductive material on electrodes where seed NDs were thick. This would explain the extreme variability in performance of the DREAMS4 chips. Since SNRs of 36 and 40 were observed, it is worth pursuing improvemnts in the fabrication process to assure that seed NDs are uniformly applied and then removed from the sensor area. If this can be achieved, devices with superior SNR to metal MEAs should be achievable.

The reason for the improved performance of the DREAMS4 chips may have severals sources. First, the plasma cleaning may leave a favorable surface topology for signal detection (low impedance in a small lateral area of the substrate). Second, unintentional thinning of the passivation layer dur-

ing the plasma cleaning may result in a smaller cleft height, and corresponding closer interfacing of the cell with the electrode. For further discussion see Section 6.4.

3.6 NanoDiamond Surfaces

In addition to their use as seed crystals for growing naonocrystaline diamond, with or without dopant, nanodiamonds can be used themselves as a diamond coating. ND suspensions applied by a wet ultrasonification process to a surface increase roughness and generate a carbon surface to present to the cells. Since neurons tend to prefer rough surfaces [67, 43] and in partiuclar surfaces that cells can wrap processes around [143] the application of a thin ND coating may improve the adhesion of cells to a device surface. However in the face of the difficulties with DREAMS4 devices, the question remained if an ND coating would decrease the signal detected by conventional devices beyond usefulness.

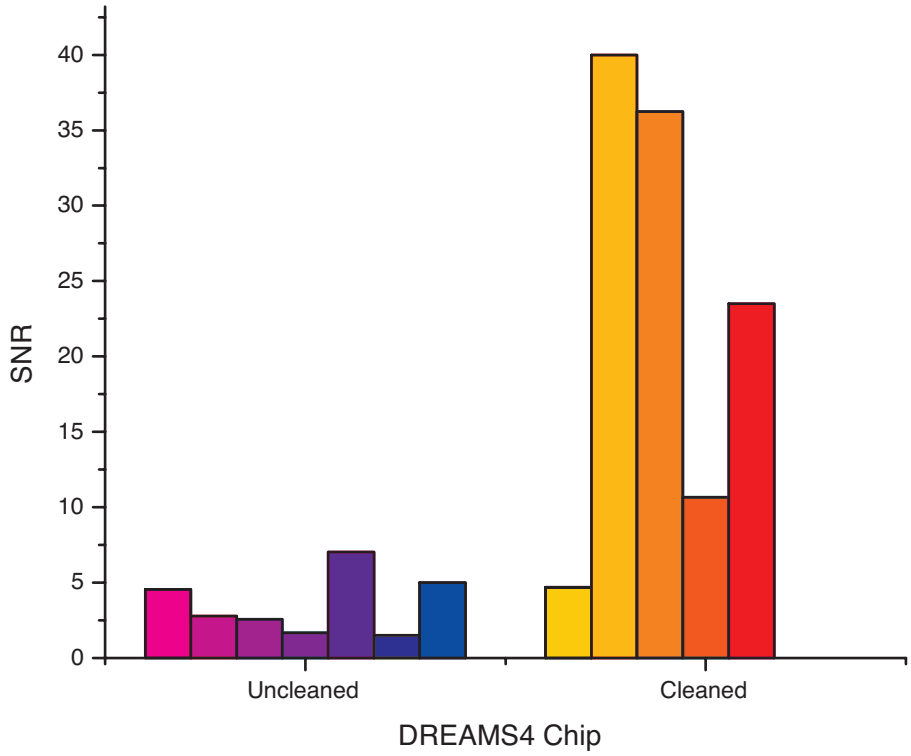

Figure 3.10: The SNR of each chip tested from the DREAMS4 production cycle divided into chips that were cleaned with a procedure that included an oxygen plasma treatment and those that were not. The results after cleaning are highly variable, but in general better than chips without cleaning.

To investigate the possibility of ND coatings, traditional planar metal MEAs were sent to UCL for coating with an unfixed ND suspension. Briefly, encapsulated metal MEAs were masked on the back of the carrier to protect the socket contacts and then treated with an ND solution in ultrasound. The solution depositied NDs are expected to cover the entire surface of the device and increase roughness, with the potential for features with an overhang (see Figure 3.11. UCL returned the chips with a reported ND thickness of 10 nm [47]. These chips were electrically characterized and then subjected to HL-1 cultures.

3.6.1 NanoDiamond Coating Electrical Effects

Bandpass measurements of ND coated MEAs showed fluctuations in performance in both the positive and negative direction. The performance of an electrode on each chip before and after ND coating can be seen in Figure 3.12. It should be noted that the metal chips sent for coating had already been used several times for cell culture and are not expected to be the best example of metal MEA performance. All comparisons are therefore made to the before and after case. The average percent change in real amplification from before ND coating to after ND coating was $-0.2\% \pm 18.3\%$ (mean $\pm$ standard deviation, $n = 8$) with positive values for an increase in maximum amplification and negative values for a decrease in maximum amplification. Therefore, we can state that the NDs themselves are not systematically reducing the signal detection of the metal electrodes. These results suggested that the chips could still be suitable for cell measurements through the 10 nm ND layer on the electrodes. Further testing in cell culture would determine if changes in the cell adhesion or cell coupling to the surface affected signal detection.

3.6.2 NanoDiamond Coatings in Cell Culutre

HL-1 were cultured on ND chips coated with fibronectin/gelatin, as is standard for this cell type, as well as on ND chips without any protein coating. Cells cultured on ND coated chips with and without protein reached maturity at a normal rate and were visibly contracting on DIV4. Surprisingly, even on chips without protein coating, cells remained healthy and continued to contract until DIV8, at which point the culture was terminated. Typical

Figure 3.11: A smooth surface (A) is contrasted with a rough surface without overhangs as is produced by CVD growth (B) and a rough surface that includes overhangs as is produced by wet deposition of crystals (C).

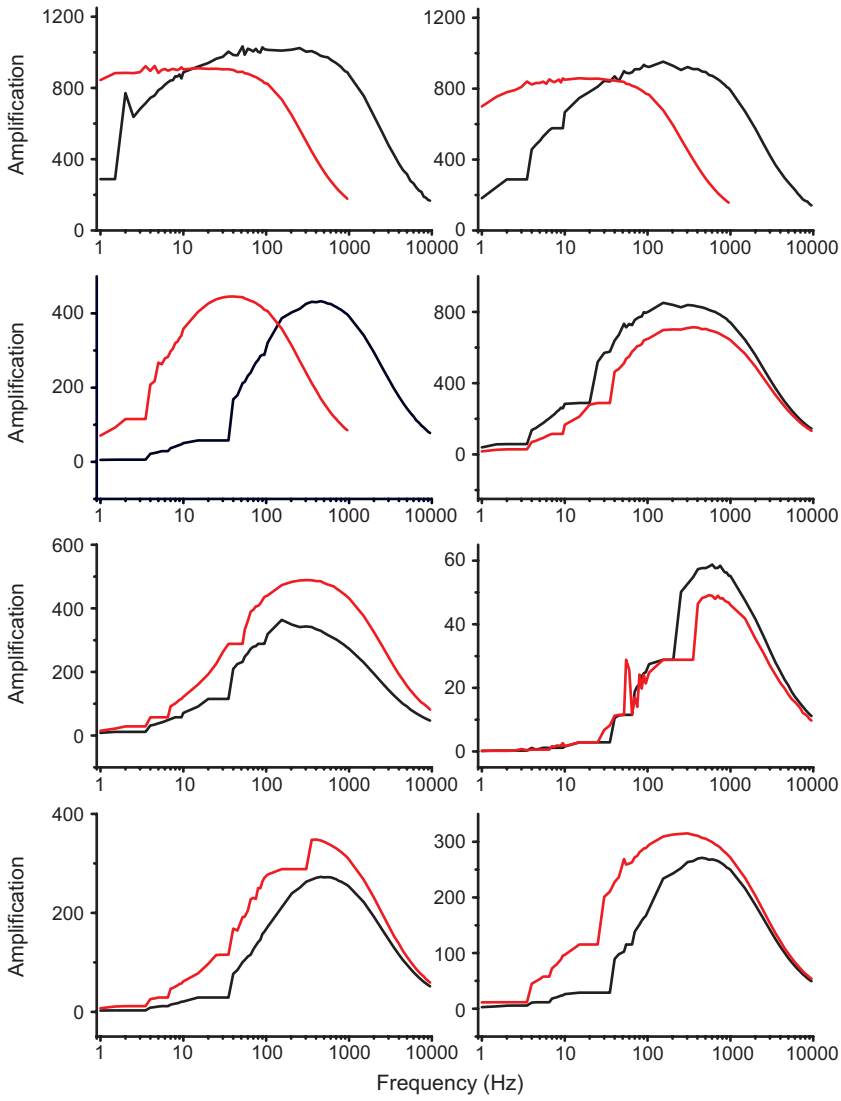

Figure 3.12: Bandwidth measurements from metal MEAs before and after ND coating are shown. In red is the measurement before coating and in black the recording after coating. There is no consistent trend among devices for improvement or worsening.

HL-1 cultures on fibronectin/gelatin coated ONO surfaces beat for only 1-2 days after reaching maturity. Electrical recordings of this activity on ND coated chips were possible as seen in Figure 3.13. This shows that ND layers of 10 nm are not effective insulators on the electrodes to block cell signals. The discrepancy between these results and the seed ND effects described in Section 3.5.2 appears to be in the thickness of the ND layer, or changes the ND seeds undergo in the subsequent CVD process.

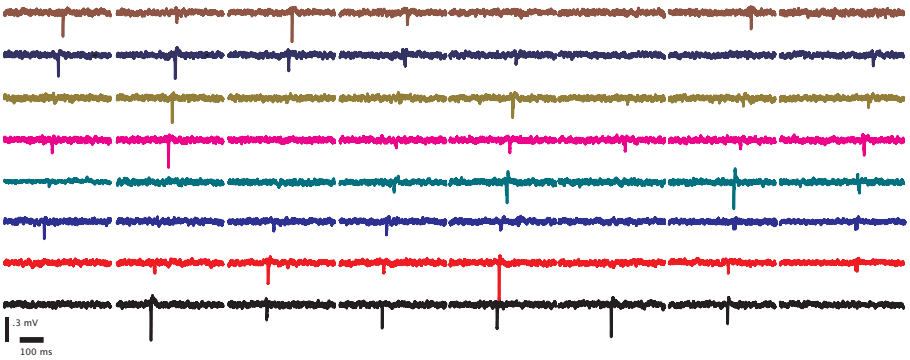

Figure 3.13: Cell recordings from a metal MEA coated with NDs, and without protein coating. Cells are recorded at DIV8 after 4 days of beating on chip. Vertical scalebar is 0.3 mV, horizontal scalebar is 100 ms.

Several attempts were made to confirm the location of the NDs after HL-1 culture on ND coated metal MEAs. If the NDs were no longer adhered to the surface, this would explain why no electrical interference was seen. The first piece of evidence that the NDs were still on the surface when the cells were recorded is that the substrate resisted the cells' mechanical force of contraction. One may expect that if the NDs were loosely adhered to the surface or removed by the cells, then the force of contraction would tear the cells off of the substrate.

Two addional attempts were made to positively confirm the location of the NDs. When the culture was terminated, cells were removed from the surface by trypsin EDTA digestion (see Section 3.1.2). In this process, all solutions and the removed cells were collected from the chips. The suspension was then centrifuged to pellet the cells so that the cells and all fluid contibutions could be separated. The chip surface, the liquid fraction removed from the chips, and the cell pellet were then examined under UV, in search of the NDs' natural red fluorescence. However, in the available illumination systems ND fluorescence could not be detected in any of the three fractions. Others have also encountered difficulties in detecting ND fluorescence in the complex environment of cell culture [47].

Therefore, a second attempt was to use AFM to analyze the roughness of the surface. This involves de-encapsulation of the chip to provide access for the AFM probe. It was intended that the area previously under the carrier could serve as a ND-free control surface compared to the array surface. Though some differences were seen between the array area and the formerly shielded area, the roughness is not the same as the reported roughness for NDs [47]. The use of roughness to confirm NDs on the surface after culture is further complicated by the need to use gentile cleaning proceedures to ensure that if the NDs are on the surface after the culture, they are not detached during cell removal. This may lead to debris or protein on the

surface which alter the roughness detected. The difficulty in getting a clear AFM image from this chip suggests some soft or sticky organic material may have remained on the surface.

The use of ND coatings to generate a rough and biocompatible surface therefore remains a viable possibility for bioelectronic sensing devices. Electrical characterization should be carried out again in the before and after situation with unused, clean chips to have accurate data on the effects of ND coatings on electrical performance. Furthermore, for biological applications, particularly *in vivo* uses, the location of the NDs must be positively confirmed. The best method for this would be the use of improved optical systems, such as confocal microscopy, to detect the intrinsic fluorescence of the NDs.

3.7 Summary

This body of work showed that diamond based MEAs are suitable for recording electrical signals from cells at a size that allows single cell resolution. The SNR performance of the different versions of diamond chips are compared with planar gold and platinized planar gold in Figure 3.14 and Table 3.3. Results from DREAMS2 and DREAMS3 chips show that diamond MEAS are not significantly different from planar gold. Since the variability in the DREAMS4 measurements can be attributed to the production process, the high average SNR suggests that if prodction can be made more consistent, the good interaction between cells and an all diamond surface can lead to a superior recording MEA. If the production inconsistencies of the DREAMS4 format cannot be improved, then ND coatings of established metal devices may provide and alternative route to achieving the benefits of carbon at the cell-device interface. Further characterization should focus on where the NDs are after the culture period, as this method would also be suitable for more complicated structures fabricated from established materials, such as coatings for 3D metal electrodes. Of further interest is the geometric layout of the NDs on the surface and if they provide a matrix which the cells can enter into. This would provide further insight to the question of how cells respond to roughness, or in this particular case the difference between roughness of an impenetrable surface and a navigable matrix. This distinction would be of interest for use of diamond surfaces with cells who have more complex protrusions, such as neurons.

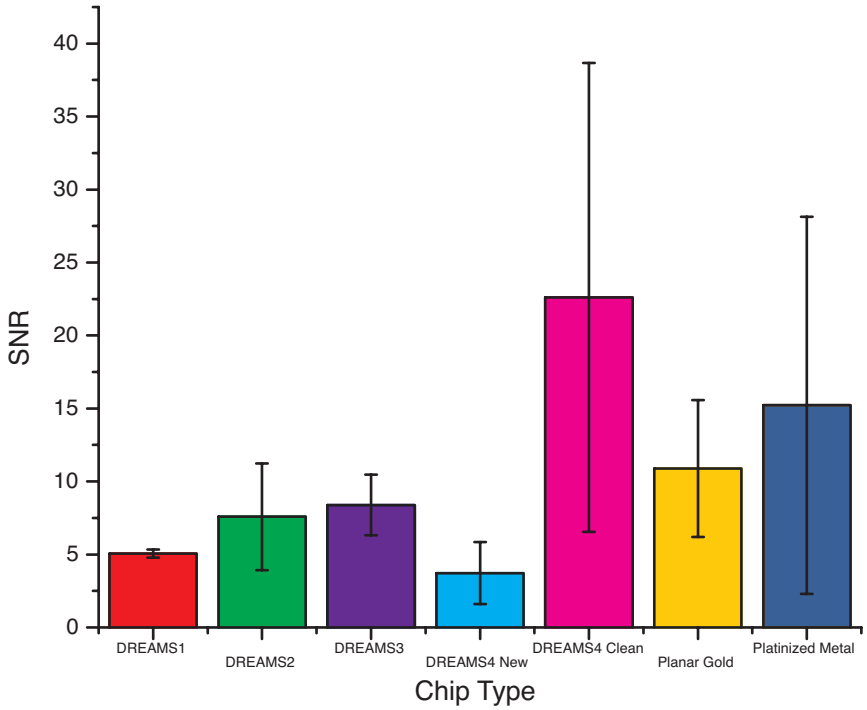

Figure 3.14: Overview of DREAMS performance in SNR, mean with standard deviation bars. Planar gold electrodes of the same size and platinized gold electrodes of approximately 20 μm $\varnothing$are given as reference to the current state of the art for planar MEAs.

Device	**SNR**	**Bandwidth (Hz)**	**Signal Loss**
DREAMS1	5.1	55 – 2000	33%
DREAMS2	7.6	50 – 800	15%
DREAMS3	8.4	40 – 2000	26%
DREAMS4 uncleaned	3.7	NA	NA
DREAMS4 cleaned	22.6	NA	NA
Gold	10.9	30 – 2000†	30%†

Table 3.3: Summary of the performance of the different iterations of diamond chips in terms of SNR and bandwidth performance. † best performance data from D. Brüggemann using planar gold MEAs of 20 μm $\varnothing$.

Chapter 4

Evaluation of Channelrhodopsin 2 Constructs

Optogenetic stimulation of electrogenic cells compliments the extracellular recording of cell networks using microelectrode arrays (MEAs) described in Chapter 3. A brief re-introduction to the optogenetic tool Channelrhodopsin will be followed by how this protein has been used and modified in the scope of the current work. The constructs are then evaluated for electrophysiological properties and viability. In the following discussions DIV#, DPT#, and DPA# are provided for Day In Vitro, Day Post Transfection, and Day Post Activation, respectively. For methodological reasons, DPAs are only given for stably transfected cell lines, and cells transiently transfected by electrofection must have equal DIV and DPT.

Several challenges are faced to integrate optogenetically sensitive neurons on MEA recording devices. First, is the low metabolism of neurons compared to other common expression systems such as HEK cells. This makes it difficult to achieve sufficiently high channel densities in the membrane to reliably trigger action potentials. The solution may be found in improving the protein's expression by modification of the expression vector. Alternatively, the protein itself can be engineered to have a higher efficiency of trafficking and incorporation into the membrane, or a higher efficiency of passing charges in response to light.

Second, is the sensitive state of neurons cultured on chip. The number of cells per unit culture volume has a strong effect on the health of the culture, and since all transfection methods risk killing some cells (with exact viability depending on both transfection parameters and cell type), the final cell concentration can be difficult to determine. Use of a second floor co-culture as described by Hofmann [74] partially alleviates this problem by allowing a wild type culture to accompany the experimental network without

connecting to it. In this position, the wild type cells are able to condition the media. However, the issue remains for determining a network density suitable for ensuring an optimal number of sensors are in contact with cells, which varies depending on the type of adhesive coating used (patterned or unpatterned for example).

Third, is the question of the cell's viability. The design of a system for long term stimulation and recording of a cell network with single cell precision is of little use if the construct is toxic to the cells on the timescale of weeks. Also, if optical intensities required to induce sufficient current for depolarization are so high that the membrane is damaged, the changes in potential seen cannot be clearly attributed to cell signaling events. Achievable current at a given light level must largely be addressed by the specific optogenetic construct used.

The variety of channelrhodopsin constructs discussed in the literature have been optimized for different applications. For use with MEA chips for single cell stimulation important qualities include driving sufficient protein expression and trafficking it to the membrane, a non-toxic expression construct and product, and the generation of high currents at safe illumination levels.

4.1 Molecular Constructs of Channelrhodopsin 2

As in most cases of gene technology, various versions of the protein and its expression vectors have been developed. These modifications improve the plasmid DNA or the expressed protein for use in different experimental systems. In this section several expression constructs and different molecular versions of Channelrhodopsin 2 are presented in terms of their molecular composition. This chapter will continue with an evaluation of their performance in terms of both electrophysiology and viability.

4.1.1 Molecular Overview

Two factors play a role in the expression of foreign genes in host cells. The first is the DNA coding of the plasmid. The base sequence used to code for each amino acid may be optimized for various species to promote more efficient expression. Furthermore, the promoter coded in the plasmid will determine which cells express the protein. In addition to restricting expression to specific types of cells, this region of the plasmid may be used to control the timing or level of expression. The second factor is the amino acid coding of the protein itself. This sequence will determine the molecular properties of the protein and may be varied by mutation or by exchanging large pieces of protein, i.e. by swapping functional domains such as fluorophores.

All of the molecules investigated here are based on the algal rhodopsin Channelrhodopsin 2. The rhodopsins are a broad class of light sensitive

proteins or protein complexes that undergo conformational changes due to exposure to light. The chromophore bound by these proteins changes isomeric form upon absorbtion of a photon, and this in turn results in a comformational change in the protein, allowing it to pass charges across the membrane. Though rhodopsins are prevelant in mammalian light sensitive systems, they are not optimal for genetically engineering optical sensitivity into other mammalian cell types. That is due to the mammalian rhodopsins' dependence on G-coupled protein responses that lead to cell depolarization or hyperpolarization [80]. The coupling to G-protein signaling cascades leads to a drastic amplification of the electrophysiological signal produced per photon, but means that the response is governed by the many proteins in the downstream cascade. This cascade can be either depolarizing or hyperpolarizing depending on the host cell [121]. If one were to engineer these systems into a new cell, many proteins could be necessary, and the role of the G-coupled proteins in the cell's normal operation would be perterbed.

In contrast, simple single cell organisms were found to use directly light-gated ion pumps [124, 24] or channels [121]. A more extensive discussion of light sensitive proteins can be found in Section 1.3.2. Briefly, these proteins have the ability to alter membrane currents without any additional proteins or pathways. Channelrhodopsin 2 of *C. reinhardtii* is one such algal rhodopsin forming a passive, directly light-gated channel. Upon absorbtion of blue light, trans-retinal is changed to cis-retinal, initiating conformational changes that allow positive ions to pass through the channel [121] (see, Figure 4.1).

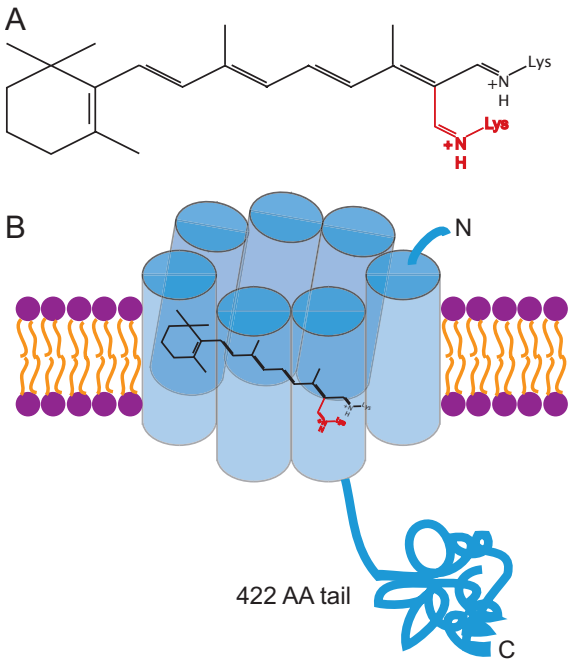

Figure 4.1: The seven transmembrane domains forming a channel in Channelrhodopsin 2 are depicted with a bound molecule of retinal. The retinal binding site is based on structural studies of bacteriorhodopsin, a protein with similar light sensitive domains [65]. The light induced rotation from all-trans to 13-cis is shown in red on the molecular illustration of retinal. The cytoplasmic C-terminal of the native protein may be replaced by a fluorescent marker such as YFP without hindering channel function [121]. All protein schematics are based on [8, 93, 157, 125].

The light sensitive and current passing domain of the native 737 amino acid protein of Channelrhodopsin 2 was found to be the first 315 amino acids [121]. These comprise seven transmembrane domains. To create an easily detectable fusion protein, most published constructs of Channelrhodopsin 2 replace the cytoplasmic, C-terminal tail of the native protein with a fluorophore (see Figure 4.1 vs Figure 4.2). It was first shown that the protein could be cloned into cells to induce a change in membrane potential with light using Xenopus oocytes and HEK 293 cells by Nagel et al. [121]. The use of Channelrhodopsin 2 soon expanded into neurons *in vitro* [98] and later *in vivo* [163]. Current use has further progressed into cardiac tissues [78, 19]. The first published construct transfected into cells to depolarize them with light was a truncated Channelrhodopsin 2 called Ch2_K315_YFP [121].

4.1.2 Ch2_K315_YFP Construct

The first construct tested for use of Channelrhodopsin 2 in primary rat cortical neurons on chip was supplied by the Bamberg group, MPI Frankfurt. The plasmid, Ch2_K315_YFP (See Figure 4.2), codes for the first 315 amino acids of Channelrhodopsin 2 using the original algal DNA sequence. This form removes the native intracellular C-terminal tail and replaces it with a YFP tag. This modification allows the expression of Channelrhodopsin 2 to be easily identified by fluorescence. The construct utilitzes the pcDNA3 plasmid and results in a final size of 7094 base pairs. The plasmid has a high copy number in standard *E. coli* strains and could readily be produced and purified by standard culture methods. The plasmid controls expression by the Cytomegalo virus (CMV) promoter, a sequence widely recognized in mammalian cell types and therefore expected to confer expression in most experimental systems. This construct was previously published by Nagel et al. [121].

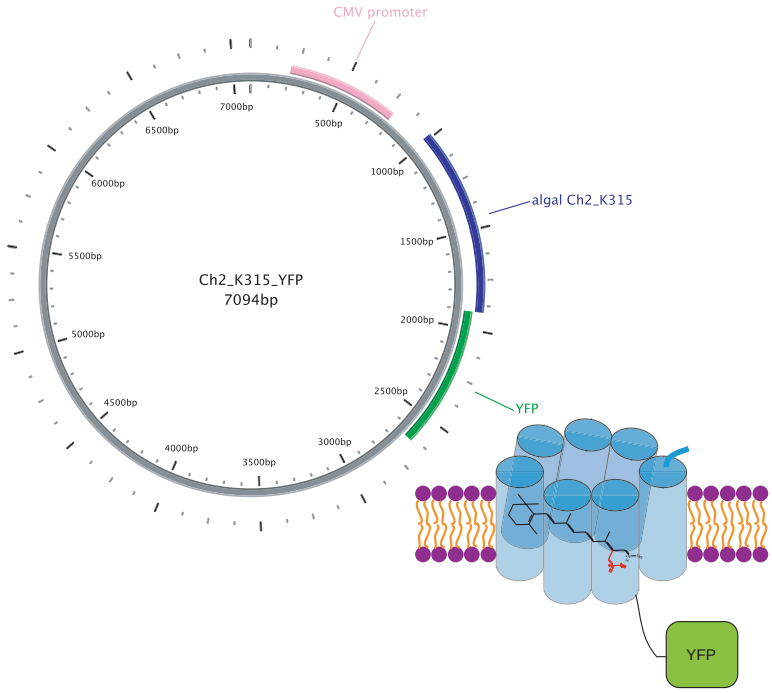

Figure 4.2: Map of the Ch2_K315_YFP plasmid showing the CMV promoter (pink), Channelrhodopsin 2 (blue), and the YFP tag (green). Note that the Channelrhodopsin and YPF are intended to be a fusion protein. A schematic of the CH2_K315_YFP protein is shown inserted in a membrane. The cytoplasmic tail of the native Channelrhodopsin 2 (see Figure 4.1) has been replaced by YFP.

4.1.3 CUCY Construct

Since the construct described above was shown to be electrophysiologically active in HL-1 cells [74], one approach undertaken to improve the performance in primary neurons was to focus on increasing the expression levels in this cell type. Based on the published evaluation of promotor performance in cortical neurons [15], the human ubiquitin C (hUbiC) promoter was selected as a better candidate promoter than CMV. The hUbiC promoter was cloned out of the commercially available plasmid pUB [1] and into the Ch2_K315_YFP construct. Due to the proximity of the cut sites,

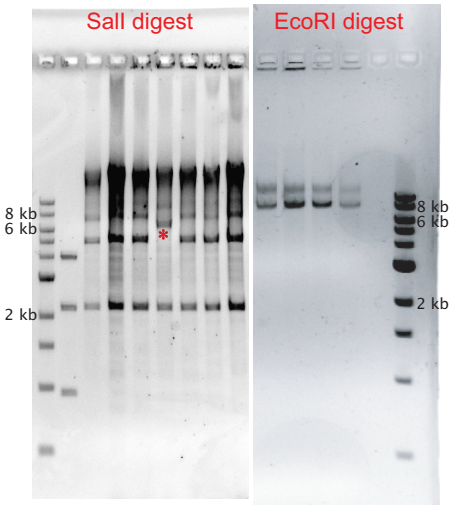

Figure 4.3: Evaluation of the CUCY plasmid by restriction enzyme digestion and gel electrophoresis shows the clone with an insertion of the correct size to be the hUbiC promoter (∗) in a SalI digest and that it is inserted in the correct direction by EcoRI digest. Backwards inserted fragments maintain two EcoRI sites, and would result in bands of 1246 and 7104.

directional cloning using the SalI-EcoRI pair of pUB-GFP and the PspXI-EcoRI pair of Ch2_K315_YFP was not possible. Instead, non-directional cloning using a heat inactivated single PspXI digest of Ch2_K315_YFP and the gel electrophoresis purified, 1299 bp hUbiC band from a single SalI digest of pUB-GFP was carried out. This scheme resulted in a high number of transformed bacteria. However, many were found to carry the un-cut, or self-religated Ch2_K315_YFP. The cloning efficiency of the correctly inserted CMV_hUbiC_Ch2_K315_YFP (CUCY) plasmid was 2%. CUCY is an 8350 bp plasmid with hUbiC inserted 146 bp downstream of the pcDNA3i CMV promoter and 61 bp upstream of the start of Channelrhodopsin 2 coding sequence (see Figure 4.4). This means that hUbiC is well within range of driving Channelrhodopsin 2 expression.

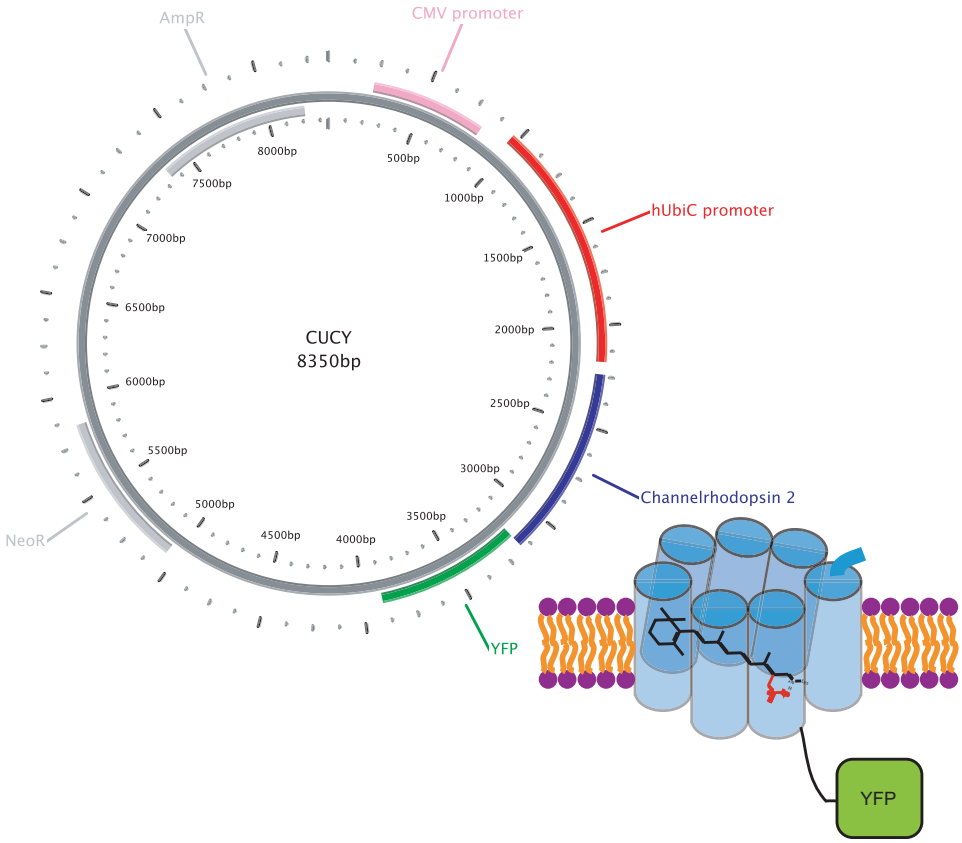

Figure 4.4: Map of the CUCY plasmid showing the prior CMV promoter (pink), new hUbiC promoter (red), channelrhodopsin 2 (blue), and the YFP tag (green). Note that the channelrhodopsin and YPF are intended to be a fusion protein. In gray are the plasmid regions associated with production, such as antibiotic resistance. The schematic of the incorporated protein shows that there are no structural differences expected compared to Ch2_K315_YFP (see Figure 4.2), only the level of expression is expected to change.

4.1.4 Ch2_mKATE_ssHK: A Multifunctional Construct

As an alternative construct, the Bamberg group kindly provided a second optogenetic plasmid, Ch2_mKATE_ssHK. This construct was intended to have spectrally seperated regions for optical depolarization, fluorescence detection, and optically controlled hyperpolarization, see Figure 4.6. The depolar-

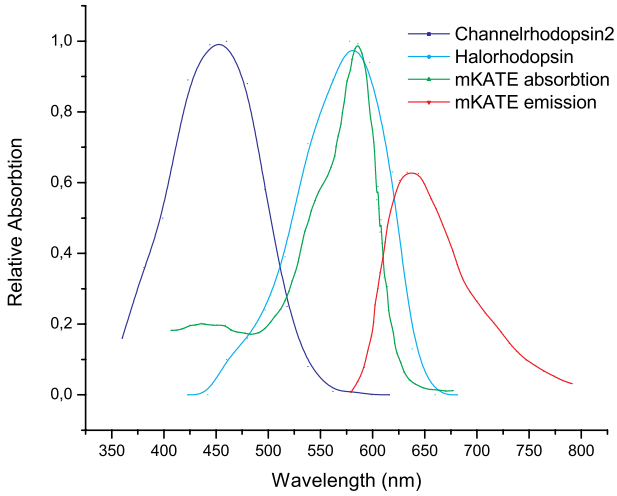

Figure 4.5: Spectral separation of the activation wavelength of Channelrhodopsin 2, halorhodopsin (NpHR, as the proxy for the ssHK pump, which is as yet unpublished), the excitation wavelength of mKATE and the emission wavelength of mKATE. Since this data was taken from different investigations, the normalization is to the peak performance of the individual proteins, i.e. one cannot say that the maximum peak current of Channelrhodopsin 2 is equal to the maximum peak current of Halorhodopsin. The absorbtion and emission of mKATE are from the same study and their relative peaks are to scale. However, the range of useful illumination wavelengths is accurately depicted across the different proteins. This construct should allow identification of transfected cells without inducing electrical changes, as well as assuring that any transfected cell can be both excited and hyperpolarized. This plot is adapted from [162, 141, 68].

ization was to be achieved via the blue light responsive Channelrhodopsin 2 channel while the hyperpolarization was to be achieved by a Cl^- pump derived from Halorhodopsin that would respond to yellow light [157]. Aside from the linkers engineered at the C-terminal of channelrhodopsin and N-terminal of the Cl^- pump, the membrane spanning regions were separated by a mutated version of the mKatushka fluorophore (mKATE) [141]. The presumed spectral separation can be seen in Figure 4.5. If high transfection rates of this consturct could be achieved, wide field yellow illumination could quiet spontaneous neural network activity by activating the Cl^- pump,

while point illumination with the blue laser coud stimulate single cells via Channelrhodopsin 2 activation. Furthermore, the change of fluorophore to mKATE (excitation at 588 nm, but with a shoulder at ∼530 nm, emission at 635 nm, [141]) would prevent activation or hyperpolarization of the neurons while searching for successfully transfected cells.

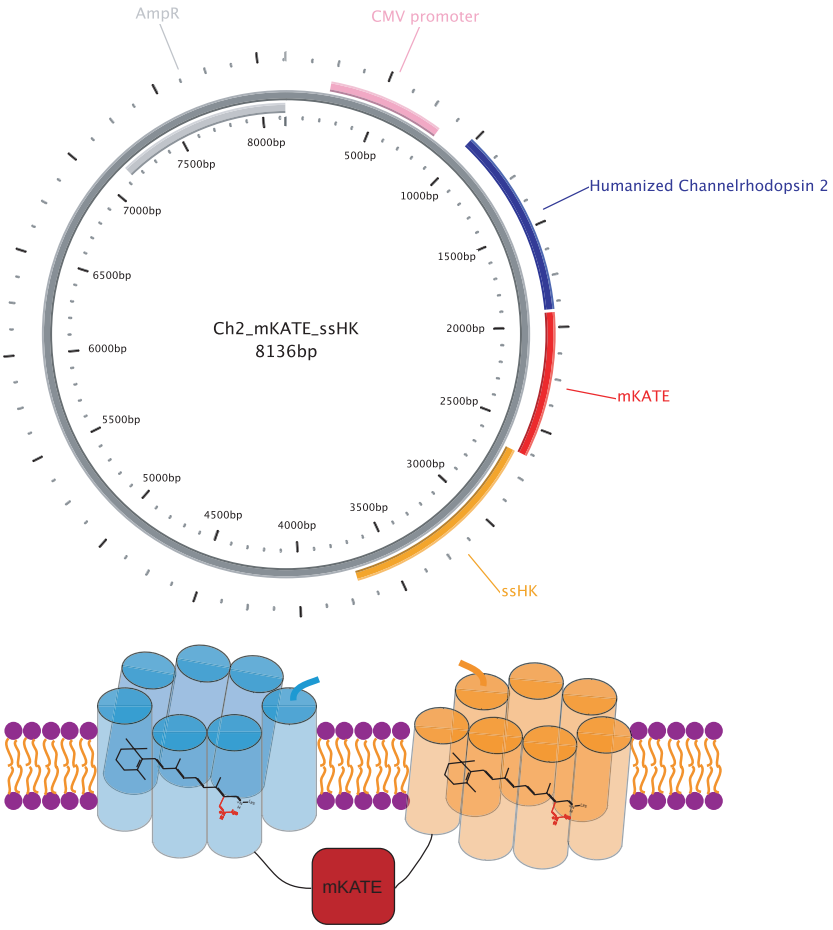

Figure 4.6: The map of the Ch2_mKATE_ssHK plasmid shows the humanized Channelrhodopsin 2 channel (blue), the mKATE fluorophore (red), Cl^- pump (orange) and CMV promoter (pink). The final construct is 8136 bp and bears a single fusion protein.The schematic shows the proposed dual membrane spanning region with different light sensitivities, separated by a fluorophore.

4.1.5 Ch2opt_mKATE Construct

In a further attempt at optimization, a novel Channelrhodopsin 2 construct was designed. Synthetic gene generation was selected so that in addition to changes to the intended protein, coding could be optimized for our model organisms, namely rodents. The protein sequence designed (see Figure 4.7) fused the leading 314 amino acids of the original Channelrhodopsin 2 to the 265 amino acids of commercially available mKATE [4] via a linker based on that used by Bamberg (TAVATI) [25]. The removal of the methionine

MDYGGALSAVGRELLFVTNPVVVNGSVLVPEDQCYCAGWIESRGTNGAQTASNVLQWL
AAGFSILLLMFYAYQTWKSTCGWEEIYVCAIEMVKVILEFFFEFKNPSMLYLATGHRV
QWLRYAEWLLTCPVILIRLSNLTGLSNDYSRRTMGLLVSDIGTIVWGATSAMATGYVK
VIFFCLGLCYGANTFFHAAKAYIEGYHTVPKGRCRQVVTGMAWLFFVSWGMFPILFIL
GPEGFGVLSVYGSTVGHTIIDLMSKNCWGLLGHYLRVLIHEHILIHGDIRKTTKLNIG
GTEIEVETLVEDEAEAGAVTAVATIVSKGEELIKENMHMKLYMEGTVNNHHFKCTSEG
EGKPYEGTQTMRIKVVEGGPLPFAFDILATSFMYGSKTFINHTQGIPDFFKQSFPEGF
TWERVTTYEDGGVLTATQDTSLQDGCLIYNVKIRGVNFPSNGPVMQKKTLGWEASTEM
LYPADGGLEGRADMALKLVDGGHLICNLKTTYRSKKPAKNLKMPGVYYVDRRLERIKE
ADKETYVEQHEVAVARYCDLPSKLGHRGGGGSGLRSRAQASNSAVDGTAGPGSTGSRF
CYENEV

Figure 4.7: The amino acid sequence designed for Ch2opt uses the leading 315 amino acids of Channelrhodopsin 2 (blue) linked to mKATE (red) without a methionine to avoid transcription of mKATE without attached Channelrhodopsin 2. The linker AVAT (black) is based on that used by Bamberg [157] and is only a spacer so the channel and fluorophore do not interfere with each other. Channelrhodopsin contains the H134R mutation (orange) published by Nagel et al [119]. The end of mKATE (green) is based on the publicly available Katushka sequence [4] rather than the inter domain linker used in Ch2_mKATE_ssHK [157]. Finally, the export sequence (purple) [8] is added at the end. The amino acid sequence is confirmed by the resequencing of the plasmid (sequencing [3], translation of DNA sequence [2]).

ahead of mKATE destroys the Kozak sequence in the coding DNA, which was present in the Ch2_K315_YFP construct, and is intended to prevent production of the fluorophore without an attached channel. mKATE was maintained as the fluorophore of choice because of its spectral separation from current optogenetic electrophysiological actuators (this spectra overlaps with the red light control of transcription reported by Tabor et al [149], but it is not intended that this construct be used for combined transcriptional and current induction). The C-terminal of mKATE was adjusted to include the seven amino acid export sequence FCYENEV [8], to alleviate the strong cytoplasmic expression seen in Ch2_K315_YFP and the clumping or vesical disruption observed in Ch2_mKATE_ssHK. The final change to the amino acid sequence was the incorporation of the H134R mutation

in Channelrhodopsin 2 to increase the efficiency of the channel as reported previously [119]. Figure 4.7 shows the final amino acid sequence of the new construct and highlights the changes made.

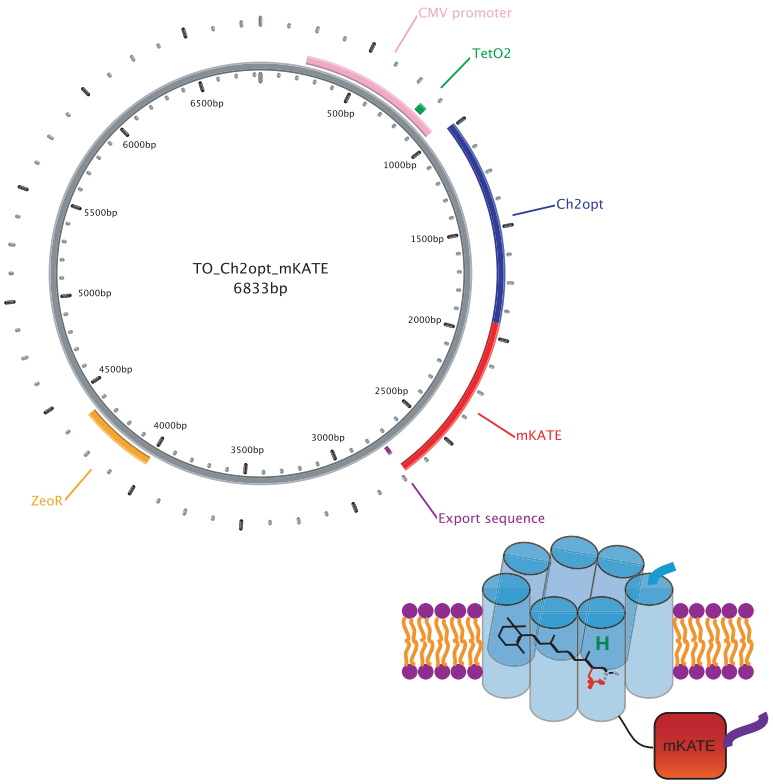

Figure 4.8: Map of the tetracycline inducible TO_Ch2opt_mKATE plasmid showing the CMV promoter (pink), TetON repeats (green), mouse coding optimized Channelrhodopsin 2 (blue) and mKATE (red) fusion protein without an intervening Kozak sequence, and the export sequence (purple). Also shown is the Zeocin resistance gene (orange) for selection of transfected cell lines.

JCat software [64] was used to optimize coding for this amino acid sequence in mice. The 5' coding region was given an 11 base pair leading sequence (`AGCTTGCCACC`) and flanked by a HindIII recognition site, while the 3' end was trailed by a single guanine before the BamHI restriction site. The new construct was supplied in an inducible expression vector to allow greater control of protein production. The TRex™ system (Invitrogen) is a means of generating stable cell lines that can be induced to express a protein of interest by adding tetracycline to the media. It comprises two standardized plasmids, pcDNA4_TO and pcDNA6_TR. Used alone, the pcDNA4_TO vector uses the constitutively active CMV and TetON promoters to express a gene of interest in eukaryotic cells. When combined with the pcDNA6_TR repressor plasmid, the tetracycline repressor prevents expression from the pcDNA4_TO plas-

mid until repression is inhibited by addition of the antibiotic tetracycline, see Figure 2.7 for a schematic depiction of this expression system. Each plasmid of the TRex system also has an antibiotic resistance gene to allow stable transfection of cell lines. The new Channelrhodopsin 2 construct was therefore supplied in the pcDNA4_TO vector. The new protein construct was named Ch2opt_mKATE, and when cloned into the pcDNA4_TO expression vector the plasmid was named TO_Ch2opt_mKATE.

The four molecular constructs discussed were all tested within the current body of work. A further discussion of the electrophysiological behavior of Ch2_K315_YFP and Ch2opt_mKATE will be presented (Section 4.2), with the Ch2_K315_YFP taken as the existing control case. CUCY was not seperately characterized electrically because the channel dynamics are assumed to be the same as Ch2_K315_YFP and characterization is not carried out in the cell type (neurons) for which the promoter was changed. CUCY will be further discussed in the viability evaluation (Section 4.3). Due to Ch2_mKATE_ssHK's viability, see Section 4.3.3, it is only further discussed in viability studies and not in electrophysiological characterization.

4.2 Electrophysiological Results

The various versions of channelrhodopsin have particular advantages and disadvantages, as reviewed by Lin [100]. Here, I shall evaluate the performance of Ch2opt_mKATE in comparison to the Bamberg group's published Channelrhodopsin 2 construct, Ch2_K315_YFP [121] and the published values for several other versions of the Channelrhodopsin 2 protein. In particular the delay between the start of illumination and the onset of current, the channel opening kinetics τ_{on}, the sustained plateau current during long illumination, and deactivation of the channels during long periods of illumination or short recovery periods will be addressed. The channel's ability to quickly pass current will determine the time resolution of stimulation, whereas the total current achieved will determine the overall efficacy of triggering action potentials in electrically active cells. Deactivation of channels, or failure to recover in the dark will contribute to the reliability of subsequent stimulations.

The major channel kinetics were calculated from series of laser illuminations of HEK cells expressing Ch2_K315_YFP or TO_Ch2opt_mKATE in voltage clamp mode. The delay between laser triggering and illumination is 0.02 ms [58] while the recordings are always more than twice that time between data points, therefore this delay can be neglected. Analysis pools the results once the cell response had settled to a steady state, except for deactivation which embodies the change to reach the steady state from the initial response. Steady state was from the seventh to the last flash for illuminations of 100 ms. The first six flashes showed strong decreases in

peak currents from one to the next, and are used to calculate the channel inactivation. Figure 4.9 shows a typical recording averaged over 41 flashes from the seventh onwards and indicates the regions of interest outlined below: delay to the onset of current, the plateau current, and the region fit with a single exponential function to extract τ_{on}. For specific calculation of the boundaries of each of these regions see Appendix C.2. Since the boundaries of the region to be fit for τ_{on} were defined in terms of the average and standard deviation of the plateau current, measurements from one HEK cell expressing Ch2opt_mKATE (80 illumination events) were omitted from the analysis because an interfering 4 Hz sine signal caused a deformation in the plateau region of the average trace, which made it impossible to analyze the data in the defined format.

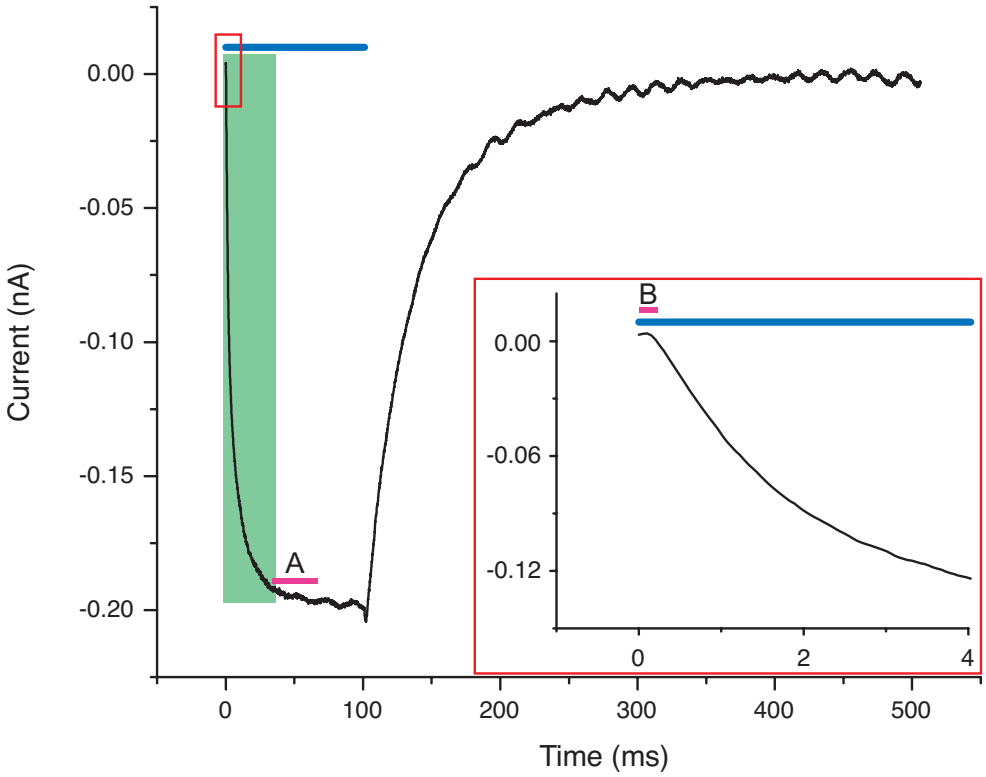

Figure 4.9: Average of the current response of the cell to 41, 100 ms laser flashes from the seventh onward flash. The delay to onset (B) can be seen in the inset. The green area is the region fit with a single exponential decay to extract τ_{on}. The current plateau is indicated by A. It can be seen that the population of channels has mostly reached a steady state of deactivation and reactivation.

A series of sub-second flashes shows two general trends in the raw recording. First, is a decrease in the plateau current over the first few illuminations as noted above. Figures 4.10 and 4.13 show the decline in peak current

achieved by each subsequent illumination in a series of 44 and 50 flashes, respectively, demonstrating the deactivation of a subset of the channels and the leveling off at a steady state, which supports the previously mentioned division of flashes into a declining group from the first to the sixth and a steady state group from the seventh onwards when flashes long enough to reach a plateau phase are used. A deeper analysis of Figure 4.13 shows that when the average and standard deviation are taken in increasingly larger data sets from the last flash to the first, the division between the sixth and seventh flash is when the preceeding point is no longer within one standard deviation of the subsequent average.

Second is a baseline drift between illuminations. The baseline drift shows the need to subtract the average current at the end of the preceeding dark phase from the subsequent flash's current recording. Traces were baseline corrected to the dark condition for the average of 5 ms before illumination. This corrects for baseline drift and for channels that are still activated from the previous flash. The drift can be seen in the raw data trace Figure 4.10. The average channel response is the mean of the baseline corrected flash responses in the steady state group. Since the baseline tends to drift to negative values, failure to perform baseline correction would artificially inflate the initial amplitude of the response to each flash.

A series of negative controls were performed to rule out effects due to the light directly influencing the patch pipette and/or additional channels in the HEK cells contributing to the recorded currents. In a first control, after a Ch2opt_mKATE expressing cell was confirmed to respond to light stimuli, concentrated sodium dodecyl sulfate (SDS) was added to the medium. This treatment should dissolve the cell membrane. After approximately one minute, the pipette resistance was seen to drop from 27 MΩ to 6 MΩ (the initial series resistance of the pipette and the extracellular solution was 5 MΩ). After this, another series of 100 ms, 20% laser stimuli were applied. This is a nominal 20% of the 100 mW laser before the fiber coupling into the microscope. No response was seen, meaning that recordings were not photochemical reactions occurring in the solution that were detected by the pipette. Nor were they photovoltaic effects occurring within the pipette due to the laser light. 20% laser output is the most common illumination intensity used for the characterization experiments, and this confirms that at this power output, the laser alone cannot be detected with the patch-clamp setup. Furthermore, 3 seperate wild type HEK 293 cells that were never exposed to Channelrhodopsin DNA were patched and each underwent a series of 50 laser flashes ramped from 0 to 100% laser output power for 100 ms per stimulation. Again, no response was observed. From this, it can be concluded that there is no visible effect on the patch pipette recording due to exposure of the pipette to laser light. Nor is there any native light sensitive electrical response in wild type HEK 293 cells.

The HEK cells supplied by the Bamberg group with tetracycline in-

ducible expression of Ch2_K315_YFP were measured at DIV2 or DIV3 and DPA1. Measurements at later DPAs were not possible (see Section 4.3). HEK Ch2opt_mKATE cells were transfected on DIV1 and measured from DPT2 to DPT5.

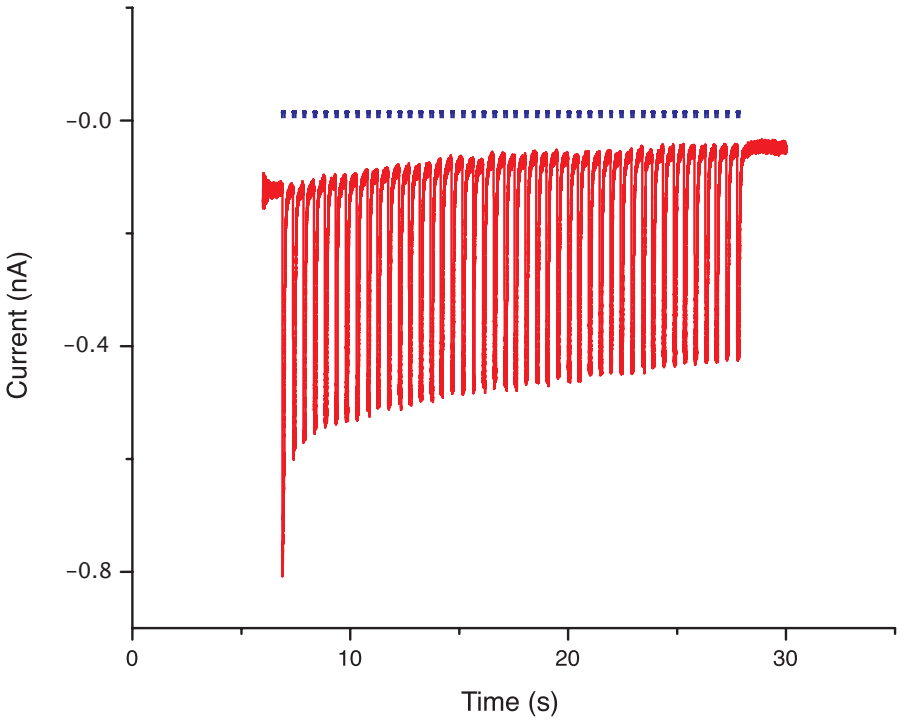

Figure 4.10: The raw recording of a series of illuminations of a single HEK cell expressing Ch2opt_mKATE with recorded current in red and period of illumination marked in blue. The decline in the amplitude of the peak current in the early flashes can be seen, as well as a baseline drift over time. Baseline correction shifts the onset of each illumination event to current zero, within the noise of the unilluminated recording.

In summary, an evaluation in the HEK cell expresison system is validated to study the new Ch2opt_mKATE construct in relation to published Channelrhodopsin 2 results, as well as to a previously published construct tested directly in parallel. The HEK expression system was shown to be a suitable model system for evaluating the proteins and measured responses are confirmed to be due to the expressed construct and not due to light affecting the patch clamp system directly, or inducing a light based response in the wild type or non-expressing HEK cells. The calculation of the channel dynamics and performance can therefore be attributed as characteristics of the introduced protein itself.

4.2.1 Onset of Current

Channelrhodopsin 2 is thought to proceed through four photostates in a linear fashion upon illumination [86]. For a full description of these states see Chapter 1. Of these states, only the second and third are expected to conduct cations [23]. The transition from the first to second state begins with illumination, but undergoes a gaussian distribution of photostates. Therefore we expect a brief delay from the onset of illumination to the onset of detectabled current flow. From Bamann et al. we can see that the relative concentration of the P1 non-conducting form begins to dissipate on the order of 10^{-5} seconds, however, some population of P1 persists into the millisecond regime. At the same time, P2 concentrations (the first conducting form) do not peak for several hundred microseconds [23]. This interplay is further complicated by distinguishing the very first channel related current from the baseline noise.

To achieve the clearest analysis, channel opening was determined using the average of whole cell voltage clamp recordings from the 7th flash applied to the cell onwards. The onset of detectable current represents the subset of the channel population capable of responding the fastest. The response of the rest of the population is captured in τ_{on} (see Section 4.2.2). For the purpose of the following discussion, let t_0 equal the data point at the time a laser flash is initiated. The onset of current is then defined as the time when the average current exceeds one average standard deviation of the noise in the baseline (the average of the standard deviation determined for 5.1 ms from t_{-100} to t_0 over all flashes). Ch2opt_mKATE was shown to have an opening delay of .77 ms (mean, n=161). The delay to the onset of opening has not been previously published in the evaluation of Ch2_K315_YFP, but in control experiments a delay of 1.33 ms was observed (mean, n=52).

The faster onset of current may be due to higher efficiency conferred by the H134R mutation or by faster dynamics of the channel itself. The fact that the published τ_{on} for ChR2_H134R is longer than the τ_{on} for ChR2_K315_YFP (1.92 ms vs. 1.21 ms [100]) suggests that the efficiency gained by the H134R mutation mostly improves the peak current passed by the channel, and that slower channel dynamics conferred by H134R dominate over higher current amplitudes. Furthermore, published constructs which were designed for high speed stimulation describe a trade-off between high currents of the H134R mutation and fast channel dynamics. For example, combination of the H134R mutation with the E123T mutation used for the ultrafast ChETA channel partially negates the speed gains of the E123T mutation [100]. One therefore does not expect the H134R mutation introduced in Ch2opt_mKATE to be the source of the faster channel opening. Therefore, the reduced time for channel opening reflects a change in overall channel dynamics due to the new structure of the protein as a whole i.e. the use of mKATE instead of YFP, and this specific combination of linkers and

protein tail.

4.2.2 Channel Kinetics: τ_{on}

τ_{on} is a measure of how quickly the whole pool of channelrhodopsin proteins absorbs light and becomes conductive. This parameter is important for reaching peak currents, and therefore depolarization, with very short illumination events. In combination with τ_{off} this dynamic determines the maximum frequency with which cells can be stimulated. While a long τ_{off} will prevent the cell from repolarizing between illuminations and therefore be likely to miss subsequent spikes, a long τ_{on} will result in failure to evoke action potentials with a single, short, light flash. In both cases, τ is determined from experimental data by a single exponential fit between the baseline and the plateau.

In determining τ_{on} in this work, the definition of baseline was maintained as points within one standard deviation of the preceeding dark condition in the average of flash seven and later. This is consistent with the definition used for the determination of the delay to onset of current, see Section 4.2.1. Similarly, the end of the region to be fit for τ_{on} was defined as when the average of flash seven and later came within one standard deviation of the plateau current, see Section 4.2.3. τ_{on} was fit in this region using Origin 8, with the equation:

$$Y = Y_o + A_1 e^{\frac{-t}{\tau_{on}}} \tag{4.1}$$

Where Y_o is the plateau current and A_1 is the amplitude of the plateau current to the baseline. Since the baseline correction brings the starting point of the current trace to zero, Y_o was a fixed parameter, set as the plateau current, and A_1 as the absolute value of the plateau current. Using these fitting parameters, a τ_{on} of 2.96 $\pm$ 0.01 ms (mean $\pm$ standard deviation, n = 161) was found for Ch2opt_mKATE in HEK 293 cells, with the adjusted R^2 of the fit ranging from 0.868 to 0.994, average adjusted $R^2 = 0.949$.

This methodology differes from the literature analysis of τ_{on}, which first of all uses only the response to the first flash to fit τ_{on}. This is an artificial inflation of how fast threshold breaking depolarization currents can be reached because most useful applications of optogenetic depolarization aim at inducing series of APs via series of flashes. Furthermore, when only the first flash is used, a sharp definition of the onset of current and the plateau are more difficult to achieve. The literature's solution to this is to fit the region between 15% and 85% of the first flash's maximum current. If the first flash only approach is applied to the data recorded here, a τ_{on} of 2.51 $\pm$ 0.02 ms (n = 4) is found, which is still not as fast as reported by Lin [100], but is closer to the literature values. I maintain that the more useful quantity is the time response in the steady state condition, and that Ch2opt_mKATE offers fast enough opening kinetics to achieve biologically

relevant stimulation frequencies.

4.2.3 Plateau Current

When Channelrhodopsin 2 is steadily illuminated, the number of inactivated channels reaches a steady state when the rate of channel reactivation in the presence of light balances conducting channels that become inactive. This results in a current plateau that is substantially less than the peak current during prolonged light exposure. The absolute value of the peak and plateau current depends heavily on the density of functional Channelrhodopsin incorporated in the membrane, with inactivation of the channel as the other major contributing factor. Since the laser illumination spot is of fixed diameter within the focal plane, and this area is less than the total area of the cell, the current induced in each experiment should be a function of the amount of active channels incorporated into the membrane. This is in contrast to electrically or chemically gated channels expressed in HEK cells, where the total size of the cell is critical in determining the total current achieved because all channels over the entire membrane are activated. While in whole cell voltage clamp mode, the effect of one positive charge moving into the cell must be balanced by one negative charge entering the cell from the patch pipette. Therefore, the currents from sub-cellular illumination spots can be compared across different cells.

Illumination spot size was measured optically using the Zeiss camera and AxioVision software. Initial measurements of spot size relied on imaging the laser spot projected onto a solid fluorescent substrate and measuring the illuminated area. In this case a spot diameter of approximately 5 μm was determined with a laser power of 5% maximum output. However, later experiments with cells showed that blooming in the camera at long exposure time and flicker at low exposure time made this a rather unreliable measurement. Instead of trying to improve the camera performance, transfected cells were bleached under the laser spot and the bleached area evaluated as a proxy for laser spot size. After exposure to a 40% laser flash for 1 min, investigation of bleached mKATE within 2 min of the end of bleaching indicated an approximately 4 μm diameter spot. One can attribute the smallest bleach spot size to the focal diameter of the laser and larger spots to diffusion of the fluorophore in the membrane. Bleach spots varied from 3.76 to 6.73 μm. This variability can be accounted for by diffusion of protein into and out of the spot during the change in measurement setup. This change is necessary because the UGA software to control the laser is not optimized for high quality images or distance measurements. However, since the UGA software calls the camera, it cannot be run simultaneously with the AxioVision imaging software. This switching is, at best, on the order of one minute.

Plateau current was calculated as the central third of the illuminated

period for light flashes longer than 50 ms. Figure 4.11 shows single responses to varying duration flashes, indicating the duration necessary to reach a steady state of active channels.

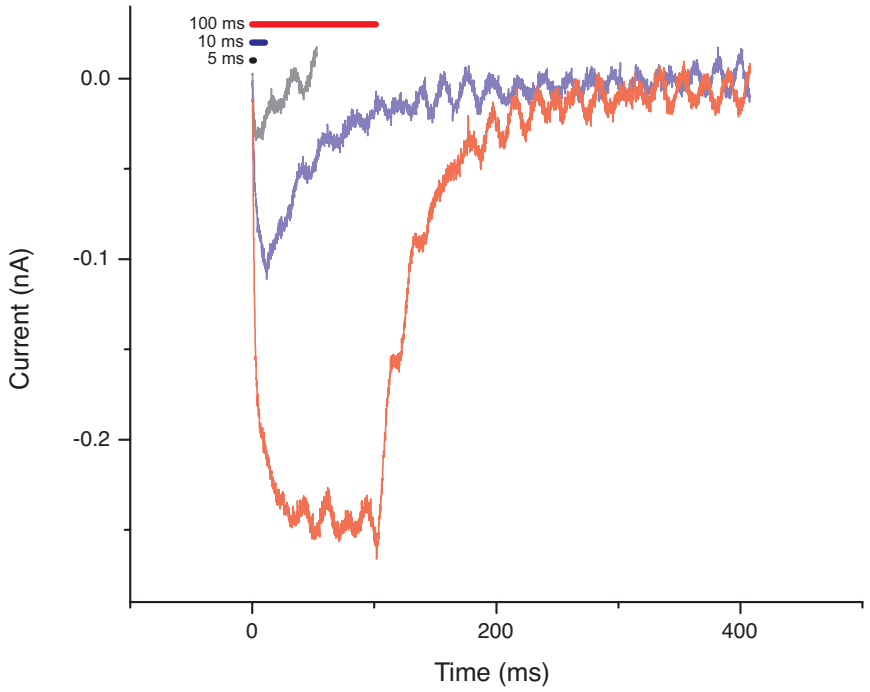

Figure 4.11: The current response to laser flashes of various lengths are shown. Horizontal bars indicate the illumination period for the traces of the corresponding lightened color (black bar indicates the gray trace's illumination, blue bar for light blue trace, and red bar for pink trace). The horizontal bars are depicted with an offset for visualization and do not correspond to a real current. All measurements shown were with 20% laser power.

The plateau current acheived by cells transfected with Ch2opt_mKATE was -225 ± 1 pA (mean±standard deviation, n=118). In contrast, the plateau current for the Bamberg group's Channelrhodopsin 2 was -125 ± 1 pA (mean±standard deviation n=34). The published value for the original ChR2 is less than 100 pA and newer versions range from less than 50 pA to approximately 400 pA, with ChIEF achieving the highest sustained currents [100]. ChIEF achieves these high sustained currents by consisting of a chimera of Channelrhodopsin 1, which has a low inactivtion, and Channelrhodopsin 2, which allows conductance of positive ions other than protons [101]. The performance of the chimera channelrhodopsins can be seen in Figure 4.12 where it can also be noted that the increased plateau currents come at the cost of slower channel kinetics.

The plateau currents sustained by Ch2opt_mKATE are comparable to plateau currents reported in the literature [100] for Channelrhodopsin 2,

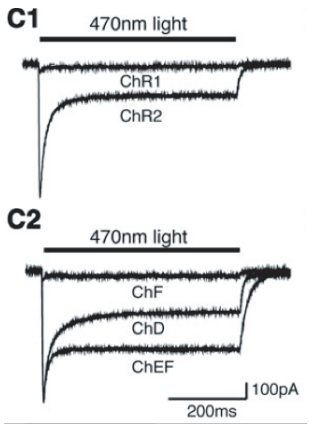

Figure 4.12: Improved plateau currents are reported for the chimeras of Channelrhodopsin 1 and Channelrhodopsin 2. Reproduced from [101].

and in direct comparison experiments, 1.8 times the current of the original Channelrhodopsin 2 construct. This sustained ability to elicit high currents should improve the construct's ability to reliably induce action potentials in response to light. Furthermore, after the initial flash to flash settling (approximately the first six illumination events) the current elicited from one flash to the next is stable and does not show the strong initial peak of isolated illuminations. Though this means the current elicited during later flashes in the train is somewhat lower than the peak achievable current (see Section 4.2.4 for a discussion) the current applied is more consistent.

4.2.4 Deactivation

Deactivation of channels during prolonged illumination or rapid short flashes reduces the overall performance of the Channelrhodopsin. This can most easily be seen in the reduction in peak current amplitude from the first flash to subsequent flashes. The fraction of the channel population that recovers during the dark phase can further be seen in the small peak, which sometimes preceeds the plateau region in response to individual flashes.

The deactivation of Ch2opt_mKATE was calculated by comparing the peak current of the first flash (the mean of 60 data points, 3 ms, with maximal current) to the plateau current in the average of flash seven and later. The percentage of the first flash current lost before reaching the plateau current corresponds to the percent of deactivated channels. For Ch2opt_mKATE, this was 42% (mean, n=4). Though it may seem a poor performance to lose more than one third of the functioning protein, the inactivation of Ch2_K315_YFP in control experiments was 55%, and the published deactivation for ChR2_H134R and ChR2_K315_YFP are 78% and 61%, respectively [100, 101].

The decline in peak current from flash to flash can be seen in Figure 4.13 for Ch2opt_mKATE. The number of flashes required to reach a steady state of current response is similar between Ch2opt_mKATE and Ch2_K315_YFP,

but as a fraction of the initial current, Ch2opt_mKATE retains more functional channels. This suggests Ch2opt_mKATE is more suitable for stimulaiton trains, since high deactivation may prevent later flashes from triggering an action potential without an increase in illumination spot size or illumination power.

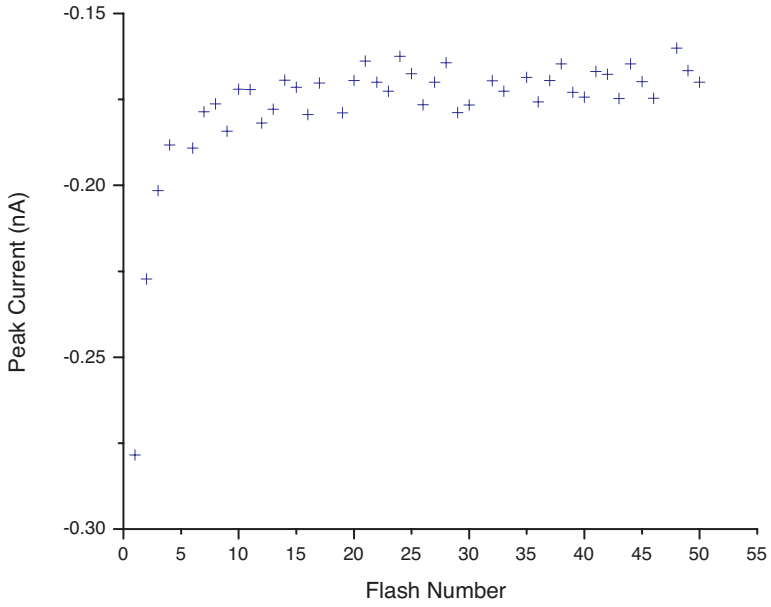

Figure 4.13: In a series of illumination events, the first flash elicits the strongest current from Ch2opt_mKATE. The decline in peak current is most severe in the first five flashes and then oscillates around a steady state. This is the reason for excluding the first six flashes from the plateau analysis and averages used to fit τ_{on} and to determine the delay to onset.

4.2.5 Summary

It has been shown that small changes in the protein construct can alter its electrophysiological performance. Here, the factors of onset of current, plateau current, and channel kinetics were investigated as key parameters for selection of a suitable optogenetic tool. For a brief overview of the new protein Ch2opt_mKATE's performance in the context of literature and the controls performed in this work see Table 4.1. The new construct achieves competitive sustained currents and is second only to the chimeric construct ChIEF for lowest deactivation.

Version	**Delay to Opening (ms)**	τ_{on} **(ms)**	**Plateau Current (pA)**	**Percent Deactivation**	τ_{off} **(ms)**
Ch2opt	0.77	2.96	-225 ± 1	42%	
ChR2♯	1.33	5.58	-125 ± 1	55%	
ChR2∗		1.21∗	$193 \pm 177\bigtriangledown$	61% ∗	13.5∗
H134R		1.92∗		78% ∗	17.9∗
ChETA		0.86∗		40%‡76%∗	4.8‡−8.5∗
ChIEF		1.62∗		20% ∗	

Table 4.1: Comparison of the electrical performance of differrent versions of Channelrhodopsin. ChR2♯ is the Channelrhodopsin 2-YFP construct expressed in HEK cells supplied by Bamberg and tested within this investigation. ∗ denotes values published by Lin [100], ‡ marks values published by Gunaydin et al. [65], $\bigtriangledown$ are values publlished by Boyden et al. [29].

4.3 Viability Results

Electrophysiological performance is not the only consideration in choosing a gene construct for use in on-chip studies. The viability of cells expressing the construct is equally if not more important. Ideally, a construct should confer light sensitivity with no other perturbations of the cell's behavior. Unfortunately, this is near impossible in genetically manipulated systems. At the very least, there is a short term difference in gene expression due to the transfection [32]. Of greater concern are long term effects due to the metabolic requirements of producing the construct, the cell's ability to utililze resistance to a selective agent for the plasmid, and potential toxic effects of the protein itself. Therefore, to complement the electrophysiological investigation, a review of the viability of cells expressing the various constructs is provided below. The decision of which construct to use for further investigations must incorporate trade-offs from these two performance criteria.

Viability of HEK cells is analysed here based on adhesion and morphology. A healthy HEK 293 culture carrying no foreign plasmids will adhere to tissue culture plastic or poly-L-lysine (PLL) coated surfaces (such as glass). Cells spread on the surface and continue to divide approximately once per day until they reach confluence. Once they reach confluence the health of the culture begins to degrade due to lack of access to a good adhesive substrate, and to restriction of nutrients from the media as cells form a multilayered tissue. One therefore expects a healthy culture to have flattened, irregularly shaped cells, which increase in number, as long as there is unoccupied substrate available.

4.3.1 Ch2_K315_YFP Viability

The viability of cells expressing the Ch2_K315_YFP construct was evaluated by examination of activated HEK Ch2 cells (supplied by the Bamberg group) and transient transfection of cortical neurons with the Ch2_K315_YFP plasmid. HEK ChR2 cells [121] were induced to express the Bamberg group's Ch2_K315_YFP construct by addition of 1μg/mL tetracycline to the growth media.

HEK ChR2 cells (supplied by the Bamberg lab) cultured in selection media without tetracycline show behavior similar to that noted for wild type HEK 293, with the exception of a slightly faster rate of division. If cells are examined for fluorescence, only a few cells can be seen to have weak YFP expression. HEK ChR2 cells were removed from tissue culture flasks using trypsin digestion and EDTA. Cells were plated onto PLL coated cover slips and allowed to adhere overnight in unactivated culture media. On DIV1 the media was changed to selection media with 1 μg/ml tetracycline and 1 μM transretinal. Cells were brightly fluorescent on DIV2, DPA1. After activation, almost every cell showed fluorescence to some detectable level, see Figure 4.14. However, after media was changed, a decrease in cell number could be seen on DIV3, DPA2. Fluorescent cells continued to round up and detach from the substrate until a steady state was reached when only several cells per field of view (0.44 mm^2) remained. This number persisted for up to one week, suggesting it was not the case that some cells have an inappropriate plasmid level and those cells are overtaxed by the construct. It was unclear if the cells that did remain were able to divide with a death rate equal to their rate of division, or if the cells were quiescent. HEK 293 cells without any plasmid construct survived until a confluent culture was reached in tetracycline containing media, indicating that the cell death was not a direct reaction to the extra antibiotic used for activation (1 μg/ml tetracycline). This indicates that at high expression levels, necessary to achieve depolarizing currents with Ch2_K315_YFP, can be too metabolically taxing to maintain over long times.

4.3.2 CUCY in Cells

CUCY was transiently transfected into HL-1 cells using either the Amaxa electrofection system or Roche's Fugene HD. CUCY was not evaluated in HEK cells because only its expression level in different cell types is expected to be changed. Laser manipulation of the HL-1 beat rate [78] showed that the new construct still produced a light activated cation channel suitable for depolarizing cells. Transfection rates were not calculated for HL-1 because the cultures were allowed to divide until a confluent layer formed before they were evaluated. This means that without specific data on if or how the foreign DNA alters the rate of division, the cells observed cannot be used

to extrapolate a transfection efficiency. Confluent cultures were more than 50% fluorescent, with variable fluorescence intensities. The above mentioned transient transfection techniques were then applied to primary embryonic rat cortical neurons. Transfection efficiency in these cells was assessed by fluorescence only. Neurons remained viable for three weeks in culture and fluorescence levels did not appear to decrease over this time. The transfection efficiency, evaluated at least two weeks after transfection to allow sufficent time for expression, ranged from 2.4 to 15.6% (n=5 cultures) using Fugene HD. The two week timepoint also assures cell viability up to an age when mature synapses can form in the network. Electrofection produced several more YFP positive cells per field of view, but the cells tended to form neurospheres, making determination of the total number of cells per field of view difficult.

Despite being brightly fluorescent, the CUCY transfected neurons could not be stimulated to produce action potentials with laser illumination. Failure to stimulate action potentials was initially attributed to low expression levels in the neurons due to their reduced metabolism compared to HL-1 cells, or as published in HEK cells [118]. However, it may be due to a Kozak sequence ahead of the YFP coding region that allows production of the YFP tag without any attached Channelrhodopsin 2. If this happened in even a fraction of the fluorescent population, the reduced expression due to the neurons' slow metabolism would only be compounded. Western blotting or a similar protein analysis method may clarify the exact failure of the Channelrhodopsin 2-YFP protein when expressed in primary neurons (by either the original Ch2_K315_YFP plasmid or the CUCY plasmid), however, it would not solve the problem of failure to achieve stimulation. Additionally, continuing to pursue higher expression levels could stress the cell which is producing tagged Channelrhodopsin 2 and YFP alone before affective levels of Channelrhodopsin 2 could be reached. Therefore, further investigation of the Ch2_K315_YFP construct in neurons was halted and an alternative Channelrhodopsin was sought. The constructs discussed above may still be useful in other cell types where metabolic differences deliver sufficient Channelrhodopsin 2 to the membrane.

4.3.3 Ch2_mKATE_ssHK Viability

Primary neurons were transiently transfected with Ch2_mKATE_ssHK using Fugene HD. At DIV4, DPT3 neurons were visibly fluorescent. In full color detection, autofluorescence from debris could be distinguished from the more red shifted mKATE fluorescence, however, the HS DSRed/AP660 filter combinations (Zeiss) were not able to seperate this appearance onto the black and white camera. When high concentrations of Fugene HD were used, red fluorescent neurons tended to round up, and appeared unhealthy. Rounding up and poor adhesion in transfected cells was also seen in HL-1

transiently transfected with Ch2_mKATE_ssHK at DIV4, DPT2. These HL-1 also had a high incidence of large mKATE excluding vesicles crowding the cell or were multi-nucleate. This suggests that independent of cell type, the Ch2_mKATE_ssHK construct makes the cells unhealthy over time.

4.3.4 Ch2opt_mKATE Viability

Unless otherwise stated, these initial tests used transiently transfected HEK 293 cells expressing the TO_Ch2opt_mKATE, see Section 4.1.5 and Figure 4.8. These cells do not need to have expression induced because the second plasmid, repressor pcDNA6_TR, is not present.

In contrast to Ch2_mKATE_ssHK and Ch2_K315_YFP, HEK 293 transfected with the TO_Ch2opt_mKATE plasmid alone were adhered and spreading from DIV2 DPT1 to DIV9 DPT8. Since these cells do not contain the Tet Repressor plasmid, they should constitutively express the construct irrespective of tetracycline. The cells were not cultured in selection media to provide an internal control via the unsuccessfully transfected cells, though media was supplemented with 1 μM transretinal. Red fluorescence was detectable in TO_Ch2opt_mKATE containing HEK cells on DPT1. Furthermore, fluorescent cells tend to appear in clusters, suggesting that expressing cells are still healthy enough to divide and spread. At DIV9 the cultures were already a multilayer, confluent cell mass, so it can be concluded that the expressing cells were capable of surviving the entire duration of the culture. Deterioration after DIV9 could not be assigned to the construct or overcrowding of the cells and was therefore not investigated. It may be possible for the transfected HEK cells to survive even longer if cell density is continually thinned. The better adhesion, proliferation, and persistance of the Ch2opt_mKATE expressing cells compared to HEK ChR2 suggests the construct is less harmful to cells. HEK ChR2 and HEK TO_Ch2opt_mKATE cells were cultured under the same lighting conditions, and show simimlar electrical properties, see 4.2. Therefore, the reduced viability of the HEK ChR2 cells is inferred to be a direct result of the construct's toxicity to cells rather than an effect due to currents induced during the culture period, i.e. from room lighting during media changes.

Neurons transiently transfected with TO_Ch2opt_mKATE also showed considerably better viability than those transfected with Ch2_mKATE_ssHK. Red fluorescent neurons were morphologically normal (see also Figure 4.15) and electrically active at DIV9 DPT9. Fluorescence could be detected in morphologically normal neurons as late as DIV38 DPT38, however the fluorescence became patchy over time and the number of healthy fluorescent cells decreased. Given the performance of the Ch2opt_mKATE construct in HEK cells, loss of plasmid or a reduction in expression over time may be the cause of fewer fluorescent cells after long culture times. Unlike DIV7 DPT7 or older cultures of neurons transiently transfected with Ch2_mKATE_ssHK,

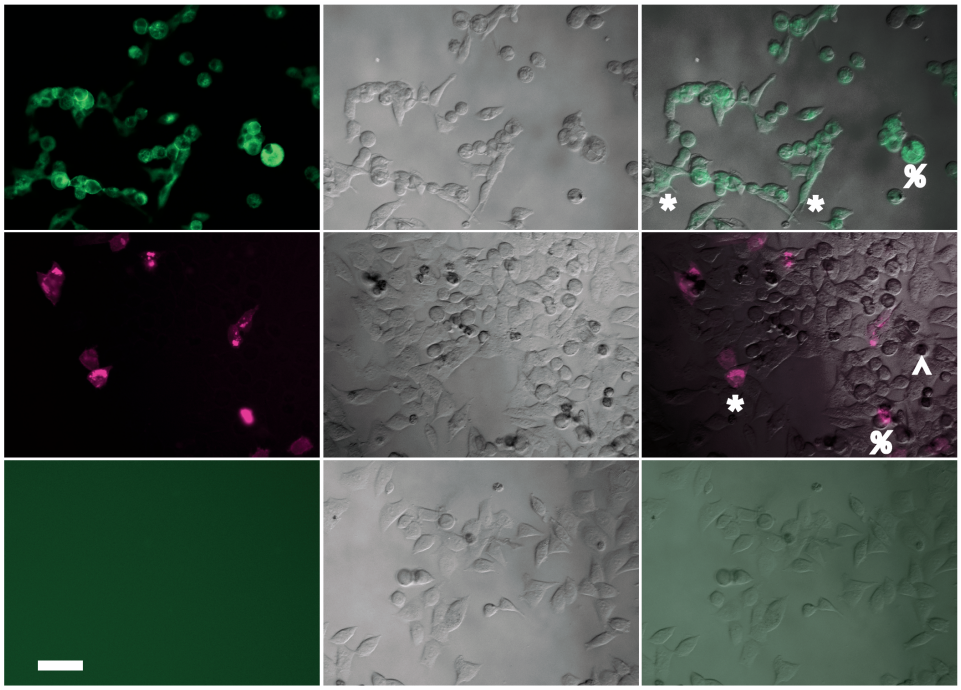

Figure 4.14: Expression of Channelrhodopsin constructs after one day of activation (HEK ChR2 cells, top row), or one day after transfection (TO_Ch2opt_mKATE HEK 293, middle row), or wild type HEK 293 cells after two days in culture (bottom row). The left column shows the fluorescence channel, center column the DIC channel, and right column the merged image. The star marks well adhered and spreading cells that also express construct. The % marks examples of cells that are expressing but rounding up and detaching from the substrate. The $\wedge$ marks round cells that are not expressing, which were likely injured by the transfection process but did not take up or did not express construct. Scale bar is 50 μm.

remains of disintigrated fluorescent cells are not seen in TO_Ch2opt_mKATE transfected cultures at DIV > 7 DPT > 7. Taken thgether these evidence support the assertion that expression of Ch2opt_mKATE is not specifically toxic to the cells.

4.3.5 Summary

From previous work [74] and experiments in this work, it is known that the Ch2_K315_YFP plasmid and the CUCY plasmid do not decrease the viability of transfected neurons. However, these constructs were also not able to confer reliable excitation of neurons.

In summary, the TO_Ch2opt_mKATE construct was shown to be less harmful to transfected HEK cells than the publicly available tetracycline induced Channelrhodopsin 2 construct from the Bamberg group. Confounding effects due to light exposure and the antibiotics used to induce expression

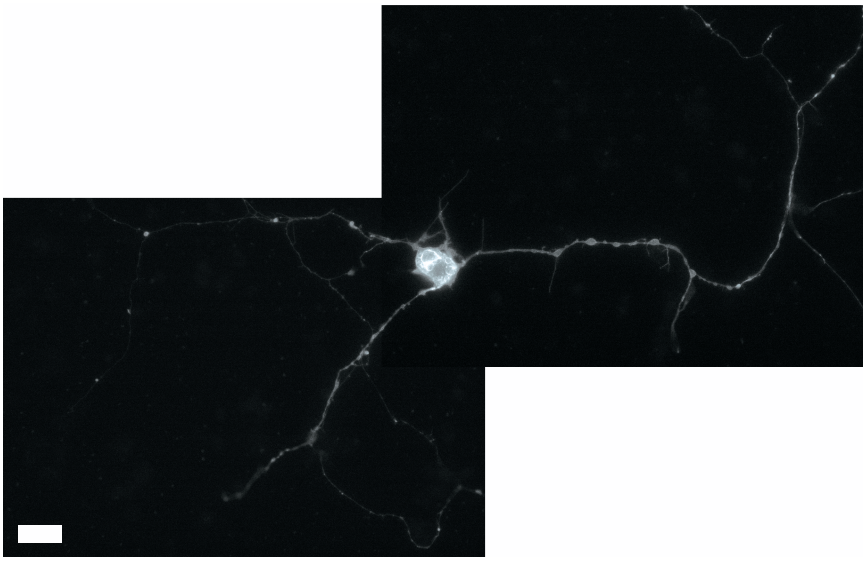

Figure 4.15: A DIV8, DPT8 neuron expressing TO_Ch2opt_mKATE is shown. Neurite extension and cell morphology suggest the neuron is not negatively affected by the construct. Scale bar is 20 μm.

were ruled out, and cells expressing the Ch2opt_mKATE construct survived until their normal endpoint (confluency of the culture). The improved viability of the Ch2opt_mKATE construct was further shown in primary neurons, in comparison to the Ch2_mKATE_ssHK construct, indicating that this is not a cell specific effect.

4.4 Further Use of Channelrhodopsin 2

The field of optogenetics continually improves the available toolbox for light sensitive actuators. These tools may be engineered for highly specialized performance (i.e. ChETA [65]). To establish reliable light stimulation of electrogenic cells on extracellular recording arrays a protein with well balanced characteristics is optimal. The aim of the Ch2opt_mKATE construct was to blend viability and spectral separation with reliable electrophysiological performance, and the electrophysiological and biological evaluation in HEK cells and neurons has shown it has done so. There exist other constructs more suited for specific investigations. For example Ch2_K315_YFP may be best suited for studying the photocycle of the protein due to its resemblance to the native form and high expression levels in protein production systems such as *Xenopus* oocytes.

Ch2_mKATE_ssHK is the most promising construct to allow precise control of activation and inactivation in a cell network. However, it requires further modifications to increase viability of transfected neurons at least to

an age when mature synapses have formed. However, a further mutational screening, or directed mutagenesis of this construct is beyond the scope of this work.

Considering the good viability in multiple cell lines, moderate currents in combination with reasonably fast kinetics, and greater ability to control expression, TO_Ch2opt_mKATE was selected as the construct for further use in cell experiments. This construct was introduced into PC-12 cells and HL-1 cells to generate stable lines with inducible expression. It was also transiently transfected into primary neurons in the absence of the pcDNA6_TR plasmid to induce immediate and constant expression in these cells.

Chapter 5

Ch2opt_mKATE in Cells

The now well characterized Ch2opt_mKATE variant of Channelrhodopsin 2 was selected to combine optogenetic stimulation with MEA recording. The goal was to establish a system that allows single cell manipulation of an electrogenic network over timescales greater than several hours.

5.1 Ch2opt_mKATE HL-1 Cells

The HL-1 cell system was again chosen for first proof-of-principle evaluation (see Section 2.4.1 for a full description of this system). In addition to validating the use of Ch2opt_mKATE in electrogenic cells, a stably transfected cardiomyocyte-like cell with optogenetic stimulation capability would allow additional studies of cardiac cell function. For example, cardiac conduction assymmetry could be modeled by subsequent stimulation of multiple artificial pacemaker cells within the network before the propagation wave spreads over the whole sheet. With the use of an underlying MEA array, the interference pattern of the colliding wave fronts could be analyzed. Such a model system could then be used, for example, in pharma screening to mediate conduction interference.

With the aim of establishing a stably transfected cell line capable of expressing Ch2opt_mKATE the TRex™, tetracycline inducable expression system (see also Section 2.4.3) was transfected into HL-1 cells. The use of un-repressed TO_Ch2opt_mKATE in HL-1 cells was tested to see if constitutively expressing cells are viable. One confluent T-25 flask of HL-1 cells was electrofected with the TO_Ch2opt_mKATE plasmid only and re-plated into a fresh T-25 flask. Cells were cultured in standard HL-1 media with the addition of zeocin to select for the transfected cells. Cells were kept in the dark to avoid confounding effects of light during growth. After one week in culture, only small islands of cells remained in the culture flask, indicating that the antibiotic selection had killed the non-transfected cells. The remaining cells showed normal spreading and adhesion to the culture flask.

However, by DIV22 a confluent layer still had not formed. This suggests that in the absence of the Tet repressor, expression of the Ch2opt_mKATE construct was too metabolically taxing to maintain a proliferating cell line.

To allow the cells to be used in a proliferating phase without Channelrhodopsin expression, followed by an induced expression for the duration of an experiment the TO_Ch2opt_mKATE plasmid was combined with the pcDNA6_TR plasmid in HL-1 cells (the HL-1 Tet Repressor line was established by B. Hofmann). HL-1 cells containing both plasmids were cultured without tetracycline but in the presence of zeocin and blastocidin to select for both plasmids. The doubly transfected cells were named HL-1 Ch2opt-TRex. This line continued to proliferate and could be routinely passaged in culture, though the proliferation speed was markedly slower than wild type HL-1 cells (doubling time of 3 days vs. approximately 24 hours). The HL-1 repressor line also showed a slower doubling time, therefore this delay cannot be attributed directly to either the stress of antibiotic selection or to the presence of the additional plasmid. The proliferating and doubly transfected HL-1 Ch2opt cell line could then be used in electrophysiological experiments.

HL-1 Ch2opt-TRex cells were plated onto fibronectin/gelatin coated MEAs with an 8 x 8 electrode array and 200 μm pitch. The sensing area of these MEAs covers 1.4 x 1.4 mm in the center of a 7 mm diameter culture area. On DIV2 cell culture media was additionally supplemented with tetracycline to induce expression of Ch2opt_mKATE. Cells continued to divide, albeit at a slow rate, until a confluent layer formed. Cells were measured at least one day after confluency, from DIV5 to DIV10, corresponding to DPA3 to DPA8.

Fluorescence examination of the cells showed a variable level of expression, see Figure 5.1. Laser pulses of varying intensity were applied to fluorescent cells through the 20x, water immersion, objective. These failed to induce a wave of action potentials propagating across the cell sheet. However, in DIV10, DPA8 cultures the HXP fluorescence light source (Zeiss) was found to stimulate propagating action potential waves. As this is a lower power light source, it suggests that the area illuminated by the laser was too small ($\sim$4 μm $\varnothing$) to activate sufficient Ch2opt_mKATE channels. The laser pulses were then targeted through the 5x non-immersion objective to obtain a larger spot diameter. However, this also did not elict a propagating AP wave. This suggests that the critical level of Ch2opt_mKATE incorporation is below the ability of the user to target the correct cells without quantitative analysis of the fluorescence. This may be further complicated by targeting difficultites because the non-immersion lens is calibrated with a dry substrate and the on-chip culture introduces an additional air-liquid interface in the beam path. Given these considerations, had every cell been systematically targeted with a laser illumination spot equal to the cell diameter, it is expected that the sufficiently expressing cell(s) could be found. Alter-

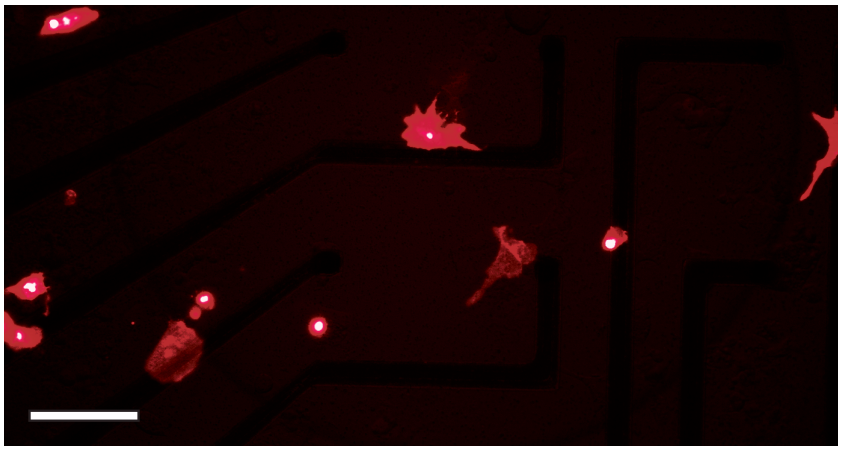

Figure 5.1: Fluorescence image of HL-1 Ch2opt-TRex cells at DIV4 DPA3 shows variable expression of the construct. Scale bar equals 100 μm.

natively, experiments were continued using the HXP light source filtered to excitation wavelengths of 450-490 nm. It could also be possible that the modification of the Channelrhodopsin 2 construct in Ch2opt_mKATE has shifted the absorbtion spectra of the protein, such that the broader spectrum stimulation of the HXP is more effective than the single wavelength laser illumination.

Illumination of the HL-1 Ch2opt-TRex cells was manually carried out with the full power output of the HXP light source with varying illumination duration and varying recovery (dark) periods. MEA recordings showed the onset and end of illumination with a bi-lobed peak of interference (see Figure 5.2 for an example and Section 5.3 for a full discussion of light effects on MEAs). These peaks could then be used to correlate the illumination with the cell activity. The first notable feature is that not every illumination event was able to trigger an action potential wave. The shortest dark recovery period after which an action potential could be generated was 1.9 seconds and the longest observed dark period which did not permit the subsequent triggering of an action potential was 1.5 seconds. This means that the steady state channel activity, see Section 4.2, was insufficient to trigger action potentials and part of the inactivated pool needed to recover before APs could be triggered. This limited the artificially triggered pacemaker to 32 beats per minute, whereas a naturally occurring mouse pacemaker can achieve 120 beats per minute.

Despite the necessity of widefield, multi wavelength illumination, AP waves could be stimulated from various points on the cell sheet. Cultures that had formed gap junctions but not yet developed a pacemaker cell could have individual AP waves generated by individual illuminations. The propagation of these waves could be traced back to the area of illumination. Thus,

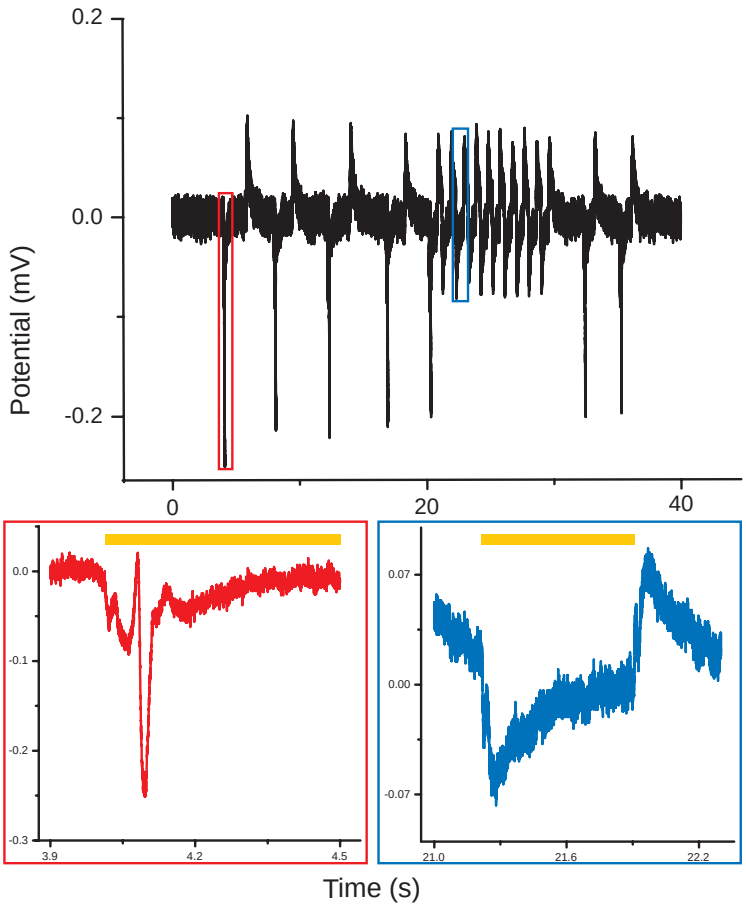

Figure 5.2: A single channel's recording of the HL-1 Ch2opt-TRex cell's response to illumination with blue light. Interference from the lamp is visible as a bi-lobed peak which, due to the baseline compensation, appears as a peak in the opposite direction when the light is switched off. The period of illumination is marked in the insets by the yellow bar. Illumination following a sufficient dark recovery period triggered an AP (red inset), while rapid series of illuminations failed to trigger APs (blue inset). See text for the biological limitations of beat rate.

illumination to the left of the array resulted in an AP wave propagating left to right, illumination near one corner of the array led to propagation along the diagonal of the array, etc. In spontaneously beating cultures, individual AP waves with different propagation directions could be induced by the artificial light-induced pacemaker. Furthermore, in one culture several illuminations were used to generate AP waves, and these AP waves triggered the regular firing of an intrinsic pacemaker cell at a different location. In this culture, prior treatment with NorA failed to elicit spontaneous activity. This suggests that electrical AP induction may be more effective as a defibrilation method than drug treatment, and optogenetics provides an

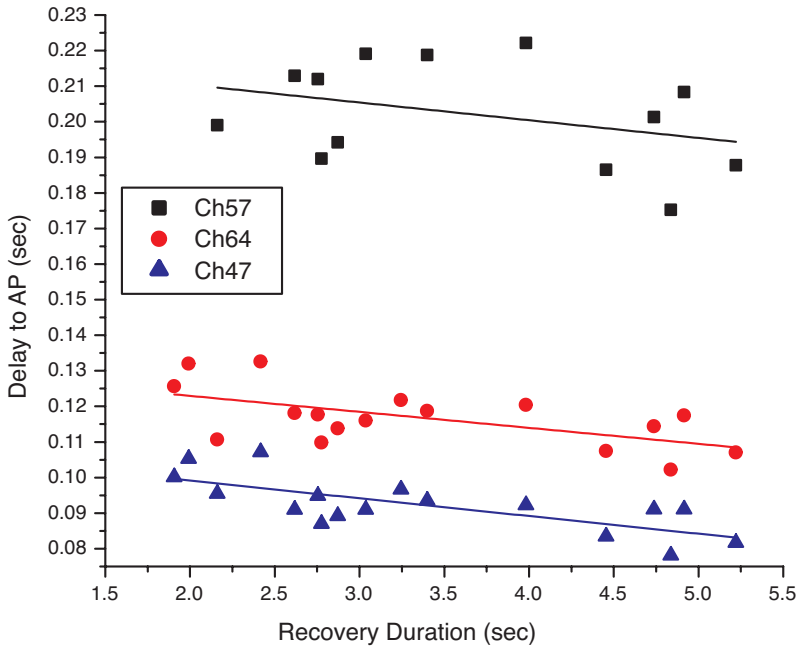

Figure 5.3: It can be seen that with longer preceeding recovery periods, the AP arrives at the electrode sooner after the onset of illumination. This delay is consistent across multiple channels and the correlation between recovery time and delay to AP can be linearly fit to find a reduction of 4-5 ms for each additional second of dark recovery time.

alternative method to extracellular electrodes for electrically inducing APs.

Another notable feature is an apparent negative correlation between the length of the recovery period and the time from the onset of illumination to the time of arrival of the AP when the stimulated cell(s) are in the non-array culture area. The longer the Ch2opt_mKATE had to recover, the earlier the AP was detected, for each propagation distance (see Figure 5.3). This measurement has a larger standard deviation in channels further away from the stimulation point, as one would expect since the signal passes through more unmodulated cells before it arrives at the electrode. The delay suggests that even in cases where enough current can be injected to induce an AP wave, currents produced by a partly inactivated population of Ch2opt_mKATE are slow to depolarize the artificial pacemaker cell. This is surprising because results in HEK cell patch clamp experiments suggested Ch2opt_mKATE currents should be higher and more consistent than those of Ch2_K315_YFP, see Section 4.2. Whereas, Ch2_K315_YFP was already shown to trigger AP waves in transiently transfected HL-1 cell cultures in response to point stimulation with the 473 nm laser spot [78].

One possible reason for poor light response may be the incomplete activation of transcription in the presence of tetracycline, in other words, the

tetracycline in the media may not bind all of the Tet Repressor to allow full expression of the Ch2opt_mKATE. It was hypothesized that the cells with a higher plasmid ratio of TO_Ch2opt_mKATE to pcDNA6_TR should be less susceptable to this effect. Therefore, selection pressure with zeocin was increased and selection pressure with blastocidin was decreased or selection pressure of zeocin was increased alone. Changes in the media concentration of each antibiotic were varied by up to 20%. After 3 months and 11 passages in culture, both of these groups had more than 75% of cells without fluorescence after activation with tetracycline. A similar loss of plasmid and development of antibiotic resisitance was seen in PC-12 cells doubly transfected with TO_Ch2opt_mKATE and pcDNA6_TR, but this cell line is beyond the scope of the current work.

Pending the validation of cell stimulation using a point light source and Ch2opt_mKATE, re-transfection of HL-1 cells followed by single clone cell line derivation may be undertaken to generate a stable line. It has also been suggested that mycoplasma infection may be a means of mammalian cells retaining zeocin resistance without themselves maintaining the plasmid of interest [161]. Therefore, all cell lines to be transfected should be verified mycoplasma free.

5.2 Neurons

One long term goal of Channelrhodopsin 2 based cell stimulation is to modulate the firing pattern of single neurons in *in vitro* neural networks. To test this, primary cortical neurons were electrofected with TO_Ch2opt_mKATE plasmid on the day of preparation. Cells were plated on either glass coverslips or MEA chips. Cells were measured from DIV9 DPT9 to DIV17 DPT17 using the EPC9 patch clamp amplifier. For patch clamp experiments the light response of the cell was measured in current clamp mode adjusted to a resting state of -50 mV. It must be noted that the patch clamp recording is divided into data blocks in order to manage the stimulation program applied and the recording in smaller data sets. This means that for a 100 ms laser flash every second, each one second of recording is saved in one data block. The blocks are recorded end to end, but there is a block switching delay in the EPC9 system of approximately 30 ms, and varies slightly from recording to recording. For the EPC9 controlled investigation of cell response at different frequencies of flash trains, nine or ten flashes are applied in a single block and defined extended dark periods flank the block switching times so that the block switching time should be in a period of long recovery, where fluctuations of a few milliseconds are a small percent of the total recovery period. This concept can be seen in Figure 5.4

Patch clamp data showed that 57% of electrically active cells (n = 14) could be depolarized by laser illumination. Voltage clamp pulses of varied

depolarizaton were used to confirm that the neuron was electrically active before light depolarization experiments were performed. From these validation recordings, the threshold potential of the neuron can be estimated. It was observed that in most cases light evoked depolarization was below threshold (as determined by voltage clamp experiments) and failed to trigger APs. To increase the number of channels activated by the laser illumination, the laser spot was de-focused. This achieved a larger illumination area and targetable spot position at the cost of reduced light intensitiy. With the larger spot size cells were depolarized to above threshold with light and action potentials were recorded in 25% of light depolarizable cells (14% of electrically active cells).

At 20% nominal laser output with the de-focused beam, light induced depolarization triggered action potentials 7% of the time with 100 ms flashes at 1 Hz. The cell also showed spontaneous spiking activity in the dark periods. However, if analyzed in spikes per second of illuminated period vs. spikes per second in darkness, spikes are 15 times more likely to occurr in the illuminated phase, see Figure 5.5. Due to the reduction in intensity by de-focusing the laser beam, laser output was then adjusted to 40% nominal output and the cell probed with further series of flashes.

At 40% laser output, 100 ms flashes at 1 Hz elicited an action potential with every flash. At this intensity, 6% of illuminated periods also elicited two action potentials. In this case APs were 134 times more likely to occurr in the illuminated period than in the dark, see Figure 5.6. This improvement suggests that with the de-focused beam, the 20% nominal laser output is not of sufficient intensity to activate all of the channels within the illumination spot. Cell illumination of greater than one minute at nominal 40% output failed to produce a bleach spot on the transfected neurons for size determination. However, use of the laser in this configuration was able to generate bleach spots in supported lipid bilayers of approximately 10 μm $\varnothing$ using full laser power and long illumination periods [14]. DIC images suggest that the objective focal plane should have been tangent to, or slightly below, the cell surface at the point of illumination. This would imply a reduction in the

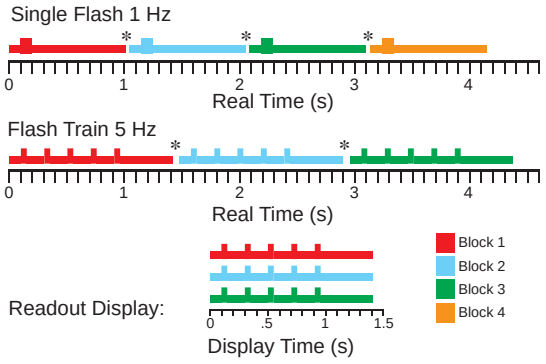

Figure 5.4: A schematic depiction of the relation between real time and recorded time using the EPC9 and how it relates to frequency stimulaiton tests is shown. Raised bars indicate illumination while the low bar indicates darkness. The $*$ indicates the block switching delay.

illumination intensity by a factor of three compared to a 4 μm $\varnothing$ focused spot of 20% laser output, but covering a six times larger area.

Experiments with trains of pulses in HEK cells that were expressing Ch2opt_mKATE (Section 4.2) showed that channel deactivation reached a steady state of inducable current after the sixth illumination event when recovery times were less than one second. The recovery from the inactive state adds an additional complexity in determining the necessary stimulation illumination because one would ideally need to know the critical de-activation at which cells could no longer be triggered to fire APs. If de-activation is the cause for failed APs, then increases in the illumination intensity will not improve performance. However, in this case, increases in illuminated area (as in laser spot defocusing) may improve stimulation success rate because the steady state inducable current over a larger area is expected to be larger than that of the small illumination spot and therefore more likely to bring the cell above AP threshold.

To investigate the effect of deactivation, flash trains were applied to the cell. The goal was to determine if firing frequencies in the physiological range could be achieved. Furthermore, how error rate relates to the frequency of stimulation applied was investigated. Finally, the source of the frequency limitation was investigated. These parameters determine what biological systems are reasonably manipulated by this construct.

Using the 40% nominal laser intensity and focal plane, which previously had a 100% success rate of eliciting APs at 1 Hz, the cell was stimulated in trains of ten flashes with 50 ms illumination and 100 ms darkness (roughly 7 Hz). Over 30 applications of this stimulation program, eight APs were missed, one flash triggered two APs, and four spontaneous events occurred

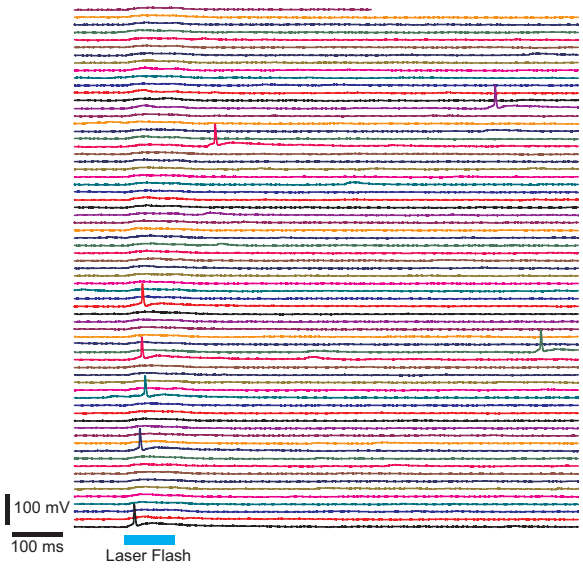

Figure 5.5: Traces show the voltage response of a TO_Ch2opt_mKATE transfected neuron in current clamp mode during 100 ms illumination at nominal 20% laser output at 1 Hz. Data blocks are stacked with an offset. Most illuminations fail to depolarize the cell above threshold, however, APs are more likely to be fired during the illuminated period than to occurr spontaneously in the dark.

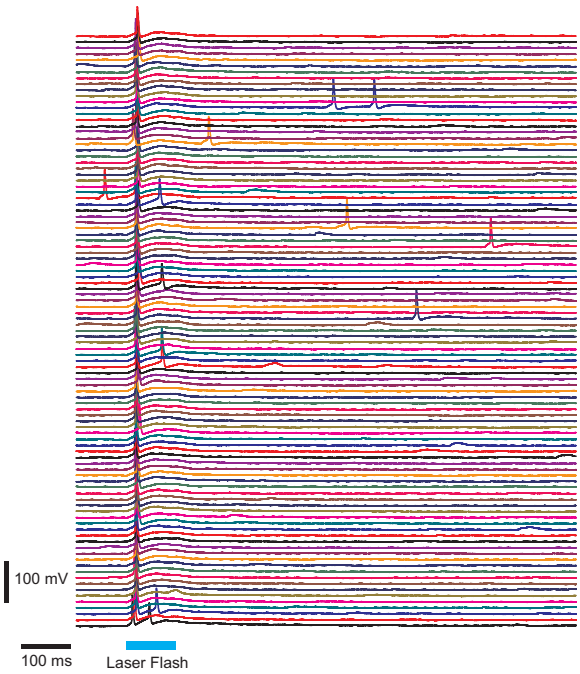

Figure 5.6: The voltage response of the same TO_Ch2opt_mKATE transfected neuron as in Figure 5.5 in current clamp mode during 100 ms illumination at nominal 40% laser output at 1 Hz, with 100 ms flash length. Data blocks are stacked with an offset. All illuminations trigger at least one AP.

within the stimulation train. The eight missed APs were each in different trains and scaling for the amount of time recorded in a flash train sequence versus in the long dark periods flanking the block change, extra spikes were only 1.5 times more likely in the dark flanking period than during the train, suggesting that these spikes are part of the spontaneous background activity. Grouping all errors together, this gives as 96% success rate of neuronal response at this frequency.

To test the effect of higher frequency stimulation on error rate, stimulation trains were then applied at the same intensity (40%) and focal plane with an illumination period of 40 ms and 50 ms dark period (representing 11 Hz). In this case a 84% success rate was observed with no stray spikes within the train but a similar rate of spontaneous spiking in the flanking dark period compared to the 7 Hz trains. The lack of spontaneous spikes observed within the trains is not surprising. Due to the reduced total time within this series of stimulation trains, there is only a 36% chance that any spontaneous activity would be observed within any of the 31 trains measured, assuming an equal rate of spontaneous firing to that observed in the low frequency experiment and the block flanking darkness. The distribution of missed APs within each train supports that the six times poorer performance is due to the shortened dark recovery period. Figure 5.7 shows the chance that a particular flash within the train (first, second, third, etc.) resulted in a missed spike from the cell in 40 ms on 50 ms off flash train experiments.

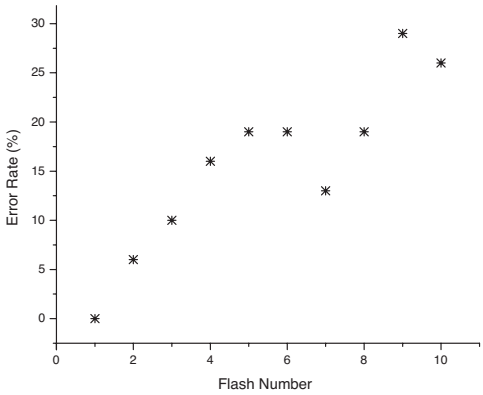

Figure 5.7: The likelihood of a flash failing to trigger an AP increases with flash number when the dark recovery period is short.The number of missed APs also increases with subsequent trains. Data from 31 trains.

In another patch clamp experiment, the source of the frequency limitation was investigated. A Ch2opt_mKATE expressing neuron underwent flash trains at 40% nominal laser output power with 50 ms flashes and 150 ms darkness (control case), 30 ms flashes and 150 ms darkness (fast flash case), and 50 ms flashes and 100 ms darkness (short recovery case). In initial 1 Hz verification of light excitability, no double APs in response to the 100 ms flash were seen, eight APs were missed, and 21 spontaneous APs occurred. This was a stimulation success rate of 95%. However, the higher rate of spontaneous activity in this cell compared to the previous experiment led to a total success rate of 58% for the light programmed activity. This is because the majority of errors occurred from spontaneous activity in the long dark period. When the fast flash case was applied, an increase in missed APs was again observed later in the train of flashes (Figure 5.8). However, the success rate only decreased to 77%. In contrast, the short recovery case showed an overall success rate of only 22%, though the success rate of the first flash in each train was 96%. This suggests the importance of channel inactivation and recovery in fast reliable stimulation of single cells from small illumination points (see full discussion in Section 6.2).

If the failure of light to trigger APs was due to persistent opening of the activated Channelrhodopsin 2, one would expect that when action potentials are successfully triggered, APs from later flashes should have a shorter delay between the onset of illumination and the triggering of the AP. This is expected due to the current already flowing from channels that had not closed after the previous flash contributing depolarizing current even before the illumination began. In fact, the opposite case is observed (see Figure 5.9). When APs in the middle and end of the train are successful, they have a longer delay from the onset of illumination, suggesting there is not a substantial residual current flowing during the dark phase. In addition to the increase in delay from flash to flash within a single train, a gradual increase in delay for the entire train is observed in subsequent trains. This shows that the longer dark periods flanking each block are sufficient to allow reliable

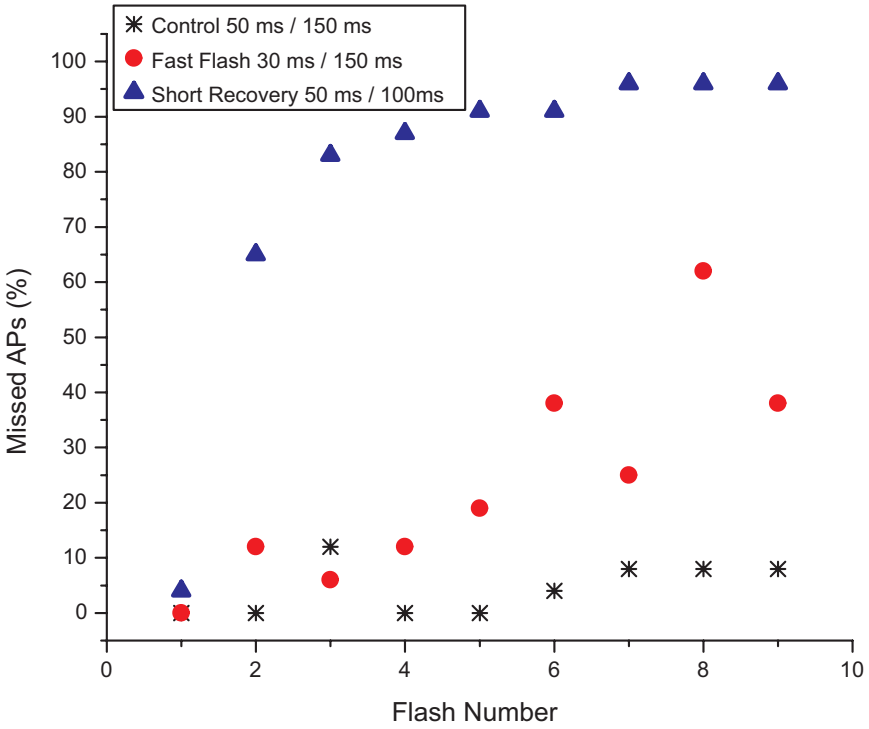

Figure 5.8: The likelihood of a flash failing to trigger an AP increases with flash number, particularly when the dark recovery period is short.

triggering of the first AP, but are not long enough to completely eliminate the deactivation of the previous train's illumination.

5.3 Light Effects on MEAs

Laser illumination had previously been used with the 8 x 8 gold MEA on Borofloat glass described in Chapter 2 [74, 78]. In these cases, it was shown that only when illumination was directly over an electrode and applied at greater than 10% of laser output, could the effect of the light alone be detected by the MEA. In this case, even the illumination directly over the electrode did not cause effects that were large enough to obscure cell signals. This was confirmed in experiments using cells without optogenetic constructs. Non-cell light effects (NCLEs) from the laser were generally not seen on nanostructured gold MEAs on silicon wafer substrates either. In some channels of these chips an 80% laser flash with 4 μm diameter, caused a spike of approximately 0.02 mV accompanied the switching of the laser. This was compensated for by the amplfier in approximately 20 ms, and the peaks were present on channels with peak to peak noise of 0.04 mV. In this case, even if the NCLE overlays the cell recording, cell signals should be dis-

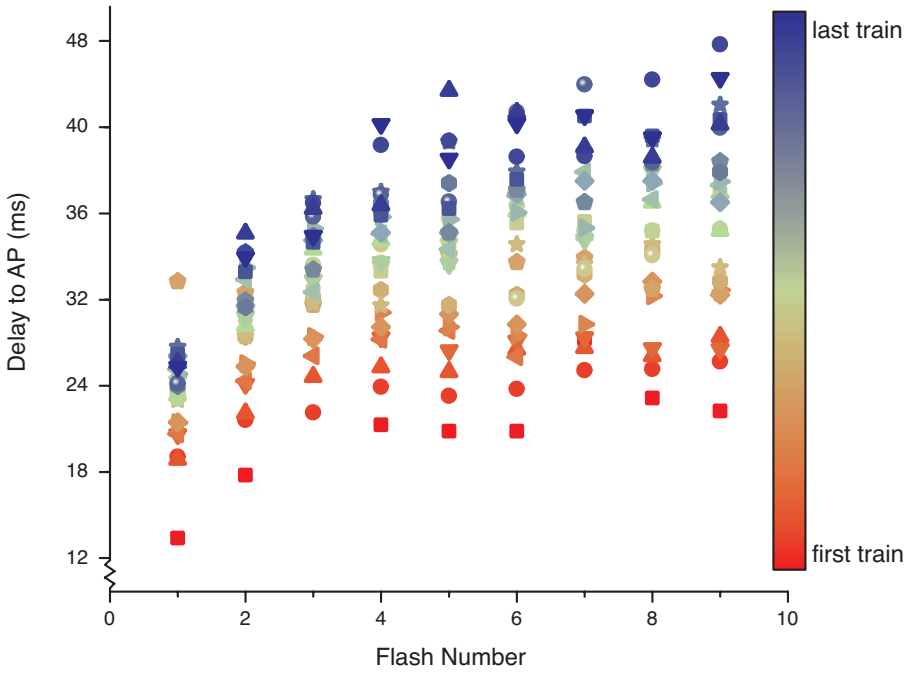

Figure 5.9: When APs are successfully stimulated in flash trains, the delay from onset of flash to triggering of AP varies. It can be seen that within each train (color coded) the delay to the AP in response to the first flash is the shortest. The delay to AP increases sharply in the first several flashes, then maintains a more consistent level. From one train to the next an additional shift of the whole train to longer delays is observed, showing that the dark period between blocks is not long enough to make the individual train responses independent of one another.

cernable, as in the case of the slightly distorted spike shapes recorded from HL-1 cells using HXP based illumination (see Section 5.1). The NCLEs of the HXP on nanopillar gold MEAs on silicon substrates caused more sever distortion of the baseline than the laser spot when both were applied away from the electrodes. In this case some of the observed disturbance may be from the switching of the lamp instead of the light itself. This is supported by the irregular shape of the disturbance, as seen in Figure 5.2.

However, as observed in the HL-1 light stimulation experiments of Section 5.1, wide field illumination with the HXP light source generated the bilobed NCLE which was used to measure the timing of the illumination. The increase in noise of DREAMS1 chips discussed in Section 3.2 also suggests the possibility of NCLEs on BNCD electrodes. However, DREAMS2 and DREAMS3 chips did not show severe NCLEs in response to off-electrode laser flashes. Unfortunately, the durability and production shortcomings prevented their use with Channelrhodopsin 2 expressing neurons (see Sections 3.3.2, 3.4.2 and 3.4.2).

The SNR of the cleaned DREAMS4 chips that were not destroyed by cleaning suggests they would be good candidates for detecting neuronal signals (see Section 3.5.3). However, these chips proved extremely light sensitive. To eliminate a small contribution from the coupling of the electronic trigger into the amplifier at channel 1, the signal to the UGA laser system was reduced to the minimum that was still detected by the UGA device when using external stimulation programs from the EPC9 system. In chips with electrolyte on the surface, NCLEs of up to 0.3 mV were induced by a 25 mV laser flash applied to the center of the chip (not on any electrode or feed line), and visible across the whole chip. Also changes in ambient lighting were visible on the DREAMS4 recordings, i.e. a shadow generated between the setup and the room lighting. These NCLEs were of moderate amplitude, but due to their prevalance in ambient conditions (see in particular Figure 3.9), the effects could not be positively correlated with illumination to reasonably disregard them. In other words, shadows could not be distinguished from low amplitude signals. Since extracellularly recorded neuronal APs are of much lower amplitude than patch clamp recordings (compare for example Figure 3.7 and Figure 5.6), even low levels of interference make neuronal AP detection difficult. Furthermore, because patch clamp cannot be applied at all 64 electrodes, nor can the spike verification methods used for HL-1 (see Section 2.4.1) be applied, APs must be robustly distinguishable in the recorded signal.

An alternative method for improving the MEAs' detection of neuronal signals is to electrodeposit platinum on the gold electrodes. For this, the nanostructured gold chips used for experiments described in Section 5.1 were covered with a spongy platinum layer as described in Section 2.2.1. These chips detected all stray light at the experimental setup in both the dry and electrolyte covered condition (for the dry chip test, the reference electrode was immersed in a neighboring bath containing KCl). In the case with electrolyte, weak light sources up to a meter away saturated the amplifier (more than 10 mV). This response made them unsuitable for use with optogenetic systems.

The highest SNR with lowest NCLEs were achieved by platinizing planar gold MEAs deposited on BoroFloat glass substrates and passivated with ONO. Care must be taken in the platinization of these chips to maintain consistent performance. In particular the chips should be monitored optically during the platinization process and the platinization program stopped in the event of bubble formation, creeping of the platinum out of the electrode, or platinization of pinholes over the feed lines. The stability of the platinization was also found to be lower than that of standard metal MEAs and the contactless cleaning method (see Section 3.1.2) is recommended to extend the usable life of the chip. Individual electrodes were seen to have the platinum removed by single mechanical cleanings.

5.4 Summary

The extension of Ch2opt_mKATE expression in electrogenic cells shows that this tool has the potential for single cell level studies in cardiac and neural tissues. The illumination area is of critical importance and could be optimized by using a light spot with a diameter as close to the cell diameter as possible. Decoupling the stimulation light from the objective lens would also assist consistent depolarization because the spot diameter at the membrane surface could be made independent of microscope focal volume. Both HL-1 and neurons were shown to be manipulated by light flashes when sufficient illumination areas were used.

In neurons, the limiting factor for stimulation reliability is the recovery of Ch2opt_mKATE from the inactive state after illumination. This is in contrast to other published Channelrhodopsin 2 variants where slow closing kinetics or poor currents have been addressed.

Finally, a MEA format with high enough sensitivity to cell signals for neuronal monitoring has been found which lacks significant NCLEs. This is the platinized, planar gold MEA, with platinized electrodes, and ONO passivation on a Borofloat glass substrate. This will allow investigations using the complimentary techniques of MEAs and optogenetics, though novel combinations are sought that also have suitable resistance to photovoltaic and photoelectric effects.

Chapter 6

Discussion

In this chapter, the relevant outcomes of the work presented are revisited and expanded. The principles underlying the effects observed are considered and possible means for improvement or futre investigations are presented. In particular the relevant parameters for use of Ch2opt_mKATE to stimulate single cells *in vitro* will be discussed, followed by the performance of diamond MEAs and their future use for extracellular recordings. Finally, the compatibility of optogenetic stimulation with MEA recordings (including those from diamond devices) is considered.

6.1 Channelrhodopsin Selection

Achieving single cell excitation using Channelrhodopsin 2 has typically relied on specificity conferred by genetic targeting rather than by precise illumination. In this work, it has been shown that the Ch2opt_mKATE construct can be expressed in cells at a level that allows subcellular illumination to trigger action potentials. Neurons remained viable while expressing the protein for over 50 days. This is in contrast to other constructs tested. The re-engineering of the protein for better expression in rodent systems, higher current efficiency, and improved trafficking to the membrane proved more effective for achieving neural stimulation than changing the promoter alone. It was also found more beneficial to incorporate only one functionality in the protein, as the viability of cells transfeced with the Ch2_mKATE_ssHK construct suffered toxic effects that prevented electrical measurements in both cell types tested.

The new Ch2opt_mKATE construct showed better viability in HEK cells than the Bamberg group's Ch2_K315_YFP, with cells surviving to confluence in culture. τ_{on} of Ch2opt_mKATE was found to be very slow compared to literature values for other Channerhodopsins. One contributor to this factor is that the values reported here are for the τ_{on} of the steady state condition. When methods are reported in detail, some literature values are

calculated using only the channel response to the first flash, prior to any deactivation. This is arguably a less useful figure than the behavior of the protein after multiple illuminations, as would be expected in a stimulation experiment. The control case (Ch2_K315_YFP) also had a much longer τ_{on} in these experiments than literature values (5.58 ms vs. 1.21 ms). This suggests the discrepancy is largely methodological and the results may better be interpreted as a τ_{on} that is 47% faster in Ch2opt_mKATE than in Ch2_K315_YFP.

6.2 Recovery, Delay to AP, and Frequency Implications

Related to the channel kinetics, Ch2opt_mKATE was evaluated for its ability to stimulate single cells in controllable frequencies. The inverse relationship between length of dark recovery period and delay from onset of illumination to generation of AP suggests that channels do not remain open through significant parts of the dark phase. If channels remained open, a depolarizing current would be expected to exist before the onset of the subsequent flash. This would lead to greater currents in the subsequent flashes, and an expected decrease in the delay to AP. Furthermore, if currents persisted in the dark, trains with short flashes and short recovery periods would be expected to behave similar to a single illumination, therefore some double spikes would be expected in the beginning of the train, followed by a plateau state or overall deactivation to below threshold crossing depolarization. This is not the case, as no double spikes are seen in short recovery time trains, and missed spikes can later be followed by successful stimulations, even though the missed AP rate increases with flash number (see Figure 5.7). Published analyses of Channelrhodospin constructs for use in electrogenic cells focus on factors such as closing kinetics, maximum currents, and ion specificty. This result shows that the inactive state in the photocycle is a further point where constructs could be optimized.

This also suggests that contrary to reports from other Channelrhodopsin constructs [65], a steady spike frequency in response to sustained illumination is not expected for Ch2opt_mKATE. Steady illumination can be considered as recovery time of zero from spike to spike and the continually increasing delay to AP in pulse trains predicts a decreasing AP frequency of the steadily illuminated neuron. One can see the onset of this phenomena in the 100 ms illuminations that trigger double spikes. In the case of the first 100 ms illumination two APs and one depolarization to near threshold is observed. The delay to the first AP is 12 ms, the delay from the first to the second AP 33 ms, and assuming the third AP was immediately below threshold when illumination ended, it would have a minimum delay of 56 ms. It remains an open question at what point this near doubling of AP delay

would cease. However, it suggests that in the case of continued illumination frequencies not higher than 17 Hz could be sustained. This would reach into the slow beta wave frequencies, but suggests that Ch2opt_mKATE is better suited for work in the delta or theta range, where flash trains can make the spike spacing more consistent. By modulating recovery time, precisely spaced trains between 1 and 7 Hz were demonstrated, see Section 5.2.

In the Ch2opt_mKATE construct, recovery period can be considered the dominant determinant of stimulation frequency. The relationship found between recovery period and delay to AP shows that alteration of the recovery period will scale the minimum necessary illumination time in an inverse fashion. The total memory of the protein, or the recovery period necessary to completely erase the effects of a prior flash, has not been determined exactly, but is at least 800 ms. This does not mean that stimulation frequencies are limited to 1.25 Hz, but means that there will be variation in the exact spike to spike time at higher frequencies due to the fluctuating delay to AP. The standard deviation of this fluctuation in a series of spike trains with 96% success rate was 8 ms. At the presumed 17 Hz maximum stimulation frequency, this would amount to 14% variation from spike to spike, though the variability may increase with decreasing recovery period. Additional samples are needed to confirm this.

6.3 Importance of Illumination Area

A restricted illumination area has advantages for specific cell targeting and timed multi-site stimulation with light. It also removes the variable of cell size from the determination of currents achieved. Therefore for sub-cellular illumination spots, current is determined by the amount of protein expressed in the membrane, the dynamics of the protein, the illumination intensity and area, and the intracellular and extracellular ions.

The likelihood of laser spot illumination depolarizing cardiomyocyte-like cells or neurons to cross the AP threshold was shown to be strongly influenced by illumination spot size in Sections 5.1 and 5.2. In the current setup, the laser coupling through the microscope optics allows ease of use and targeting ability. However, it also makes the illumination area dependent on the focal plane of the microscope and the objective's focal volume. Stimulation of transfected HL-1 with the HXP light source was possible when the entire cell surface was illuminated. This light source has a theoretical intensity of 14 mW/cm^2 with the filter set used. This is far lower than the 50-3000 mW/cm^2 typically used to stimulate cells with Channelrhodopsins [65, 132, 28, 63, 17, 19]. The only report of similar intensities being used is from Sugiyama who stimulated transfected HEK cells with 12 mW/cm^2 illumination [148].

Previous work with Ch2_K315_YFP in this institute showed that the level

of depolarization without triggering an AP was continuously scalable with increasing laser intensity up to maximum power output of the laser setup [76]. This means that with the small focal point (4 μm $\varnothing$), the boundary between light induced channel opening and light induced membrane damage could not be distinguished. Therefore, it is desirable to work with intensities known to be well tolerated by the cells. For example, the 40% power output with 4 μm $\varnothing$ spot size was applied repeatedly to beating HL-1 cultures for more than 30 minutes without observed degradation of performance as would be expected from membrane damage. It also raises the question of how long cells could survive being stimulated with the high illumination intensities more commonly used with Channelrhodopsins. It is therefore preferable to maintain low illumination intensities and increase the illuminated area of CH2opt_mKATE expressing cells.

One approach to increase the area illuminated would be to scan the laser spot over the surface of the cell. This may allow activation of APs while maintaining spatial precision of illumination. The disadvantage to this approach is that it would add time to the required illumination period. As shown in Section 5.2 and discussed in Section 6.2, the recovery period of Ch2opt_mKATE limits the frequencies of attainable stimulation. Therefore, the shorter the illumination period necessary to trigger an AP, the larger the range of physiologically relevant AP frequencies can be stimulated. An alternative to scanning the laser spot would be to use a light source that does not pass through the microscope optics (i.e. illumination from below through an optically clear substrate). This would allow a column of illumination without a restricted focal volume. There would not be the dependence on the focal plane of the microscope, and curvature of the membrane would add channels to the illumination volume instead of bringing channels out of the focal plane. This approach would also allow more accurate determination of the power density in the illuminated area than the current method of defocusing the laser spot prior to the targeting mirror. It would of course also mean that for use with extracellular recording, the recording device would have to be specifically optimized for lack of light sensitivity, see Section 6.5.1, and optical clarity in the excitation wavelength.

6.4 Diamond SNR

It was shown (Chapter 3) that MEAs made with BNCD electrodes performed statistically at least as well as planar gold MEAs of equal electrode size in terms of SNR. Furthermore, it was seen that MEAs with BNCD electrodes and NCD passivation have the ability to achieve very high SNRs (over 35). If production of these devices can be standardized, an improvement of approximately four fold is expected over planar gold devices. Here, the discussion will focus on the possible sources of such a high SNR.

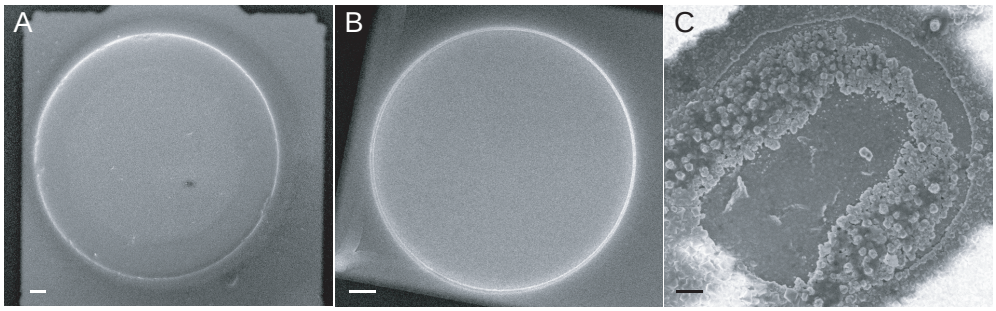

Figure 6.1: The surface of effectively cleaned diamond electrodes with diamond passivation compared to other electrode materials. (A) Planar gold MEA as processed in the cross structure (Section 2.2.1). Photo by S. Eick. (B) Planar gold MEA as processed in Bonn. Photo by D. Brüggemann. (C) DREAMS4 chip with good performance after cleaning. All scalebars represent 2 μm.

6.4.1 Effect of Roughening

One source of the improved SNR in successfully cleaned DREAMS4 chips may be roughening of the electrode surface. "Planar"gold MEAs produced by the University of Bonn have a better SNR than those originally produced by this institute (10.9 vs. 5.3, respectively). While some of this difference may be attributed to changes in the feedline layout from cross to star shaped to make all feedlines similar length, the dominant difference is in how the electrodes were patterned. The Bonn chips were patterned by reactive ion etching (RIE) instead of a liftoff process, which can leave the electrodes rougher. Studies on nanostructured gold [31] further support that a textured electrode surface achieves a better SNR.

In particular for the DREAMS4 chips, a dispersion of ND particles on the surface of the electrode would lead to a differential etching of the electrode surface during the oxygen plasma cleaning step. Irregularities in the electrode surface can be seen in the chips that were cleaned and showed improved SNR (see Figure 6.1).

6.4.2 Effect of Etching

The etching of the oxygen plasma is not limited to the electrode surface during the cleaning proceedure. This means that the passivation NCD is expected to be etched away by at least the 70 nm of ND seeds that were to be removed. In the ideal case of removing only the NDs and not etching deeper into the BNCD electrodes, the plasma would have reduced the passivation from 400 nm to 330 nm of NCD. Therefore, the volume of the diamond cleft over the electrode is 100 μm^3 instead of the 470 μm^3 produced by SU8 or ONO passivation (assuming a flat membrane sealing the top of the cylinder at the height of the passivation). Even if the plasma etch over etched the

NDs and began to remove chip material, etching beyond the NDs is expected to reduce the electrode and the surrounding passivation at a similar rate, so that the volume of the cleft would then remain constant. The smaller the cleft, the larger the impact of a single charge moving into or out of the cleft, and therefore the larger the signal expected.

The difficulty in achieving thin, yet completely sealed, passivation layers with other biocompatible materials (i.e. SiO_2 or SU8) usually prevents the use of such thin passivtion layers as was achieved with NCD. The lack of pinhole signals from DREAMS4 chips suggests that even at one fourth the typical passivation thickness the NCD passivation is well sealed. However, pinhole recorded signals can also be larger than electrode recorded signals (see Figure 3.7 for DREAMS3 chips with pinholes). This can also be due to the reduced cleft volume into which ions flow, and can be compounded by tight sealing of the cell to the entire opening of the pinhole (estimated area of the cell in close contact with the planar surface is 60 μm^2, calculated from [159]). MEAs have been designed to maintain a large electrode size with an aperture that could theoretically be completely in close contact with the cell by introducing a nanocavity between the passivation and the electrode. Nanocavity chips with 30 μm diameter electrodes and 40 μm^3 cleft volume [77] achieved SNRs comparable to the best plasma cleaned NCD passivated diamond MEAs.

The oxygen plasma may in fact combine the effects of reduced cleft size and larger electrode surface. The larger surface is achieved by the roughening of the surface, and the reduced cleft size by the etch.

6.4.3 Production Consistency

Some parameters of MEA production are inherently more inconsistent in diamond MEA production than in metal MEA production. For example, diamond deposition results in a thicker diamond layer in the center of the three inch wafer than at the edges, whereas metal MEAs can routinely be processed on eight inch wafers with little variation from one position to the next. The diamond MEAs in this work were therefore processed in groups of four MEAs per wafer. This proximity from MEA to MEA and disuse of the edges of the wafer should have given the greatest reproducability possible. However, this resulted in generally low numbers of chips. Prior to the confirmation that the devices do not degrade from culture to culture, achieving low standard deviation of measurements on a small number of devices is difficult, particularly when the biological measurements add an additional source of spread. Future production may take advantage of wafer rotation or movable screens to grow larger batches of diamond at consistent thicknesses.

Avoidable sources of production consistency stemmed from different production partners using their standard methods for different parts of the de-

vice production. Some of these processes were originally designed for high throughput while others were intended for specialist applications, some material processes were aimed at high quality material but with a high percent variation in material quality, while other processes produce lower quality material but produce it more consistently. For this reason, the expansion of diamond MEA use should involve the development of a dedicated production process, either in a single location or across collaborators but with processes specifically designed to fit together in the production run.

Furthermore, the state of a substrate should be confirmed each time it changes production partners. A standardized wafer history sheet to travel with the material is also advisable. This should prevent assumptions about results when partners use similar but not identical processes. For example, this would have prevented the seed NDs on the DREAMS4 MEAs (see Section 3.5.3) from being left behind by the etch. The promising results obtained in the rare cases of successfully cleaned fully diamond MEAs suggests a dedicated production process is worth pursuing.

6.5 Compatability of the Methods

After parallel optimization of light stimulation and diamond electrode devices, their use as complimentary technologies was tested. This came with the surprising result that the chips with the best signal to noise ratios, and therefore the most promising for detecting neuronal action potentials, were themselves the most sensitive to light. The implications of this are discussed in this section.

6.5.1 Light Effects on MEAs

In order to bring together light stimulation and MEA recordings, a MEA configuration must be found that does not have NCLEs which obscure cell signal and that is sensitive enough to detect neuronal signals. An offset due to illumination would not be a problem if its onset was fast enough and its magnitude small enough that the baseline compensation of the amplifier could bring the recording to baseline before the AP is triggered (or arrives, for the case of propagating signal). In contrast, slow onset NCLEs distort the cell signals and high amplitude NCLEs may mask the AP's presence. This section addresses what was found to be unsuitable for combined neural MEA recordings and optogenetic stimulation, followed by promising results where further chip development may allow clear extracellular recordings in the presence of varying illumination.

Sources of NCLEs

The irregularity of the HXP induced NCLE suggests that it is not only related to illumination intensity changes on the chip. This may involve disturbance of the setup as a whole due to manual switching applied, or to inconsistent movement of the shutter when manually operated. The long duration of changing NCLE is also less desirable than an NCLE that quickly reaches a steady state and can then be compensated for by the baseline correction. Therefore, it is preferable to use spot illumination, in this case available via the laser. The rest of the NCLE discussion will focus on physical sources of NCLEs with the aim of minimizing them in chip design.

The chips most sensitive to NCLEs were those with dark surfaces and high surface area contacts between two materials. Porous platinum applied to nanostructured gold showed the strongest NCLEs, with the amplifier going in to saturation from even low light levels. Since platinizatoin and surface structuring are the two major means of improving neuronal signal detection, it suggests utilizing the reduced cleft volume discussed in Section 6.4.2 could be an alternative for chips intended for optogenetic investigations. Optically clear substrates also perform better in terms of low NCLEs, and would furthermore allow illumination from below. While Borofloat glass has been investigated with planar gold electrodes for NCLEs, flexible substrates such as polyimide should also be tested. NCD passivated BNCD electrodes could also be tested on the clear substrates to eliminate the possibility that the interactions are between the light and the substrate. In this case alternative adhesion layers to $TiSi_2$, such as gold, should be tested.

DREAMS2 and 3 Light Resistance

Surprisingly, DREAM2 and DREAMS3 chips showed very little response to light. Their performance over the DREAMS1 design has been linked to better electrical contact between the silver glue and the $TiSi_2$ than to the BNCD. However, their lower light sensitivity compared to the DREAMS4 chips suggests a role for the passivation layer in light sensitivity. Though the NCD passivation has a much lower conductance than BNCD, the grain boundaries of the diamond allow sp^2 phases, which may act as hopping points for charge carriers. This combined with the NCD's high optical clarity may be the source of the increased NCLE on DREAMS4 chips. If the DREAMS3 design were produced without pinholes, this would be a suitable chip for optogenetic neural studies on MEAs, even though it does not perform as well in SNR as the DREAMS4 design. Furthermore, roughening of the non-diamond passivated BNCD electrodes could improve the SNR of these chips, as would reduction of cleft height, for example by alternating very thin layers of Si_2N_3/SiO_2 to maintain a tight seal.

6.6 Summary

A novel Channelrhodopsin2 construct, Ch2opt_mKATE, has been introduced and has shown the importance of recovery dynamics in optogenetic construct design. With this construct, reliable stimulation can be achieved with a sub-cellular illumination spot, though the exact area of the membrane illuminated has proven critical for the success rate. Furthermore, diamond MEAs have shown the ability to reach fourfold higher signal to noise ratios than planar metal MEAs, while maintaining sizes and bandwidths suitable for single cell recording.

Finally, it was shown that parallel optimization of MEA and optogenetic technology has resulted in a divergence of compatability instead of an exploitation of complementarity. The principles of improved diamond MEA recordings learned from the DREAMS4 chips should therefore be applied to new diamond MEAs that are specifically designed for optogenetic studies. The roughened BNCD electrodes on clear substrates with thin and well sealed passivation layers are expected to have suitably low NCLEs for optogenetic use, while achieving high enough SNRs for neuronal signal analysis.

Chapter 7

Zusammenfassung

Obgleich die Neurowissenschaft ein hoch entwickeltes Forschungsgebiet ist, sind noch immer viele Fragen bezüglich der Informationsverarbeitung in mittelgroßen Netzwerken elektrogener Zellen offen. Solche Experimente, die die bidirektionale Kommunikation mit Einzelzellauflösung untersuchen, stellen hohe Anforderungen an die zeitliche Genauigkeit, Stabilität und Unschädlichkeit des Verfahrens. Ein möglicherweise geeignetes Paar von Werkzeugen, das für diese Untersuchungen entwickelt werden kann ist die optogenetische Stimulation und die Messung über extrazelluläre Mikroelektroden. Dieses Paar besitzt sich ergänzende Eigenschaften, die der Flexibilität bei der Stimulation zum einen, und die der örtlichen und zeitlichen Auflösung bei der Messung zum anderen. Beide Felder können von Neuentwicklungen profitieren.

Verbesserte Stabilität, Biokompatibilität und Transparenz im Optischen machen Diamant zu einen guten Kandidaten fr die Entwicklung von neuen extrazellulären Mikroelektroden. In dieser Dissertation wird zunächst die Leistungsfähigkeit von Mikroelektroden Arrays verschiedener Entwicklungsstufen, hergestellt aus borgedoptem nanokristallinem Diamant untersucht und bewertet. Es wird gezeigt, dass diese Chips die Fähigkeit besitzen, Signale, mit einem Signal zu Rauschen Verhältnis ähnlich oder besser dem von Metallelektroden, zu detektieren. Ein hohes Signal zu Rausch Verhältnis wird erreicht, obwohl die Elektroden nicht vorsätzlich mikrostrukuriert wurden und sie Abmessungen aufweisen, wie sie für Einzelzell Messungen notwendig sind.

Zweitens werden die Ergebnisse von Untersuchungen meherer optogenetischer depolarisierender Proteine, die aus der Literatur bekannt sind, im Zusammenhang mit dem neuen, das heißt in Rahmen dieser Arbeit erschaffenen, Ch2opt_mKATE, einer Variante von Channelrhodopsin 2, präsentiert. Es wird gezeigt, dass Zellen die mit Ch2opt_mKATE transfiziert wurden, eine höhere Überlebensrate auf weisen, als Zellen die mit verschiedenen anderen Channelrhodopsin 2 Varianten transfiziert wurden. Darüber hinaus

besitzt Ch2opt_mKATE Kanaldynamiken die für eine Vielzahl von Anwendungen geeignet sind. Dies steht im Gegensatz zu publizierten Varianten, bei denen eine Eigenschaft zu Lasten der Gesamteigenschaften optimiert wurde, zum Beispiel wurden höchste Ströme durch verlangsamte Kanaldynamik erkauft.

Drittens wird die Anwendbarkeit von Ch2opt_mKATE durch den Einsatz in zwei elektrogenen Zelltypen evaluiert. Hierbei wird im Gegensatz zu den oft diskutierten "on" und "off Kinetics" und den höchsten beobachteten Strömen des Kanals, festgestellt, dass die beleuchtete Fläche sowie die Dunkel-Erholungszeit die kritischen Faktoren sind, die die dauerhaft mögliche Stimulationsfrequenz bestimmen. Es wird gezeigt, dass Stimulation mit einer beleuchteten Fläche von sub-zellulärer Größe möglich ist, die Wiederholbarkeit der Stimulation aber von einer Beleuchtung die sich nicht nuf auf ein kleines Fokusvolumen beschränkt, profitieren würde.

Die nachstehende Arbeit beschreibt eine Parallelentwicklung die sowohl die optogenetische Stimulation, als auch die Mikroelektroden Array Messung um ein neues Protein bezeihungsweise ein neues Material erweitert. Die zukünftige Intergration dieser beiden Techniken, um eine dauerhafte nicht-invasive Kommunikation mit elektrogenen Zellen zu erreichen, macht eine konsolidierte Optimierung notwendig.

Chapter 8

Summary

Though the study of neuroscience is an advanced field, there remain many questions to be answered about information processing in mesoscale networks of electrogenic cells. This is because such investigations require temporally precise, robust, and non-damaging bi-directional communication with single cell resolution. One possible pair of tools that can be developed towards this end is optogenetic stimulation and extracellular electrode recording. This pair has the complimentary traits of flexible stimulation and spatio-temporal precision of recording, and both fields can benefit from new developments.

Improved stability, biocompatibility, and optical clarity make diamond a good candidate for development of new extracellular recording electrodes. This thesis first evaluates the performance of micro electrode arrays made from boron doped nanocrystalline diamond through several design iterations. The devices' ability to detect cell signals with signal-to-noise ratios comparable to, or better than achieved with metal electrodes is shown. A high signal-to-noise ratio is achieved despite the electrodes not being intentionally micrstructured, and having dimensions suitable for single cell resolution recordings.

Second, the evaluation of several optogenetic depolarizing proteins from literature, as well as the novel Ch2opt_mKATE variant of Channelrhodopsin2 is presented. Ch2opt_mKATE is shown to have better viability than several other Channelrhodopsin 2 constructs. Furthermore, Ch2opt_mKATE posess channel dynamics that make it suitable for a range of applications. This is in contrast to published variants, which sacrafice performance in one area to be the best in another, such as achieving the highest currents reported at the cost of channel kinetics.

Third the use of Ch2opt_mKATE is evaluated in two electrogenic cell types. Here it is found that contrary to the oft-discussed on and off kinetics of the channel, or peak currents passed, it is illumination area and dark recovery period that are the critical factors for determining the frequency

of maintainable stimulation at the single cell level. Stimulation is shown to be possible with subcellular illumination areas, but would benefit from illumnination not restricted to a small focal volume.

The included work shows that a parallel development approach has advanced both the techniques of optical stimulation and MEA recording with new materials. Going forward, integration of these techniques for long term non-invasive interfacing with electrogenic cells requires consolidated optimization.

Chapter 9

Acknowledgments

Prof. Andreas Offenhäusser - Thank you for the opportunity to work in a challenging and inspiring environment. The institute achieves a rare integration of disciplines that has taught me much more than any project alone could.

Prof. Hermann Wagner - Thank you for providing an intellectual link to the University, and for helpful discussions on this work.

Prof. Frank Müller - Thank you for being my BioSoft supervisor and for reminding me to find the biological question.

Prof. Arnd Baumann - Thank you for all of the technical support to bring molecular genetics into a physics lab, and for reading base code with the skill that one can only gain with experience.

IHRS BioSoft and DREAMS - I would like to thank the International Helmholtz Research School BioSoft and the EU project DREAMS for funding my studies and the diamond materials respectively.

Klaus Peter - You got me through it and exacted very little revenge along the way.

Boris - For being a good teacher, a good lookout, and a good friend, thank you.

Rita - We never knew how good we had it until it was gone. Thanks for keeping us in line.

Marko - Danke für alles was ich aus dem Reinraum gebraucht habe.

Stefan, Michael, Jan E. - Thank you for patiently and carefully explaining electronics to someone who can read a plasmid map better than a wiring diagram.

Nils, Sandra, Francesca, Silke, Philipp, Alexandre, Alexey, Dzmitry, Janis, Enno, Jan S., Martin (in spatial order) - You're all a big part of why thank you number one is possible, and you mean that the early starts aren't so bad.

Kristin and Simone You have taught me things I never knew I should seek to learn.

Sven - Thank you for instilling a healthy sense of doubt.

James - I shall never fear an audience more than your questions. That makes presenting a lot easier, thank you.

Maurice - Thank you for pushing me to get out. I owe that I headed here to you.

Maren & Jessica - Ihr habt eine ausgezeichnete Zukunft vor Euch. Danke für Eure Hilfe in der Vergangenheit.

For all of the help hauling bidest, lifts to the RTB, decons, putting tools back where they were found, driving the fork lift, third hands for the filter carousel, trips to the Tierhaus, co-prepping, sharing your last backup aliquot, and translating, thank you. There are too many of you to match individually to those.

IBN-2, ICS-8, PGI-8 and every other name change that may be imposed - regardless what what they call the institute there is greater possibility for camaraderie and collaboration than any other academic institution I've been at. Thank you all for making it that way.

David, Inke, Simone - Thank you for being such good neighbors.

Dorothea - Thank you for the control chips.

Werkstatt and E-Werkstatt, Vielen Dank für Eure technische Hilfe, haupsächlich bei dem Aufbau des neuen Messsetups.

Thorsten - Thank you for listening to all our comments about the BioSoft program and always taking an interest in making it a better school. We will all not only benefit from our participation in the program, but from the program's continued growth.

Mom and Dad - I never would have made it this far without your support, especially for allowing the distances involved. I have you with me always.

John - We choose to make our mark in very different ways, but I look forward to celebrating yours with you.

Appendix A

Materials List

This Appendix first lists the suppliers of materials used, followed by mixtures specific to this work. Standard buffers and reagent mixtures are as can be found in [137].

A.1 Suppliers and Materials

Materials aside from those listed below are from Sigma-Aldrich GmbH. Equipment not listed was built in-house.

Material	Specifications (if necessary)	Supplier
Fetal Bovine Serum	EU Approved Origin South America	Invitrogen
Neurobasal™ Medium	[-] L-Glutamine	Invitrogen
Amaxa® Rat Neuron Nucleofector® Kit		Lonza
fluo-4 AM	dilute to 1 μg/μL in DMSO for use	Invitrogen
L-Glutamine	200 mM	Invitrogen
Pen Strep	10,000 Units/mL and 10,000 μg/mL respectively	Invitrogen
B-27 Supplement		Invitrogen
Trypsin EDTA	0.05%	Invitrogen
hydrogen hexachloroplatinate(IV)		Fluka
Fugene® HD		Roche
silver glue		EpoTek
epoxy	U300 and U302	EpoTek
Helmanex		Fisher Scientific

Table A.1: Material Sources

Equipment	Manufacturer
Axio Scope	Carl Zeiss GmbH
HXP illumination source	Carl Zeiss GmbH
Micromanipulators	Luigs & Neumann GmbH
Optical Filters	AHF Analyse Technik GmbH
NIDAQ	National Instruments
Nucleofector 2b	Lonza
Plasma Oven	Diener Electronics
SEM	Carl Zeiss GmbH
Apotome	Carl Zeiss GmbH
Fineplacer	Finetech

Table A.2: Equipment Sources

A.2 Reagent Recipies

Specific mixtures and solution compositions are given here. Supplements to culture media are listed seperately in Table B.13.1, as they contain a commercially available media as a base solution, rather than something made entirely by the user.

A.2.1 GpECM

GpECM is the coating nearly determined in this work to allow coating surfaces without activation. The gelatine works by an unknown mechanism to allow adhesion of the proteins to the surface. Tests with concentrations of gelatin down to half of that used in this thesis were able to support neurons, but the ratio here was found to have results most similar to pECM coatings on activated surfaces. Higher concentrations were not tested, as the goal was to be able to use pre-established plating densities on fragile substrates. Combine 0.02% Gelatin in Bidest : PDL : ECM gel : GBSS in the ratio of 2:1:1:100.

A.2.2 Patch Solutions

Patch solutions are either intracellular or extracellular. Intracellular patch solution is used to fill patch pipettes used for whole cell configuration patch clamp experiments. Intracellular patch solution is temperature sensitive due to the Mg-ATP in it and should not be re-frozen or used after the day of thawing. Extracellular patch solutions are exchanged for the culture media at the time of the experiment. Extracellular patch solution is more stable than intracellular patch solution but should always be adjusted to the osmolarity of the culture, as measured immediately before exchanging the solution for the media.

	Intracellular Solution	Extracellular Solution
NaCl	2 mM	120 mM
KCL	120 mM	3 mM
$MgCl_2$	4 mM	1 mM
Hepes	5 mM	10 mM
$CaCl_2$	-	2 mM
EGTA	0.2 mM	-
Mg-ATP	4.3 mM	-

Figure A.1: The composition of patch solutions dissolved in water. Intracellular patch solution is adjusted to pH 7.3 with 1 M KOH. Extracellular patch solution is adjusted to pH 7.3 with 1 M NaOH. Osmolarity of the extracellular patch solution is matched to that of the media with glucose immediately before the experiment.

A.2.3 Midi-Maxi Prep Solutions

Solutions I, II, III are used for Protocol B.11 and are based on the original protocol published in [137]. The specific adaptations used here are those recommended by A. Baumann (Forschungszentrum Jülich).

Solution I	Solution II	Solution III
50 mM Glucose	0.2 mM NaOH	60 mL 5M KAc
25 mM TrisHCl pH 8.0 (autoclaved)	1% SDS	11.5 mL Acetic Acid
10 mM EDTA		pH to 4.8 with HCl and fill to 100 mL with H_2O

Table A.3: Solutions for preparing plasmids from bacteria.

Appendix B

Protocols

B.1 Cortex Preparation

This protocol is performed under sterile conditions. Cortical neurons are prepared from E18 Wistar rat embryos, mechanically dissociated, and plated onto *in vitro* growth substrates by the following protocol:

1. Remove brain in 1.5 mL $HBSS^-$ on ice.
2. Isolate cortex without dura and transfer to 7 mL $HBSS^-$ in a 15 mL Falcon tube. Pool as many cortices as necessary, always storing on ice.
3. Reduce the volume of $HBSS^-$ to 1 mL per brain.
4. Mechanically dissociate cells with a silanized, fire polished, glass pipette.
5. Add two volumes $HBSS^+$ and allow to settle for 3 min on ice.
6. Transfer the top half, to two thirds, of the preparation to a clean tube.
7. Centrifuge at 200 g for 3 min.
8. Aspirate HBSS and resuspend pellet in 1 mL supplemented NB media.
9. Dilute trypan blue 1:2 in NB media, then add 1 volume of cell suspension for live dead staining. The final mixture is 1:2:1, trypan blue:NB:cell suspension. 25 μL is the standard volume for trypan blue.
10. Count live (not blue) cells in a Neubauer chamber and dilute to appropriate plating concentrations in NB. Distribute to substrates.
11. Let substrates stand at room temperature for 10 min, then transfer to a 37°C 5% CO_2 humidified incubator.
12. After 1-4 hours of adhesion, aspirate media and replace with fresh NB. Then change half of the media every 3-4 days.

B.2 Care of HL-1

This protocol is performed under sterile conditions.

1. HL-1 are maintained in supplemented Claycomb's media. Cultures should be a confluent contracting layer when split.

2. Aspirate media, and rinse cells once with 1 mL trypsin EDTA, aspirating as quickly as possible.

3. Add 1 mL trypsin EDTA and incubate at 37°C for 5 min.

4. Add 5 mL Claycomb's media and break up any remaining cell clumps by pipetting up and down. Transfer suspension to a 15 mL Falcon tube.

5. Centrifuge 5 min at 500 g.

6. Aspirate liquid and resuspend pellet in 4 mL supplemented Claycomb's media.

7. Plate desired number of cells (see Section C.1). For cells plated into culture flasks, return the culture to 37°C 5% CO_2 humified incubator and change the media every day.

8. For chips, plate cells in the inner ring or funnel at low volume (30-100 μL) and allow to adhere for 2-4 hours at 37°C 5% CO_2. Then top up chips with media.

9. For weekends, split cells on Friday and fill the culture flask with double the normal amount of media. Feed cells again Monday morning.

B.3 Care of HEK 293

This protocol is performed under sterile conditions.

1. Cells are maintained in culture flasks with DMEM media supplemented with FBS and antibiotics. Media is changed every other day.

2. Split cells at 80% confluence.

3. Aspirate media and rinse once with 1 mL trypsin EDTA.

4. Add 1 mL trypsin EDTA and incubate 3-5 min at 37°C.

5. Add 5 mL supplemented DMEM and loosen cells from the flask by pipetting.

6. Transfer the cell suspension to a 15 mL Falcon tube and centrifuge 5 minutes at 300 g.

7. Aspirate the liquid fraction and resuspend the pellet in 1 mL supplemented DMEM.

8. Count cells and dilute to the desired plating concentration in supplemented DMEM.

9. Plate in the final volume on PLL coated substrates for experimental use or plate into tissue culture flasks

B.4 Care of HEK ChR2

This protocol is performed under sterile conditions. Note these cells have a very high rate of division in the repressed state, and need frequent splitting when kept in working culture.

1. Cells are maintained in culture flasks with supplemented Ion Gate Media, and media changed every other day.

2. Split cells at 80% confluence.

3. Aspirate media and rinse once with 1 mL trypsin EDTA.

4. Add 1 mL trypsin EDTA and incubate 3-5 min at 37°C.

5. Add 5 mL supplemented Ion Gate Media and loosen cells from the flask by pipetting.

6. Transfer cell suspension to a 15 mL Falcon tube ad centrifuge 5 minutes at 300 g.

7. Aspirate the liquid fraction and resuspend the pellet in 1 mL supplemented Ion Gate Media.

8. Count cells and dilute to the desired plating concentration in supplemented Ion Gate Media.

9. Plate cells in the final desired volume onto 10-100 μg/mL PLL coated substrates.

10. Grow cells at 37°C 5% CO_2 in a humidified incubator. Do not change to activated supplemented Ion Gate Media for at least one day.

11. To induce expression of channelrhodopsin, change media to activated supplemented Ion Gate Media. Cells will express within 24 hours. Most will subsequently die within a further 48 hours.

B.5 Amaxa Electrofection

This protocol is performed under sterile conditions. The electrofection protocol presented is that optimized for use with TO_Ch2opt_mKATE and primary cortical rat neurons. It is also effective on re-suspended tissue culture cell lines, but further optimization for the specific cell type may improve performance. This protocol was used for experiments described in Chapter 4 and 5.

1. Prepare a transfection cuvette with 7-9 μg plasmid DNA in MilliQ water.
2. Pellet the cell suspension (i.e. step five in HL-1 splitting Section B.2, or step seven in cortex preparation Section B.1). For neurons use one brain's cortex.
3. Resuspend cells in 200 μL of supplemented transfection solution from the Amaxa Nucleofection Kit, and transfer to the transfection cuvette. Tap gently to mix.
4. Quickly transfer the closed cuvette to the Amaxa electrofection device and run program G-013 "Neurons, Chicken DRG". When the program is finished return the sample to the sterile bench.
5. Quickly add 1 mL RPMI recovery media and gently mix.
6. Use the provided pipette to transfer the cells to a Falcon tube. Rinse the cuvette with 1 mL RPMI for a further three times, pooling all washes together. Minimize pipetting of individual cell suspension fractions.
7. Count the number of live cells as in Cortex Preparation B.1 step nine.
8. Dilute cells to the desired concentration in RPMI and plate onto substrates.
9. Allow samples to stand at room temperature for 10 minutes, then move to a 37°C 5% CO_2 humidified incubator.
10. After 4 hours of adhesion time, change the media to supplemented NB media. Change half of the media every 3-4 days using supplemented NB media.

B.6 FugeneHD® Transfection

This protocol is performed under sterile conditions. The concentrations shown work well for CUCY and Ch2opt_mKATE plasmid in HL-1 cells or

Component	Amount
Media	225 μL
DNA	8-10 μg
Fugene® HD	12.5 μL

Table B.1: An example of the FugeneHD® transfection mix, suitable for 9 coverslips in a 24 well plate.

neurons and TO_Ch2opt_mKATE in HEK293 cells. Other plasmids or cell lines may require optimization.

1. Prepare the cell type's respective growth media without serum, B-27, or antibiotics.

2. Add the DNA to the media and mix by pipetting up and down, see Table B.1 for amounts.

3. Add the Fugene®HD to the middle of the fluid in the tube, minimizing contact with all plastics.

4. Mix by tapping the tube.

5. Incubate 15 min at room temperature.

6. Add the transfection mixture to adherent cultures, see B.1, using 25 μL mix per 0.5 mL media.

7. Gently swirl cultures to mix and return to standard culture conditions.

8. Change media to standard culture media for the cell type after 24 hours. Continue feeding as usual for the cell type.

B.7 Chip Encapsulation

This protocol is not performed under sterile conditions. A detailed protocol of the standard encapsulation process is provided here to supplement the overview in Section 2.2.2. For specific differences used for special chips see Section 3.1.2 and 2.2.2.

1. Punch out the desired number of PCB carriers and file sides flat and inner hole so that the 9 mm ⌀ glass rings pass through easily.

2. Prepare Epotek silver glue in a 1:1 ratio on a glass substrate using two toothpicks or small pipette tips. Use as little silver glue as possible.

3. Align the PCB carrier under the screenprinting foil in the plastic holder. Place a thin line of silver glue to the far side of the holes on the screen. Press the rubber scraper flat against the foil at a 45°angle and pull towards yourself in one smooth stroke.

4. Scrape excess glue off the rubber scraper and pool with remaining glue.

5. Lift the screen and check the carrier for shorts or misses. A second pass with the screen printer cannot be made once glue is on the carrier. If there are a small number of contacts without glue they can be hand spotted using the toothpick or pipette tip. If there are shorts or many misses, clean the carrier with 70% ethanol and repeat screenprinting in a clean set of holes.

6. Clean the screen after printing the glue using 70% ethanol and the toothbrush. Do not scratch the foil. Clean from both sides and wipe dry with a tissue. Do not use again until the foil is completely dry.

7. Pick up the chip with the fine placer on one of the left corners with the substrate towards the vaccuum and the MEA towards the table.

8. Align the PCB carrier glue side up under the chip, being sure to slide the microscope to the right to check one full side of the chip for the correct angle of alignment.

9. Move the microscope out of the way and bring the chips together with the fine placer. Release the vaccuum and with the vaccuum released, tap the chip on all four corners to assure even contact.

10. If the chip is on a clear substrate, check for shorts before baking. If shorts are present, separate the chip and carrier, clean both with 70% ethanol and begin again.

11. Bake chips 1 hour at 150°C.

12. Mix underfill epoxy. For most of this work including all diamond MEAs Epotek U300 at 1:10 curing agent:base was used. This product was then discontinued by the supplier. The now available Epotek U302 is used at 45:100 curing agent:base. Apply a thin layer of epoxy to the back of the PCB carrier along the edge of the chip using a toothpick. This should be sucked under by capillary forces.

13. Bake chips 1 hour at 150°C.

14. Spread 10:1 base:curing agent PDMS on a sheet of paper. Dip glass rings in the PDMS to coat the circumference. Stamp the ring once on a clean area of paper to ensure a complete circle of PDMS, remove

excess, and check there is no film of PDMS across the inner area of the ring.

15. Apply the 9 mm ring on the chip inside the hole in the carrier. Apply the 20 mm ring on top of the carrier centered at the MEA.

16. Bake 1 hour at 150°C.

17. Coat the area between the glass rings with a thin layer of 10:1 base:curing agent PDMS using a syringe with a 200 μL pipette tip.

18. (OPTIONAL) write labels to the outside of the ring and coat with a very thin layer of PDMS.

19. Bake 1 hour at 150°C.

20. (OPTIONAL) write labels on the back of opaque chips and coat with a thin layer of 10:1 base:curing agent PDMS. The underfill can also be protected with a thin layer of PDMS to increase the durability of the chips. Bake 1 hour at 150°C. This step is not advisable when stamping with large or stiff stamps later.

B.8 Chip Cleaning

This protocol is not carried out in sterile conditions. This is used for chips without fragile or chemically reactive surfaces.

1. Immediately after culture, rinse chips with 70% ethanol.

2. Rinse chips with water. Chips may be dried and stored at this point as long as desired.

3. Fill the chip with 70% ethanol and gently clean with a Q-tip.

4. Rinse with water.

5. Clean in an ultrasound bath of 2% Helmanex in bidest for 5 min.

6. Rinse excess Helmanex off with de-salted water.

7. Clean in an ultrasound bath of bidest for 5 min.

8. Dry in a stream of nitrogen.

B.9 Contactless Chip Cleaning

This protocol is not carried out in sterile conditions. This is used for chips with surface structures or reactive surfaces (see Sections 3.1.2 and 5.3).

1. Immediately after culture rinse chips with water.
2. Fill chips with trypsin EDTA and incubate at 37°C for at least 20 min. Preferably do not let the chips dry out.
3. Rinse with a stream of water, i.e. from a wash bottle.
4. Rinse with 70% ethanol, then with water. Chips may be dried and stored at this point.
5. Wash chips in 2% Helmanex in a rocking bath at approximately 50 rpm for one hour.
6. Rinse chips for 4 hours in flowing de-salted water.
7. Dry in a stream of nitrogen.

B.10 Protein Coatings

This protocol transitions from non-sterile to sterile work. See Table B.4 for the protein and concentration used for different applications.

B.10.1 Activation

Activation is possible with most MEA chips and single material substrates. There are variations using acid activation, but these were not utilized in this work and therefore are not listed.

Material	Activation Method	Requires Further Sterilization
metal MEA	5 min oxygen plasma 40% power 0.6 mbar	yes
diamond MEA	None	yes
glass cover slips	flame	no

Table B.2: Which activation methods are used for various types of substrates.

B.10.2 Sterilization

All materials must be sterile for tissue culture use. Not all materials can withstand the same sterlilization techniques.

Material	Sterilization Method
metal MEA	1 hour UV exposure
diamond MEA	70% ethanol for 1 min then sterile bidest rinse
glass cover slips	flame

Table B.3: How different substrates are sterilized.

Cell Type	Protein	Concentration	Solvent
HEK	PLL	10-100 μg/mL	HBSS
HL-1	Fibronectin/Gelatin	5 μg/mL and 2 μg/mL	bidest
Neurons	pECM	1:1:100	GBSS
Neurons on unactivated substrate	GpECM	2:1:1:100	GBSS

Table B.4: Substrate coating by cell type.

B.10.3 Protein

Protein is adsorbed to the surface for 1 hour at room temperature. The substrate is then rinsed once with the protein solution solvent to remove excess protein and aspirated dry.

B.11 Midi-Maxi Prep

The composition of Solutions I, II, and III are given in Table A.3. The volumes used are always to be based on the volume of material recovered in the previous step. The starting volume presented is for a normally growing 500 mL overnight *E. coli* culture.

1. Divide an overnight culture of bacteria and spin 15 min at 2000 g at 4°C.
2. For each 300-500 mL culture, resuspend pellets in 8 mL Bacto Solution I.
3. Add 2 volumes Bacto Solution II (16 mL). Mix.
4. Add 2 volumes Bacto Solution III (16 mL). Mix.
5. Spin 10 min at 4°C at 3800 g.
6. Filter the supernatant through filter paper.
7. Add 2.5 times the recovered volume of supernatant of isopropanol (under the filter).
8. Spin 10 min at 4°C at 3800 g.

9. Decant the supernatant and dry the tube with a tissue.
10. Resuspend the pellet in water and pool into two tubes with 2.9 mL each.
11. Add 5 mL of 4 M LiCl per tube.
12. Add 100 μL 1 M Tris HCl pH 7.5 per tube.
13. Spin 10 min at 4°C at 3800 g.
14. Collect the supernatant and transfer to a new tube.
15. To the volume of recovered supernatant, add 2.5 volumes of ethanol per tube.
16. Spin 10 min at 4°C at 3800 g.
17. Decant supernatant and dry the tube with a tissue.
18. Resuspend pellet in 500 μL Tris EDTA and digest with 3 μL RNAse A at 37°C for greater than one hour.
19. Perform three phenol - chloroform extractions, keeping the aqueous phase (usually the top).
20. Pool the DNA fractions and add 100 μL 3 M LiCl.
21. Add 3 volumes cold ethanol.
22. Spin 10 min at 4°C at 3800 g.
23. Dry the pellet and wash with 70% ethanol.
24. Dry the pellet and resuspend it in pure water.

B.12 CloneCheck

This protocol is not performed in the sterile bench, but good sterile technique is essential. This protocol is originally from James Baker (Kernan Group, University of Stony Brook).

CloneCheck Mix is 0.5% Triton-X and 2.5 mM EDTA in MilliQ

Enzyme Master Mix =
(1 μL buffer concentrate + 1 μL enzyme + 0.1 μL RNAse A) x (number of colonies)

1. Grow bacterial colonies overnignt on selective plates.
2. Prepare tubes with 6 μL sterile Luria Broth.

3. Prepare corresponding tubes with 8 μL CloneCheck Mix.
4. Flame a pipette tip and when it is cool pick an isolated colony into the 6 μL of Luria Broth. Pipette up and down to mix and transfer 3 μL into the corresponding CloneCheck Mix tube. Pipette up and down to mix.
5. Repeat 4 for the desired number of colonies.
6. Place Luria Broth tubes at 4°C for later re-streaking.
7. Boil CloneCheck tubes for 3 minutes. Then cool to room temperature.
8. Add 2 μL Enzyme Master Mix to each CloneCheck tube.
9. Incubate 20 min at 37°C.
10. Mix CloneCheck digestion with 2 μL Loading Buffer and add directly to an agarose gel with small wells.
11. Run gel, stain, and image as usual.

B.13 Media Supplements

B.13.1 Media Supplements by Cell Type

Cells	Media	Serum	Glutamine	Antibiotic	Other
HL-1	∗ 100 mL Claycomb's Media	11.2 mL FBS	1.14 mL	1.14 mL Penn/Strep	1.14 mL NorA
HL-1 TRex	⋆ 100 mL Claycomb's Media	11.2 mL FBS	1.14 mL	1.14 mL Penn/Strep 200 μL zeocin 50 μL blastocidin	1.14 mL NorA
Neurons	50 mL Neuro Basal Media	500 μL B-27	125 μL	50 μL Gentamycin	-
Electrofected Neurons	10 mL RPMI	100 μL FBS	25 μL	-	-
HEK 293	† 90 mL DMEM	9 mL FBS	-	1 mL Penn/Strep	-
HEK Ch2	‡ 90 mL DMEM	9 mL FBS	-	1 mL Penn/Strep 200,μL zeocin 50,μL blastocidin	-

Table B.5: Items to add to supplement growth media. ∗ media for HL-1 cells and ⋆ HL-1 cells using the TRex system to express Ch2opt_mKATE, † media for HEK cells and ‡ for HEK Ch2 cells in the repressed state "Ion Gate Media".

B.13.2 Activation Media

To standard growth media for the desired cell type, add:
1:100 Tetracycline stock (100 μg/mL)
1:1000 all trans-Retinal stock (optional) (1 mM in ethanol)

Appendix C

Calculations

A summary of calculations used for planning experiments and analysing data is presented. The related sections of the text are referenced under the title.

C.1 HL-1 Cell Number Determination

See also Appendix B.2.
The following calculation starts with a confluent T-25 flask of HL-1 cells with assumed normal growth rate (doubling approximately every 24 hours). The general formula for how many cells to re-plate is:

$$F = \frac{1}{2^{(d-1)}} \tag{C.1}$$

Where F is the fraction of the confluent T-25 flask plated into a new T-25 flask and d is the number of days the culture should grow before the next splitting.

When plating to chips, 50 μL of a 4 mL resuspension of a confluent T-25 flask should form a 7 mm $\varnothing$confluent and electrically active tissue on DIV4. This may be scaled for DIV3 and DIV5 assuming the 24 hour doubling rate, but deviations beyond this tend to be unhealthy on chip. Scaling for smaller chip surfaces is possible by area fraction, but the low volume of cells necessary should be plated into an initial volume of supplemented Claycomb's media to prevent the sample from drying during the adhesion period.

C.2 Channelrhodopsin Kinetics Calculations

See also Section 4.2.
The goal of the kinetic analysis was to determine how fast the population of channels responds to the flashes of light and becomes conductive. When

a single patch clamped HEK cell that expresses channels is exposed to a series of illumination flashes interspersed with periods of darkness, negative currents are observed in a shape similar to that shown in Figure C.1. The data analysis aims to extract how quickly the current reaches its plateau value, which is described by the opening kinetics τ_{on}. To determine τ_{on} a smooth current trace must be fit only in the region of channel opening, not in the region during the delay to opening or in the plateau. The calculations in this section start by describing how a smooth average current trace is established. Then, the boundaries of the region when channels are opening is defined in terms of the baseline and plateau. Finally, the extracted curve is fit with a single exponential decay and the value of τ_{on} is determined.

C.2.1 Baseline Correction

To determine the average current response of a cell to a series of flashes those flashes that are in steady state are baseline corrected to the average current of the 100 points immediately preceeding the laser flash. The raw data is always taken for this dark current. The preceeding dark current is subtracted from the current response for the trace from the onset of illumination to the onset of the next illumination. The responses are then aligned according to the beginning of the dark current region and the average is taken. This can be seen pictorally in Figure C.1.

This can be described as:

$f = 1, \ldots, N$ are the N events to be considered, or those flashes in the steady state.
$I_f(t)$ is the current of event f.
$t = 0$ is the time the flash starts
$t = t_e > 0$ is the time the flash ends.

Then the preceeding dark current is the case when: $-\Delta t < t < 0$ is the time interval of the dark current preceeding any given flash.
$I_f^d(t), -\Delta t < t < 0$ is the dark current preceeding flash f.
$\langle I_f^d \rangle = \frac{1}{\Delta t} \int_{-\Delta t}^{0} I_f(t)dt$ gives the average of the dark current, which is subtracted from the current of the event $I_f(t)$ to baseline correct it.
$I_f^c(t) = I_f(t) - \langle I_f^d \rangle, 0_f < t < 0_{f+1} - 1$ gives the baseline corrected current.

C.2.2 Extracting τ_{on}

One standard deviation (σ) of the current in the dark period preceeding the illumination gives the spread of the baseline, (the height of the red box in Figure C.1). This can be used to determine the onset of the light evoked current. The time from start of illumination to the onset of current is the delay to onset discussed in Section 4.2 and defines the start of the region to be fit for τ_{on}.

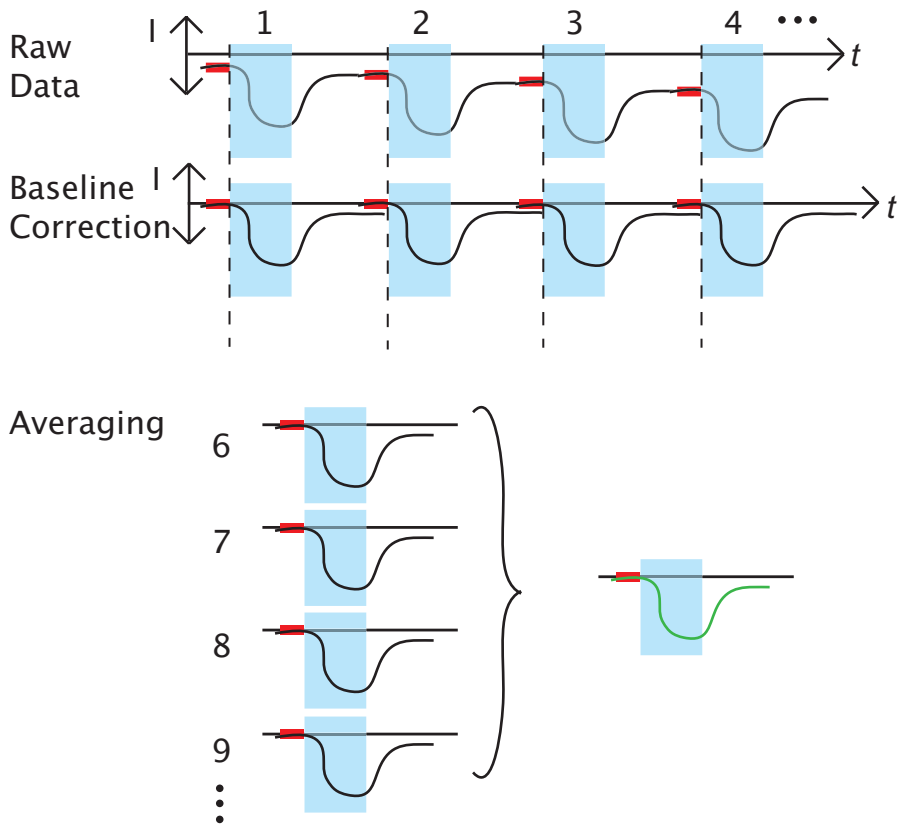

Figure C.1: A series of sequential illuminations (blue region) of a HEK cell expressing a Channelrhodopsin construct produces pulses of negative current (positive charge into the cell). This series is baseline corrected so that each response starts from zero using the preceeding dark phase (red). For averaging, only the flashes in steady state (after flash six) are considered. The responses are then aligned according to the beginning of the preceeding dark current and averaged from the beginning of the preceeding dark phase to immediately before the next illumination (average in green).

$(\sigma_f^d)^2 = \frac{1}{\Delta t}\int_{-\Delta t}^{0}(I_f^d - \langle I_f^d\rangle)^2 dt$ gives the variance of the dark current. The average spread of the baseline in the dark current was taken as: $\sigma^d = \frac{1}{N-1}\sum_{f=1}^{N}(|\sigma_f^d|)$

The baseline corrected current average is then defined as: $\bar{I^c}(t) = \frac{1}{N-1}\sum_{f=1}^{N} I_f^c(t)$

To determine the end of the interval to be fit for τ_{on}, the time when the plateau current $\langle I^p\rangle$ begins must be defined.

$\langle I^p\rangle = \frac{1}{\frac{1}{3}t_e}\int_{\frac{1}{3}t_e}^{\frac{2}{3}t_e}\bar{I^c}(t)dt$

As the dark current has a certain variance σ^d, so has the plateau a variance σ^p.

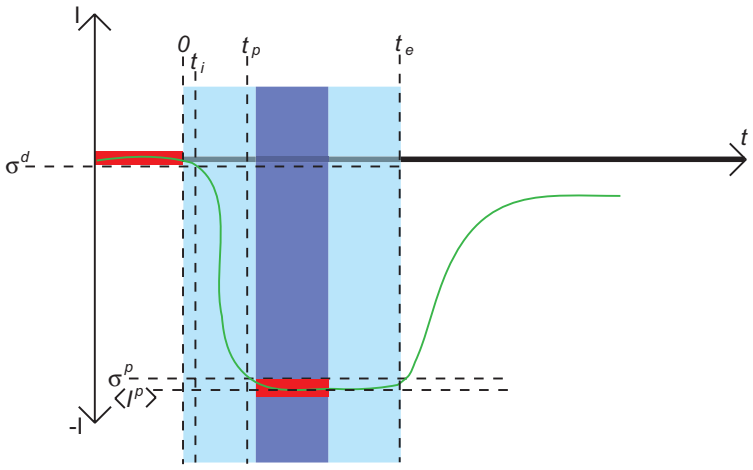

Figure C.2: The averaged current responses (green) to illumination (blue area from $t = 0$ to t_e) are plotted. The average plateau current ($\langle I^p \rangle$) is calculated using the current in the middle third of the illumination (dark blue). The average plateau current also has a spread, σ^p, similar to the spread of the baseline, σ^d. Both the spread of the baseline and the plateau are marked by the height of the red boxes. t_i denotes the onset of current and t_p denotes the onset of the plateau.

$(\sigma^p)^2 = \frac{1}{\frac{1}{3}t_e} \int_{\frac{1}{3}t_e}^{\frac{2}{3}t_e} (\bar{I^c}(t) - \langle I^p \rangle)^2$

The interval of interest for fitting τ_{on} is then defined as the region from the time of onset of current t_i to the time of reaching plateau current, t_p. These are the times when:

$\bar{I^c}(t_i) = \sigma^d$

$\bar{I^c}(t_i) = \langle I^p \rangle - \sigma^p$

τ_{on} is then determined by fitting the trace with the equation:

$\bar{I^c_{fit}}(t) = \langle I^p \rangle + |\langle I^p \rangle + \sigma^d| e^{\frac{t-t_i}{\tau_{on}}}$

This can be seen pictorally in Figure C.2.

Table C.1: Acronyms

Abbreviation	Description
AFM	Atomic Force Microscopy
AP	Action Potential
Arch	Archaerhodopsin-3
ATP	Adenosine Tri-Phosphate
BAPTA	1,2-bis-(2-aminophenoxy)ethane-N,N,N′,N′-tetraacetic acid
BNCD	Boron Doped Nanocrystalline Diamond
BPM	Beats Per Minute
CaTCH	Calcium Translocating Channelrhodopsin
CEA	Commissariat a l'energie atomique
Ch2	Channelrhodopsin 2
Ch2_K315_YFP	Plasmid encoding the first 315 amino acids of Channelrhodopsin 2 fused to YFP as generated by the Bamperg group
Ch2_mKATE_ssHK	Plasmid encoding the first 315 amino acids of Channelrhodopsin 2 fused to mutated Katushka and then to a chloride pump as generated by the Bamberg group
Ch2opt_mKATE	Channelrhodopsin 2 variant with H134R mutation, fusion to mutated Katushka, and export sequence
ChETA	Channelrhodopsin 2 mutant E123T Accelerated
ChIEF	Channelrhodopsin 1 and 2 chimera ChEF with mutation I170V
CMV	Cytomegalo Virus
CUCY	Plasmid encoding the CMV promoter, the hUbiC promoter, and Ch2_K315_YFP
DIC	Differential Interference Contrast
DIV	Days In Vitro
DMEM	Dulbecco's Modified Eagle Media
DNA	Deoxyribo Nucleic Acid
DPA	Days Post Activation
DPT	Days Post Transfection
DREAMS	Diamond to REtina Artificiall Micro-interface Systems
DREAMS1	BNCD diamond MEA with BNCD bond pads and SU8 passivation
DREAMS2	BNCD diamond MEA with $TiSi_2$ bondpads and SU8 passivation
DREAMS3	BNCD diamond MEA with $TiSi_2$ bondpads and ONO passivation

Table C.1: Acronyms

Abbreviation	Description
DREAMS4	BNCD diamond MEA with $TiSi_2$ bondpads and NCD passivation
ECM	Extracellular Matrix
EDTA	Ethylenediaminetetraacetic Acid
FET	Field Effect Transistor
FLIM	Fluorescence Lifetime IMaging
FRAP	Fluorescence Recovery After Photobleaching
FRET	Förrster Resonance Energy Transfer
GBSS	Gey's Balanced Salt Solution
GFP	Green Fluorescent Protein
GpECM	Gelatin:PDL:ECM:GBSS mixture at 2:1:1:100
HBSS +/-	Hank's Balanced Salt Solution with/without calcium and magnesium
HEK	Human Embryonic Kidney
HL-1	Cardiomyocyte-like cell line derived from the AT-1 mouse atrial tumor by Claycomb et al
hUbiC	Human Ubiquitin C
HXP	Zeiss brand metal halide illumination source
MEA	Micro Electrode Array
mKATE	Mutated Katushka fluorophore
μCD	Microcrystalline Diamond
NCD	Nanocrystalline Diamond
NCLE	Non-Cell Light Effects
ND	Nanodiamond
NorA	Norepinephrine
NpHR	*Natronobacterium pharaonis* Halo Rhodopsin
ONO	$SiO_2/Si_2N_3/SiO_2$ passivation mulitlayer stack
PCB	Printed Circuit Board
PCD	Poly Crystalline Diamond
pcDNA4_TO	Tetracycline on plasmid of the TRex expression system, with multiple cloning site downstream of a CMV promoter and Tet repressor binding site
pcDNA6_TR	Tetracycline repressor plasmid part of the TRex epxression system
PDL	Poly-D-lysine
PDMS	Polydimethylsiloxane
PECVD	Plasma Enhanced Chemical Vapor Deposition
PIF	Phytochrome Interacting Factor
PLL	Poly-L-lysine
PTL	Photo Tethered Ligand

Table C.1: Acronyms

Abbreviation	Description
RDX	Reasearch Department Explosive, cyclotrimethylenetrinitramine
RMS	Root Mean Squared
SDS	Sodium Dodecyl Sulfate
SNR	Signal-to-Noise Ratio
stack	Multilayer passivation stack
SU-8	A biocompatible epoxy-based negative photoresist
TetON	Tetracyclin on promoter
TNT	Trinitrotoluene
TO_Ch2opt_mKATE	Plasmid encoding modified Channelrhodopsin 2-mutated Katushka fusion protein with mouse optimized coding in the tetracycline on promoter of the Trex expression system
UCL	University College London
UK	United Kingdom
UGA	High speed programmable scanning spot illumination system from Rapp Optoelectronics
UNCD	Ultra Nanocrystalline Diamond
YFP	Yellow Fluorescent Protein

Bibliography

[1] Addgene plasmid pUB-GFP. http://www.addgene.org/pgvec1?f=c&identifier=11155&atqx=pUB&cmd=findpl, 2008.

[2] SDSC biology workbench. http://workbench.sdsc.edu/, 2008-2011.

[3] Eurofins MWG Operon. http://www.operon.com, 2009-2010.

[4] Plasmid pmkate2-c. www.evrogen.com/products/vectors/pmKate2-C/pmKate2-C.shtml, 2010.

[5] What do neuronal networks have to do with real neurons? http://encefalus.com, July 2010.

[6] element6. http://www.e6.com/en/businessareas/e6advancedmaterials/products, April 2011.

[7] Functional magnetic resonance imaging. gttp://en.wikipedia.org/wiki/Functional_magnetic_resonance_imaging, May 2011.

[8] Open optogenetics. http://www.openoptogenetics.org/index.php?title=Main_Page, 2011.

[9] Wikipedia, ligand-gated ion channel. http://en.wikipedia.org/wiki/Ligand-gated_ion_channel, May 2011.

[10] Wikipedia, organelle. http://en.wikipedia.org/wiki/Organelle, May 2011.

[11] Wikipedia, patch clamp. http://en.wikipedia.org/wiki/Patch_clamp, April 2011.

[12] Patrick Roland Abbott. The effect of average grain size on the work function of polycrystalline diamond films, 2002.

[13] Stephen R Adams. How Calcium Indicators Work. *Cold Spring Harb Protoc*, 2010(3):pdb.top70, 2010.

[14] Dzmitry Afanasenkau. personal communication, 2011.

[15] Cansu Agca, Jason J Fritz, Lary C Walker, Allan I Levey, Anthony Ws Chan, James J Lah, and Yuksel Agca. Development of transgenic rats producing human beta-amyloid precursor protein as a model for Alzheimer's disease: transgene and endogenous APP genes are regulated tissue-specifically. *BMC neuroscience*, 9:28, January 2008.

[16] David J Aidley. *The Physiology of Excitable Cells*. Cambridge University Press, 4 edition, 1998.

[17] Benjamin R Arenkiel, Joao Peca, Ian G Davison, Catia Feliciano, Karl Deisseroth, George J Augustine, Michael D Ehlers, and Guoping Feng. In vivo light-induced activation of neural circuitry in transgenic mice expressing channelrhodopsin-2. *Neuron*, 54(2):205–18, April 2007.

[18] P Ariano, O Budnyk, S Dalmazzo, D Lovisolo, Ch Manfredotti, P Rivolo, and E Vittone. On diamond surface properties and interactions with neurons. *The European physical journal. E, Soft matter*, 30(2):149–56, October 2009.

[19] a. B. Arrenberg, D. Y. R. Stainier, H. Baier, and J. Huisken. Optogenetic Control of Cardiac Function. *Science*, 330(6006):971–974, November 2010.

[20] O. Auciello and A.V. Sumant. Status review of the science and technology of ultrananocrystalline diamond (UNCD (TM)) films and application to multifunctional devices. *Diamond and Related Materials*, 19(7-9):699–718, 2010.

[21] Piyush Bajaj, Demir Akin, Amit Gupta, Debby Sherman, Bing Shi, Orlando Auciello, and Rashid Bashir. Ultrananocrystalline diamond film as an optimal cell interface for biomedical applications. *Biomedical microdevices*, 9(6):787–94, December 2007.

[22] James Baker. personal communication, 2008.

[23] Christian Bamann, Taryn Kirsch, Georg Nagel, and Ernst Bamberg. Spectral characteristics of the photocycle of channelrhodopsin-2 and its implication for channel function. *Journal of molecular biology*, 375(3):686–94, January 2008.

[24] E Bamberg, J Tittor, and D Oesterhelt. Light-driven proton or chloride pumping by halorhodopsin. *Proceedings of the National Academy of Sciences of the United States of America*, 90(2):639–43, January 1993.

[25] Prof. Ernst Bamberg. personal communication, 2009.

[26] Matthew Banghart, Katharine Borges, Ehud Isacoff, Dirk Trauner, and Richard H Kramer. Light-activated ion channels for remote control of neuronal firing. *Nature neuroscience*, 7(12):1381–6, December 2004.

[27] L Berdondini, P D van der Wal, O Guenat, N F de Rooij, M Koudelka-Hep, P Seitz, R Kaufmann, P Metzler, N Blanc, and S Rohr. High-density electrode array for imaging in vitro electrophysiological activity. *Biosensors & bioelectronics*, 21(1):167–74, July 2005.

[28] André Berndt, Ofer Yizhar, Lisa a Gunaydin, Peter Hegemann, and Karl Deisseroth. Bi-stable neural state switches. *Nature neuroscience*, 12(2):229–34, February 2009.

[29] Edward S Boyden, Feng Zhang, Ernst Bamberg, Georg Nagel, and Karl Deisseroth. Millisecond-timescale, genetically targeted optical control of neural activity. *Nature neuroscience*, 8(9):1263–8, September 2005.

[30] Austin L. Brown, Brandon E. Johnson, and Miriam B. Goodman. Patch clamp recording of ion channels expressed in xenopus oocytes. *J Vis Exp.*, 20, 2008.

[31] Dorothea Brüggemann, Bernhard Wolfrum, Vanessa Maybeck, Yulia Mourzina, Michael Jansen, and Andreas Offenhäusser. Nanostructured gold microelectrodes for extracellular recording from electrogenic cells. *Nanotechnology*, 22.

[32] Susan Calvin, Jay Want, Jeff Emch, Simone Pitz, and Linda Jacobsen. FuGENE®HD transfection reagent: Choice of a transfection reagent with minimal off-target effect as analyzed by microarray transcriptional profiling. *Biochemica*, 2006.

[33] N.A. Campbell and J.B. Reece. Biology, 2002.

[34] P Cesare, a Moriondo, V Vellani, and P a McNaughton. Ion channels gated by heat. *Proceedings of the National Academy of Sciences of the United States of America*, 96(14):7658–63, July 1999.

[35] H.Y. Chan, M. Varney, S. Hatch, and DM Aslam. Implantable polycrystalline diamond neural probe for in vivo and in vitro physiological recording. In *Solid-State Sensors, Actuators and Microsystems Conference, 2009. TRANSDUCERS 2009. International*, number 1, pages 1202–1205. IEEE, 2009.

[36] Kwok Feng Chong, Kian Ping Loh, S R K Vedula, Chwee Teck Lim, Hadwig Sternschulte, Doris Steinmüller, Fwu-Shan Sheu, and

Yu Lin Zhong. Cell adhesion properties on photochemically functionalized diamond. *Langmuir : the ACS journal of surfaces and colloids*, 23(10):5615–21, May 2007.

[37] Brian Y Chow, Xue Han, Allison S Dobry, Xiaofeng Qian, Amy S Chuong, Mingjie Li, Michael a Henninger, Gabriel M Belfort, Yingxi Lin, Patrick E Monahan, and Edward S Boyden. High-performance genetically targetable optical neural silencing by light-driven proton pumps. *Nature*, 463(7277):98–102, January 2010.

[38] Yun Doo Chung. Mechanosensory Transduction in. *Review Literature And Arts Of The Americas*, 29(December):419–420, 2007.

[39] W C Claycomb, N a Lanson, B S Stallworth, D B Egeland, J B Delcarpio, a Bahinski, and N J Izzo. HL-1 cells: a cardiac muscle cell line that contracts and retains phenotypic characteristics of the adult cardiomyocyte. *Proceedings of the National Academy of Sciences of the United States of America*, 95(6):2979–84, March 1998.

[40] Stuart F Cogan. Neural stimulation and recording electrodes. *Annual review of biomedical engineering*, 10:275–309, January 2008.

[41] Edward C. Conley and William J. Brammar. *The Ion Channel Facts Book:IV Voltage Gated Channels*. Academic Press London, 1999.

[42] Markus Dankerl, Stefan Eick, Boris Hofmann, Moritz Hauf, Sven Ingebrandt, Andreas Offenhäusser, Martin Stutzmann, and Jose A Garrido. Diamond Transistor Array for Extracellular Recording From Electrogenic Cells. *Advanced Functional Materials*, 19(18):2915–2923, 2009.

[43] C.M. Dekeyser, E. Zuyderhoff, R.E. Giuliano, H.J. Federoff, Ch.C. Dupont-Gillain, and P.G. Rouxhet. A rough morphology of th eadsorbed fibronectin layer favors adhesion of neuronal cells. *Journal of biomedical materials research, Part A*, 87:116–28, 2008.

[44] Sharanya Arcot Desai, John D Rolston, Liang Guo, and Steve M Potter. Improving impedance of implantable microwire multi-electrode arrays by ultrasonic electroplating of durable platinum black. *Frontiers in neuroengineering*, 3(May):5, January 2010.

[45] Elena Dreosti and Leon Lagnado. Optical reporters of synaptic activity in neural circuits. *Experimental physiology*, 96(1):4–12, January 2011.

[46] H Ecken, S Ingebrandt, M Krause, D Richter, M Hara, and A Offenhäusser. 64-Channel extended gate electrode arrays for extracellular signal recording. *Electrochimica Acta*, 48(20-22):3355–3362, September 2003.

[47] Robert Edgington. personal communication, 2010.

[48] Robert Edgington. Preliminary title: Diamond at the brain machine interface, in preparation 2011. in preparation.

[49] Stefan Eick. *Extracellular Stimulation of Individual Electrogenic Cells with Micro-Scaled Electrodes*. PhD thesis, 2010.

[50] Thomas M. Jessell Eric R. Kandel, James H. Schwartz, editor. *Principles of Neural Science*. McGraw-Hill, fourth edition edition.

[51] Jan Eschermann. Contactless cleaning of nanowire FETs. personal communication.

[52] Jan Eschermann. Silicium Nanodrähte für die extrazelluläre Ableitung elektrischer Aktivität, 2010.

[53] B. Eversmann, M. Jenkner, F. Hofmann, C. Paulus, R. Brederlow, B. Holzapfl, P. Fromherz, M. Merz, M. Brenner, M. Schreiter, R. Gabl, K. Plehnert, M. Steinhauser, G. Eckstein, D. Schmitt-Landsiedel, and R. Thewes. A 128 x 128 cmos biosensor array for extracellular recording of neural activity. *IEEE Journal of Solid-State Circuits*, 38(12):2306–2317, December 2003.

[54] P. Fromherz and A. Stett. Silicon-neuron junction: capacitive stimulation of an individual neuron on a silicon chip. *Physical review letters*, 75(8):1670–1673, 1995.

[55] W. Gajewski, P. Achatz, O. Williams, K. Haenen, E. Bustarret, M. Stutzmann, and J. Garrido. Electronic and optical properties of boron-doped nanocrystalline diamond films. *Physical Review B*, 79(4):1–14, January 2009.

[56] K. Gerwert. 42nd iff springschool 2011, macromolecular systems in soft and living matter. pages C6.1 – C6.16, Jülich, Germany, February 2011.

[57] HEKA Elektronik GmbH. *EPC 9 Manual*.

[58] Rapp Optoelectronics GmbH. Customer support, 2011.

[59] B Y David E Goldman. IN MEMBRANES.

[60] Wolfgang H. Goldman. Mechanical aspects of cell shape regulation and signaling. *Cell Biology International*, 26:313–7, April 2002.

[61] A. Grinvald, L. Anglister, JA Freeman, R. Hildesheim, and A. Manker. Real-time optical imaging of naturally evoked electrical activity in intact frog brain. *Group*, 308(26):848–50, 1984.

[62] Amiram Grinvald and Rina Hildesheim. VSDI: a new era in functional imaging of cortical dynamics. *Nature reviews. Neuroscience*, 5(11):874–85, November 2004.

[63] Nir Grossman, Vincent Poher, Matthew S Grubb, Gordon T Kennedy, Konstantin Nikolic, Brian McGovern, Rolando Berlinguer Palmini, Zheng Gong, Emmanuel M Drakakis, Mark a a Neil, Martin D Dawson, Juan Burrone, and Patrick Degenaar. Multi-site optical excitation using ChR2 and micro-LED array. *Journal of neural engineering*, 7(1):16004, February 2010.

[64] Andreas Grote, Karsten Hiller, Maurice Scheer, Richard Münch, Bernd Nörtemann, Dietmar C Hempel, and Dieter Jahn. JCat: a novel tool to adapt codon usage of a target gene to its potential expression host. *Nucleic acids research*, 33(Web Server issue):W526–31, July 2005.

[65] Lisa a Gunaydin, Ofer Yizhar, André Berndt, Vikaas S Sohal, Karl Deisseroth, and Peter Hegemann. Ultrafast optogenetic control. *Nature neuroscience*, 13(3):387–92, March 2010.

[66] Aviad Hai, Ada Dormann, Joseph Shappir, Shlomo Yitzchaik, Carmen Bartic, Gustaaf Borghs, J P M Langedijk, and Micha E Spira. Spine-shaped gold protrusions improve the adherence and electrical coupling of neurons with the surface of micro-electronic devices. *Journal of the Royal Society, Interface / the Royal Society*, 6(41):1153–65, December 2009.

[67] Aviad Hai, Dotan Kamber, Guy Malkinson, Hadas Erez, Noa Mazurski, Joseph Shappir, and Micha E Spira. Changing gears from chemical adhesion of cells to flat substrata toward engulfment of micro-protrusions by active mechanisms. *Journal of neural engineering*, 6(6):066009, December 2009.

[68] Xue Han and Edward S Boyden. Multiple-color optical activation, silencing, and desynchronization of neural activity, with single-spike temporal resolution. *PloS one*, 2(3):e299, January 2007.

[69] Yael Hanein. Guest Seminar PGI-8, 2011.

[70] Yael Hanein. How many cells does it take to change a lightbulb? carbon nanotubes, neurons, and everything in between., April 2011.

[71] F Heer, S Hafizovic, T Ugniwenko, U Frey, W Franks, E Perriard, J-C Perriard, a Blau, C Ziegler, and a Hierlemann. Single-chip microelectronic system to interface with living cells. *Biosensors & bioelectronics*, 22(11):2546–53, May 2007.

[72] Peter Hegemann. Algal sensory photoreceptors. *Annual review of plant biology*, 59:167–89, January 2008.

[73] A L HODGKIN. Ionic movements and electrical activity in giant nerve fibres. *Proceedings of the Royal Society of London Series B Containing papers of a Biological character Royal Society Great Britain*, 148(930):1–37, 1958.

[74] Boris Hofmann.

[75] Boris Hofmann. personal communication, 2008.

[76] Boris Hofmann, Stefan Eick, Simone Meffert, Sven Ingebrandt, Ernst Bamberg, and Andreas Offenhäusser. Analysis of light induced activity in defined neural networks. In 6^{th} *International Meeting on Substrate Integrated Microelectronics*, July 2008.

[77] Boris Hofmann, Enno Kätelhön, Manuel Schottdorf, Andreas Offenhäusser, and Bernhard Wolfrum. Nanocavity electrode array for recording from electrogenic cells. *Lab on a chip*, pages 0–4, February 2011.

[78] Boris Hofmann, Vanessa Maybeck, Stefan Eick, Simone Meffert, Sven Ingebrandt, Philip Wood, Ernst Bamberg, and A. Offenhäusser. Light induced stimulation and delay of cardiac activity. *Lab Chip*, pages 1–11, 2010.

[79] P. Holzer. Acid-sensitive ion channels and receptors. *Handbook of Experimental Pharmacology*, 194:283–332, 2009.

[80] William M. Horspool and Pill-Soon Song. *CRC Handbook of Organic Photochemistry and Photobiology*. CRC Press Inc., 1994.

[81] Xianju Huang, Ronxin Wang, Wei Wang, and Zhihong Li. Fabrication of flexible 3D microelectrode array with paralyene-bassed pattern transfer technique. *Transducers*, 2009.

[82] a J Ingram, H Ly, K Thai, M Kang, and J W Scholey. Activation of mesangial cell signaling cascades in response to mechanical strain. *Kidney international*, 55(2):476–85, February 1999.

[83] Toru Ishizuka, Masaaki Kakuda, Rikita Araki, and Hiromu Yawo. Kinetic evaluation of photosensitivity in genetically engineered neurons expressing green algae light-gated channels. *Neuroscience research*, 54(2):85–94, February 2006.

[84] P a Janmey. The cytoskeleton and cell signaling: component localization and mechanical coupling. *Physiological reviews*, 78(3):763–81, July 1998.

[85] Michael Jansen. BioMas Analyzer. software, May-June 2011.

[86] S. Kateriya, G. Nagel, E. Bamberg, and P. Hegemann. "Vision" in single-celled algae. *News in physiological sciences*, 19:133–137, 2004.

[87] Richard S. Kelly. Analytical Electrochemistry : The Basic Concepts. *Analytical Sciences Digital Library*, 2009.

[88] Alexandre Kisner. Synthesis and integration of ultrathin au nanowires for stimulation and signal recording from electrogenic cells. PGI/ICS-8 Seminar, 20 May 2011.

[89] Tilman Kispersky and John A. White. Stochastic models of ion channel gating. *Scholarpedia*, 3(1):1327.

[90] Thomas Knöpfel, M.Z. Lin, Anselm Levskaya, Lin Tian, J.Y. Lin, and E.S. Boyden. Toward the Second Generation of Optogenetic Tools. *The Journal of Neuroscience*, 30(45):14998, 2010.

[91] Emily B Kramer and Philip J Farabaugh. The frequency of translational misreading errors in E. coli is largely determined by tRNA competition. *RNA (New York, N.Y.)*, 13(1):87–96, January 2007.

[92] A. Krüger, F. Kataoka, M. Ozawa, T. Fujino, Y. Suzuki, A.E. Aleksenskii, A. Ya. Vul', and E. Osawa. Unusually tight aggregation in detonation nanodiamond Identification and disintegration. *Carbon*, 43:1722–30, 2005.

[93] Zhang Lab. ITASSER online, protein structure and function predictions. `http://zhanglab.ccmb.med.umich.edu/I-TASSER/`, 2011.

[94] a. Lambacher, M. Jenkner, M. Merz, B. Eversmann, R.a. Kaul, F. Hofmann, R. Thewes, and P. Fromherz. Electrical imaging of neuronal activity by multi-transistor-array (MTA) recording at 7.8?m resolution. *Applied Physics A*, 79(7):1607–1611, August 2004.

[95] J K Lanyi. Photochromism of halorhodopsin. cis/trans isomerization of the retinal around the 13-14 double bond. *The Journal of biological chemistry*, 261(30):14025–30, October 1986.

[96] M Lehmann, W Baumann, M Brischwein, R Ehret, M Kraus, a Schwinde, M Bitzenhofer, I Freund, and B Wolf. Non-invasive measurement of cell membrane associated proton gradients by ion-sensitive field effect transistor arrays for microphysiological and bioelectronical applications. *Biosensors & bioelectronics*, 15(3-4):117–24, June 2000.

[97] L Leybaert, J Sneyd, and M J Sanderson. A simple method for high temporal resolution calcium imaging with dual excitation dyes. *Biophysical journal*, 75(4):2025–9, October 1998.

[98] Xiang Li, Davina V Gutierrez, M Gartz Hanson, Jing Han, Melanie D Mark, Hillel Chiel, Peter Hegemann, Lynn T Landmesser, and Stefan Herlitze. Fast noninvasive activation and inhibition of neural and network activity by vertebrate rhodopsin and green algae channelrhodopsin. *Proceedings of the National Academy of Sciences of the United States of America*, 102(49):17816–21, December 2005.

[99] Elizabeth Licht. *A Translation of Luigi Galvani's De Viribus Electridtatis*. 1953.

[100] John Y Lin. A user's guide to channelrhodopsin variants: features, limitations and future developments. *Experimental physiology*, 96(1):19–25, January 2010.

[101] John Y Lin, Michael Z Lin, Paul Steinbach, and Roger Y Tsien. Characterization of engineered channelrhodopsin variants with improved properties and kinetics. *Biophysical journal*, 96(5):1803–14, March 2009.

[102] University College London, Paris Vision Institute INSERM, Commissariat á l énergie atomique, Walter Schottky Institute, Forschungszentrum Jülich GmbH, and Academy of Sciences of the Czech Republic. Periodic reports of the EU project DREAMS, 2008-2010.

[103] Alicia Lundby, Walther Akemann, and Thomas Knöpfel. Biophysical characterization of the fluorescent protein voltage probe VSFP2.3 based on the voltage-sensing domain of Ci-VSP. *European biophysics journal : EBJ*, pages 1625–1635, August 2010.

[104] Alicia Lundby, Hiroki Mutoh, Dimitar Dimitrov, Walther Akemann, and Thomas Knöpfel. Engineering of a genetically encodable fluorescent voltage sensor exploiting fast Ci-VSP voltage-sensing movements. *PloS one*, 3(6):e2514, January 2008.

[105] Haiming Luo, Jie Yang, Honglin Jin, Chuan Huang, Jianwei Fu, Fei Yang, Hui Gong, Shaoqun Zeng, Qingming Luo, and Zhihong Zhang. Tetrameric far-red fluorescent protein as a scaffold to assemble an octavalent peptide nanoprobe for enhanced tumor targeting and intracellular uptake in vivo. *The FASEB journal : official publication of the Federation of American Societies for Experimental Biology*, pages 1–9, February 2011.

[106] Robert Machinek. *Stimulation and Recording of Electrical Cell Signals Using Electronic Devices*. PhD thesis, RWTH Aachen, 2010.

[107] Jirí J. Mares, Pavel Hubík, Jozef Kristofik, Dobroslav Kindl, and Milos Nesládek. Quantum Transport in Boron-Doped Nanocrystalline Diamond. *Chemical Vapor Deposition*, 14(7-8):161–172, July 2008.

[108] Steve McGregor. Argonne plays important role in development of artificial retina. http://www.anl.gov/Media_Center/News?2004/news041014.html.

[109] Sven Meyburg, Michael Goryll, Jürgen Moers, Sven Ingebrandt, Simone Böcker-Meffert, Hans Lüth, and Andreas Offenhäusser. N-Channel field-effect transistors with floating gates for extracellular recordings. *Biosensors & bioelectronics*, 21(7):1037–44, January 2006.

[110] G. Miller. Optogenetics. shining new light on neural circuits. *Science*, 314(5806):1674–6, December 2006.

[111] S I Miyazaki, K Takahashi, and K Tsuda. Electrical excitability in the egg cell membrane of the tunicate. *The Journal of physiology*, 238(1):37–54, April 1974.

[112] LadyofHats Mnokel. Wikipedia, action potential. http://en.wikipedia.org/wiki/Action_potential, May 2011.

[113] LadyofHats Mnokel. Wikipedia, g protein-coupled receptor. http://en.wikipedia.org/wiki/G_protein-coupled_receptor, May 2011.

[114] Michael a Moffitt and Cameron C McIntyre. Model-based analysis of cortical recording with silicon microelectrodes. *Clinical neurophysiology : official journal of the International Federation of Clinical Neurophysiology*, 116(9):2240–50, September 2005.

[115] J Preben Morth, Bjørn P Pedersen, Mads S Toustrup-Jensen, Thomas L-M Sø rensen, Janne Petersen, Jens Peter Andersen, Bente Vilsen, and Poul Nissen. Crystal structure of the sodium-potassium pump. *Nature*, 450(7172):1043–9, December 2007.

[116] Sami Myllymaa, K. Myllymaa, H. Korhonen, K. Djupsund, H. Tanila, and R. Lappalainen. Development of flexible thin film microelectrode arrays for neural recordings. In *14^{th} Nordic-Baltic Conference on Biomedical Engineering and Medical Physics*, volume 20 Part 4, pages 286–89.

[117] Takeharu Nagai, Shuichi Yamada, Takashi Tominaga, Michinori Ichikawa, and Atsushi Miyawaki. Expanded dynamic range of fluorescent indicators for Ca(2+) by circularly permuted yellow fluorescent proteins. *Proceedings of the National Academy of Sciences of the United States of America*, 101(29):10554–9, July 2004.

[118] G Nagel, T Szellas, S Kateriya, N Adeishvili, P Hegemann, and E Bamberg. Channelrhodopsins: directly light-gated cation channels. *Biochemical Society transactions*, 33(Pt 4):863–6, August 2005.

[119] Georg Nagel, Martin Brauner, Jana F Liewald, Nona Adeishvili, Ernst Bamberg, and Alexander Gottschalk. Light activation of channelrhodopsin-2 in excitable cells of Caenorhabditis elegans triggers rapid behavioral responses. *Current biology : CB*, 15(24):2279–84, December 2005.

[120] Georg Nagel, Doris Ollig, Markus Fuhrmann, Suneel Kateriya, Anna Maria Musti, Ernst Bamberg, and Peter Hegemann. Channelrhodopsin-1: a light-gated proton channel in green algae. *Science (New York, N.Y.)*, 296(5577):2395–8, June 2002.

[121] Georg Nagel, Tanjef Szellas, Wolfram Huhn, Suneel Kateriya, Nona Adeishvili, Peter Berthold, Doris Ollig, Peter Hegemann, and Ernst Bamberg. Channelrhodopsin-2, a directly light-gated cation-selective membrane channel. *Proceedings of the National Academy of Sciences of the United States of America*, 100(24):13940–5, November 2003.

[122] Chrostoph E. Nebel, Dongchan Shin, Bohuslav Rezek, Norio Tokuda, Hiroshi Uetsuka, and Hideyuki Watanabe. Diamond and biology. *Journal of the Royal Society Interface*, (4):439–61, 2007.

[123] P O'Donnell, a Lavín, L W Enquist, a a Grace, and J P Card. Interconnected parallel circuits between rat nucleus accumbens and thalamus revealed by retrograde transynaptic transport of pseudorabies virus. *The Journal of neuroscience : the official journal of the Society for Neuroscience*, 17(6):2143–67, March 1997.

[124] D. Oesterhelt and W. Stoeckenius. Rhodopsin-like protein from the purple membrane of *Halobacterium halobium*. *Nature: New biology*, 233:149–52, 1971.

[125] University of Michingan. OPM Database. `http://opm.phar.umich.edu/protein.php?pdbid=3a7k`.

[126] Markus Pagels, Clive E Hall, Nathan S Lawrence, Andrew Meredith, Timothy G J Jones, Herman P Godfried, C S James Pickles, Jonathan Wilman, Craig E Banks, Richard G Compton, and Li Jiang. All-diamond microelectrode array device. *Analytical chemistry*, 77(11):3705–8, June 2005.

[127] Fernando Patolsky, Brian P Timko, Guihua Yu, Ying Fang, Andrew B Greytak, Gengfeng Zheng, and Charles M Lieber. Detection, stimulation, and inhibition of neuronal signals with high-density nanowire transistor arrays. *Science (New York, N.Y.)*, 313(5790):1100–4, August 2006.

[128] George H Patterson and Jennifer Lippincott-Schwartz. Selective photolabeling of proteins using photoactivatable GFP. *Methods (San Diego, Calif.)*, 32(4):445–50, April 2004.

[129] Serge Picaud. personal communication, 2010.

[130] D C Prasher. Using GFP to see the light. *Trends in genetics : TIG*, 11(8):320–3, August 1995.

[131] Leslie A. Pray. DNA replication and causes of mutation. *Nature Education*, 1(1), 2008.

[132] Stefan R Pulver, Nicholas J Hornstein, Bruce L Land, and Bruce R Johnson. Optogenetics in the teaching laboratory: using channelrhodopsin-2 to study the neural basis of behavior and synaptic physiology in Drosophila. *Advances in physiology education*, 35(1):82–91, March 2011.

[133] Peter H Quail. Phytochrome photosensory signalling networks. *Nature reviews. Molecular cell biology*, 3(2):85–93, February 2002.

[134] Marco Mank Arnaud Muller Palmer Taylor Oliver Griesbeck David Kleinfeld Quoc-Thang Nguyen, Lee F Schroeder. An in vivo biosensor for neurotransmitter release and in situ receptor activity. *Nature Neuroscience*, 13:127–132, 2010.

[135] P. Reichart, G. Dollinger, A. Bergmaier, A. Hauptner, R. Hertenberger, H.-J. Körner, and R. Krücken. Detection of Hydrogen on Grain Boundaries of CVD-Grown Diamond. `http://www.bl.physik.uni-muenchen.de/bl_rep/jb2002/p67.ps`.

[136] S. Saada, J.C. Arnault, L. Rocha, B. Bazin, and P. Bergonzo. Synthesis and characterisation of NCD films on 10 x 10 mm^2 and deposition on 2 inch wafer using rotating substrate-holder set-up. *Physica Status Solidi (a)*, 205:2121–25, 2008.

[137] Joseph Sambrook, David W. Russell, Nina Irwin, and Kaaren A. Janssen. *Molecular Cloning, A Laboratory Manual*. CSHL Press, 3 edition, 2001.

[138] Brigitte Schobert and Janos K. Lanyi. Halorhodopsin is a light-driven chloride pump. *The Journal of Biological Chemistry*, 257(17):10306–10313, september 1982.

[139] Alex K. Shalek, Jacob T. Robinson, Ethan S. Karp, Jin Seok Lee, Dae-Ro Ahn, Myung-Han Yoon, Amy Sutton, Marsela Jorgolli, Rona S. Gertner, Taranjit S. Gujral, Gavin MacBeath, Eun Gyeong Yang, and Hongkun Park. Vertical silicon nanowires as a universal platform for delivering biomolecules into living cells. *PNAS*, 107(5):1870–5, 2009.

[140] Nathan C Shaner, George H Patterson, and Michael W Davidson. Advances in fluorescent protein technology. *Journal of cell science*, 120(Pt 24):4247–60, December 2007.

[141] Dmitry Shcherbo, Ekaterina Merzlyak, Tatiana Chepurnykh, Arkady Fradkov, Galina kova, Elena Solovieva, Konstantin Lukyanov, Ekaterina Bogdanova, Andrey Zaraisky, Sergey Lukyanov, and Dmitriy Chudakov. Bright far-red fluorescent protein for whole-body imaging. *Nature Methods*, 4:741–46, 2007.

[142] D Shoham, D E Glaser, a Arieli, T Kenet, C Wijnbergen, Y Toledo, R Hildesheim, and a Grinvald. Imaging cortical dynamics at high spatial and temporal resolution with novel blue voltage-sensitive dyes. *Neuron*, 24(4):791–802, December 1999.

[143] Asaf Shoval, Christopher Adams, Moshe David-Pur, Mark Shein, Yael Hanein, and Evelyne Sernagor. Carbon nanotube electrodes for effective interfacing with retinal tissue. *Frontiers in neuroengineering*, 2(April):4, January 2009.

[144] J.C. Skou. The influence of some cations on an adenosine triphosphatase from peripheral nerves. *Biochimica et biophysica acta*, 23:394–401, 1957.

[145] Frank Sommerhage. M64. software.

[146] William R. Stauffer and Xinyan T. Cui. Polypyrrole doped with 2 peptide sequences from laminin. *Biomaterials*, 27:2405–13, 2006.

[147] Alfred Stett, Ulrich Egert, Elke Guenther, Frank Hofmann, Thomas Meyer, Wilfried Nisch, and Hugo Haemmerle. Biological application of microelectrode arrays in drug discovery and basic research. *Analytical and bioanalytical chemistry*, 377(3):486–95, October 2003.

[148] Yuka Sugiyama, Hongxia Wang, Takuya Hikima, Minami Sato, Jun Kuroda, Tetsuo Takahashi, Toru Ishizuka, and Hiromu Yawo. Photocurrent attenuation by a single polar-to-nonpolar point mutation of channelrhodopsin-2. *Photochemical & photobiological sciences : Official journal of the European Photochemistry Association and the European Society for Photobiology*, 8(3):328–36, March 2009.

[149] Jeffrey J Tabor, Anselm Levskaya, and Christopher a Voigt. Multichromatic control of gene expression in Escherichia coli. *Journal of molecular biology*, 405(2):315–324, October 2010.

[150] P. Thomas and T.G. Smart. Hek293 cell line: a vehicle for the expression of recombinant proteins. *Journal of Pharmacological and Toxicological Methods*, 51(3):187–200, May-June 2005.

[151] E. Vanhove, J. de Sanoit, P. Mailley, M.-A. Pinault, F. Jomard, and P. Bergonzo. High reactivity and stability of diamond electrodes: The influence of the b-doping concentration. *Physica Status Solidi A*, (9):2063–69, 2009.

[152] M. Volgraf, P. Gorostiza, R. Numano, R.H. Kramer, E.Y. Isacoff, and D. Trauner. Allosteric control of an ionotropic glutamate receptor with an optical switch. *Nature Chemical Biology*, 2:47–52, December 2005.

[153] Jing Wang, David A. Borton, Jiayi Zhang, Rebecca D. Burwell, and Arto V. Nurmikko. A neurophotonic device for stimulation and recording of neural microcircuits. In *32nd Annual International Conference of the IEEE EMBS*, pages 2935–8, Buenos Aires, Argentina, 2010.

[154] R Weis, B Müller, and P Fromherz. Neuron adhesion on a silicon chip probed by an array of field-effect transistors. *Physical review letters*, 76(2):327–330, January 1996.

[155] Andreas a Werdich, Eduardo a Lima, Borislav Ivanov, Igor Ges, Mark E Anderson, John P Wikswo, and Franz J Baudenbacher. A microfluidic device to confine a single cardiac myocyte in a sub-nanoliter volume on planar microelectrodes for extracellular potential recordings. *Lab on a chip*, 4(4):357–62, August 2004.

[156] Oliver A. Williams and Miloš Nesládek. Growth and properties of nanocrystalline diamond films. *Physica Status Solidi (a)*, 203(13):3375–86, 2006.

[157] Philip Wood. personal communication, 2009.

[158] G Wrobel, Y Zhang, H-J Krause, N Wolters, F Sommerhage, a Offenhäusser, and S Ingebrandt. Influence of the first amplifier stage in MEA systems on extracellular signal shapes. *Biosensors & bioelectronics*, 22(6):1092–6, January 2007.

[159] Günter Wrobel, Matthias Höller, Sven Ingebrandt, Sabine Dieluweit, Frank Sommerhage, Hans Peter Bochem, and Andreas Offenhäusser. Transmission electron microscopy study of the cell-sensor interface. *Journal of the Royal Society, Interface / the Royal Society*, 5(19):213–22, February 2008.

[160] Xingcheng Xiao, Jian Wang, Chao Liu, John a Carlisle, Brian Mech, Robert Greenberg, Dilek Guven, Ricardo Freda, Mark S Humayun, James Weiland, and Orlando Auciello. In vitro and in vivo evaluation of ultrananocrystalline diamond for coating of implantable retinal microchips. *Journal of biomedical materials research. Part B, Applied biomaterials*, 77(2):273–81, May 2006.

[161] Ian York. Cells spontaneously zeocin resistant? `http://www.molecularstation.com/forum/protocols-methods-forum/19816-cells-spontaneously-zeocin-resistant.html`, 2008.

[162] Feng Zhang, Li-Ping Wang, Martin Brauner, Jana F Liewald, Kenneth Kay, Natalie Watzke, Phillip G Wood, Ernst Bamberg, Georg Nagel, Alexander Gottschalk, and Karl Deisseroth. Multimodal fast optical interrogation of neural circuitry. *Nature*, 446(7136):633–9, April 2007.

[163] Wei Zhang, Wooping Ge, and Zuoren Wang. A toolbox for light control of Drosophila behaviors through Channelrhodopsin 2-mediated photoactivation of targeted neurons. *The European journal of neuroscience*, 26(9):2405–16, November 2007.

Author's List of Publications

Small company mergers - good for whom? **Vanessa Maybeck** and William Bains, (2006) *Nature Biotechnology* 24 (11) p. 1343-8.

A targeted gain-of-function screen identifies genes affecting salivary gland morphogenesis/tubulogenesis in Drosophila. **Vanessa Maybeck** and Katja Röper, (2009) *Genetics* 181 (2) p. 543-65.

Light induced stimulation and delay of cardiac activity. Boris Hofmann, **Vanessa Maybeck**, Stefan Eick, Simone Meffert, Sven Ingebrandt, Philip Wood, Ernst Bamberg, Andreas Offenhäusser, (2010) *Lab on a Chip* 10 (19) p. 2588-96.

Nanostructured gold microelectrodes for extracellular recording from electrogenic cells. D Brüggemann, B Wolfrum, **V Maybeck**, Y Mourzina, M Jansen, A Offenhäusser, (2011) *Nanotechnology* 22 (26) p. 265104-10.

Lebenslauf

Persönliche Daten

Name	Maybeck
Vorname	Vanessa
Geburtstag	13 Jun 1982
Geburtsort	West Islip
Staatsangehörigkeit	amerikanerin

Qualifikationen

2000	Regents Diploma - West Islip High School (Eq. Abitur)
2000-2004	Bachelor of Science, Maj. Biology, Min. Chinese Studies - Stony Brook University
2004-2005	Master of Philosophy, BioScience Enterprise - University of Cambridge
ab 2008	Promotion am Institut für Complex Systeme - 8 im Forschungszentrum Jülich

12 Oktober 2011

Declaration of Originality

I declare that this dissertation is an original work that has not been submitted for any other degree or title, at any higher education institution. I declare that this dissertation represents my own work and all work which is not my own has been cited as such.

Ich versichere eidesstattlich, dass ich diesen Promotionsantrag erstmalig einreiche und keine früheren Versuche einer Promotion unternommen habe. Ich erkläre eidesstattlich, dass ich die Dissertation selbständig verfasst und alle in Anspruch genommenen Hilfen in der Dissertation angegeben habe. Ich erkläre, dass durch die Veröffentlichung als Dissertation der RWTH Aachen bestehende Schutzrechte - inbesondere Urheberschutzrechte - nicht verletzt werden.

Vanessa Maybeck

Jül-4346
November 2011
ISSN 0944-2952